



Pilkington Library

Author/Filing Title KEYTE, R.W.

Accession/Copy No. 040129639

Vol. No. Class Mark

LOAN COPY

0401296393



BADMINTON PRESS
18 THE HALFCROFT
SYSTEM
LEICESTER LE7 1LD
ENGLAND
TEL: 0116 260 2917
FAX: 0116 268 6639

**STUDIES OF
DITHIOIMIDODIPHOSPHINATES
AND RELATED COMPOUNDS**

by


ROBIN W. KEYTE

A Doctoral Thesis submitted
in partial fulfilment for the award of

Doctor of Philosophy of the Loughborough University

Department of Chemistry
Loughborough University
Loughborough
Leicestershire
LE11 3TU

© R. W. Keyte 1996

 Loughborough University Library
Date <i>Dec 96</i>
Class
Acc No. <i>040129639</i>

96451382

This work is
dedicated to the memory of

Dorothy Bowley

10th January 1909 - 22nd April 1995

*Kind hearts are the garden,
Kind thoughts are the roots,
Kind words are the flowers,
Kind deeds are the fruits.*

ABSTRACT

The condensation reaction of ${}^i\text{Pr}_2\text{P}(\text{S})\text{Cl}$ with hexamethyldisilazane, $\text{HN}(\text{SiMe}_3)_2$, followed by oxidation with sulfur yields ${}^i\text{Pr}_2\text{P}(\text{S})\text{NHP}(\text{S}){}^i\text{Pr}_2$. Single crystal X-ray diffraction studies indicate it adopts a unique *cisoid* conformation in a hydrogen bonded chain. ${}^i\text{Pr}_2\text{P}(\text{S})\text{NHP}(\text{S}){}^i\text{Pr}_2$ was reacted with carbonates of Zn, Cd and Ni, CoCl_2 , MCl_2COD ($\text{M} = \text{Pd}, \text{Pt}$) and $\text{Pt}(\text{PMe}_3)_2\text{Cl}_2$ yielding the complexes $\text{M}[{}^i\text{Pr}_2\text{P}(\text{S})\text{NP}(\text{S}){}^i\text{Pr}_2]_2$ ($\text{M} = \text{Zn}, \text{Cd}, \text{Ni}, \text{Co}, \text{Pd}, \text{Pt}$), $\{[{}^i\text{Pr}_2\text{P}(\text{S})\text{NP}(\text{S}){}^i\text{Pr}_2]\text{Pd}[{}^i\text{Pr}_2\text{P}(\text{S})\text{NHP}(\text{S}){}^i\text{Pr}_2]\}^+\text{Cl}^-$ and $\{\text{Pt}(\text{PMe}_3)_2[{}^i\text{Pr}_2\text{P}(\text{S})\text{NP}(\text{S}){}^i\text{Pr}_2]\}^+\text{BPh}_4^-$. Crystallography revealed $\text{M}[{}^i\text{Pr}_2\text{P}(\text{S})\text{NP}(\text{S}){}^i\text{Pr}_2]_2$ ($\text{M} = \text{Zn}, \text{Cd}, \text{Ni}$) to be isostructural tetrahedrons in which the $\text{MS}_2\text{P}_2\text{N}$ rings adopted pseudo boat conformations in contrast to the $\text{M}[{}^i\text{Pr}_2\text{P}(\text{S})\text{NP}(\text{S}){}^i\text{Pr}_2]_2$ ($\text{M} = \text{Pd}, \text{Pt}$) square planar complexes where the $\text{MS}_2\text{P}_2\text{N}$ rings adopted pseudo boat conformations for $\text{Pd}[{}^i\text{Pr}_2\text{P}(\text{S})\text{NP}(\text{S}){}^i\text{Pr}_2]_2$ and chair type conformations for $\text{Pt}[{}^i\text{Pr}_2\text{P}(\text{S})\text{NP}(\text{S}){}^i\text{Pr}_2]_2$. In addition the unique $\{[{}^i\text{Pr}_2\text{P}(\text{S})\text{NP}(\text{S}){}^i\text{Pr}_2]\text{Pd}[{}^i\text{Pr}_2\text{P}(\text{S})\text{NHP}(\text{S}){}^i\text{Pr}_2]\}^+\text{Cl}^-$ complex was also studied crystallographically. Furthermore variable temperature ${}^{31}\text{P}$ NMR indicated a chair vs boat equilibrium for the $\text{Pt}[{}^i\text{Pr}_2\text{P}(\text{S})\text{NP}(\text{S}){}^i\text{Pr}_2]_2$ complex.

Analogous butyl substituted compounds were synthesised via an HBr elimination reaction between $\text{R}_2\text{P}(\text{S})\text{NH}_2$ and $\text{R}'_2\text{P}(\text{S})\text{Br}$ yielding the compounds $\text{R}_2\text{P}(\text{S})\text{NHP}(\text{S})\text{R}'_2$ ($\text{R} = {}^n\text{Bu}, {}^i\text{Bu}, {}^s\text{Bu}$; $\text{R}' = {}^n\text{Bu}, {}^i\text{Bu}, {}^s\text{Bu}$). Further crystallographic studies revealed ${}^n\text{Bu}_2\text{P}(\text{S})\text{NHP}(\text{S}){}^n\text{Bu}_2$ and ${}^s\text{Bu}_2\text{P}(\text{S})\text{NHP}(\text{S}){}^i\text{Bu}_2$ to be hydrogen bonded *transoid* dimers and ${}^i\text{Bu}_2\text{P}(\text{S})\text{NHP}(\text{S}){}^i\text{Bu}_2$ to be a *transoid* hydrogen bonded chain. These compounds were reacted with ZnCl_2 and PdCl_2COD yielding the coordination complexes $\text{M}[\text{R}_2\text{P}(\text{S})\text{NP}(\text{S})\text{R}'_2]_2$ ($\text{R} = {}^n\text{Bu}, {}^i\text{Bu}, {}^s\text{Bu}$; $\text{R}' = {}^n\text{Bu}, {}^i\text{Bu}, {}^s\text{Bu}$; $\text{M} = \text{Zn}, \text{Pd}$) and the compounds $\text{R}_2\text{P}(\text{S})\text{NHP}(\text{S})\text{R}_2$ ($\text{R} = {}^n\text{Bu}, {}^i\text{Bu}, {}^s\text{Bu}$) were reacted with PtCl_2COD yielding the coordination complexes $\text{Pt}[\text{R}_2\text{P}(\text{S})\text{NP}(\text{S})\text{R}_2]_2$ ($\text{R} = {}^n\text{Bu}, {}^i\text{Bu}, {}^s\text{Bu}$).

The compounds $(\text{EtO})_2\text{P}(\text{S})\text{NHP}(\text{S})\text{Ph}_2$, $(\text{EtO})_2\text{P}(\text{O})\text{NHP}(\text{S})\text{Ph}_2$ and $(\text{EtO})_2\text{P}(\text{S})\text{NHP}(\text{O})\text{Ph}_2$ were synthesised via an HCl elimination reaction between $\text{R}_2\text{P}(\text{S})\text{NH}_2$ and $\text{R}'_2\text{P}(\text{E})\text{Cl}$ ($\text{R} = \text{Ph}$, $\text{R}' = \text{OEt}$; $\text{R} = \text{OEt}$, $\text{R}' = \text{Ph}$; $\text{E} = \text{S} / \text{O}$). Crystallographic studies indicate the $(\text{EtO})_2\text{P}(\text{S})\text{NHP}(\text{S})\text{Ph}_2$ and $(\text{EtO})_2\text{P}(\text{O})\text{NHP}(\text{S})\text{Ph}_2$ compounds are hydrogen bonded dimers and

$(\text{EtO})_2\text{P}(\text{S})\text{NHP}(\text{O})\text{Ph}_2$ adopts the *cisoid* conformation in an hydrogen bonded chain. These compounds were reacted with ZnCl_2 and MCl_2COD ($\text{M} = \text{Pd}, \text{Pt}$) yielding the coordination complexes $\text{M}[(\text{EtO})_2\text{P}(\text{S})\text{NP}(\text{E})\text{Ph}_2]_2$ ($\text{M} = \text{Zn}, \text{Pd}, \text{Pt}; \text{E} = \text{S} / \text{O}$) and $\text{M}[(\text{EtO})_2\text{P}(\text{O})\text{NP}(\text{S})\text{Ph}_2]_2$ ($\text{M} = \text{Zn}, \text{Pd}, \text{Pt}$). Crystallographic studies of the tetrahedral $\text{Zn}[(\text{EtO})_2\text{P}(\text{O})\text{NP}(\text{S})\text{Ph}_2]_2$ complex displayed the effect of the oxygen donor atom on the $\text{ME}_2\text{P}_2\text{N}$ ($\text{E} = \text{S} / \text{O}$) ring geometry. Further crystallographic studies of the square planar complexes $\text{M}[(\text{EtO})_2\text{P}(\text{S})\text{NP}(\text{S})\text{Ph}_2]_2$ ($\text{M} = \text{Pd}, \text{Pt}$) revealed the $\text{MS}_2\text{P}_2\text{N}$ ring geometry for the Pd complex was pseudo boat in contrast to the analogous Pt complex which uniquely displayed one ligand of pseudo boat conformation and another of chair conformation. Variable temperature ^{31}P NMR indicates both conformers are present in solution at room temperature for the Pd and Pt complexes and one conformer is favoured at higher temperatures. Furthermore $\{\text{Pt}(\text{PMe}_3)_2[(\text{EtO})_2\text{P}(\text{S})\text{NP}(\text{S})\text{Ph}_2]\}^+ \text{BPh}_4^-$ was synthesised by reacting $(\text{EtO})_2\text{P}(\text{S})\text{NHP}(\text{S})\text{Ph}_2$ with $\text{Pt}(\text{PMe}_3)_2\text{Cl}_2$ revealing a complex ABCD type ^{31}P NMR spectrum. Crystallographic studies indicated the $\text{MS}_2\text{P}_2\text{N}$ ring geometry might be a hybrid of the pseudo boat and chair geometries.

Molecular modelling using MOPAC MNDO was in good agreement with the crystal structures of the non-coordinated compounds and the two zinc complexes, whilst poor agreement was observed for the ADF models of $\text{Pd}[\text{}^i\text{Pr}_2\text{P}(\text{S})\text{NP}(\text{S})\text{}^i\text{Pr}_2]_2$ and $\text{}^i\text{Bu}_2\text{P}(\text{S})\text{NHP}(\text{S})\text{}^i\text{Bu}_2$. In addition the molecular weights in solution of $\text{}^n\text{Bu}_2\text{P}(\text{S})\text{NHP}(\text{S})\text{}^n\text{Bu}_2$, $\text{}^i\text{Bu}_2\text{P}(\text{S})\text{NHP}(\text{S})\text{}^i\text{Bu}_2$ and $\text{}^s\text{Bu}_2\text{P}(\text{S})\text{NHP}(\text{S})\text{}^s\text{Bu}_2$ were studied in cyclohexane, $\text{}^s\text{Bu}_2\text{P}(\text{S})\text{NHP}(\text{S})\text{}^s\text{Bu}_2$ dissociating to a monomer in contrast to $\text{}^n\text{Bu}_2\text{P}(\text{S})\text{NHP}(\text{S})\text{}^n\text{Bu}_2$ and $\text{}^i\text{Bu}_2\text{P}(\text{S})\text{NHP}(\text{S})\text{}^i\text{Bu}_2$ which revealed degrees of dimerisation.

ACKNOWLEDGEMENTS

First and foremost I wish to thank my parents who have never doubted my choice of studies and have always given me unswerving support. I would also like to thank Siobhan for her continual belief in me and for her companionship and understanding. Next are my brothers and their respective partners to whom I am indebted for many games of golf, nice meals and encouragement throughout my academic career.

I have been fortunate to receive the attention of two excellent supervisors, Derek Woollins and Dom Cupertino, to whom I am grateful for their ideas and support (morally and financially). These three years have taught me a great deal, thank-you.

I am indebted to my old lab. mates Paul Kelly, Julian, Pravat, Stan and Eddie, who taught me the finer art of chemistry research (and kept me in one piece). Also at Imperial I would like to thank the guys in the Holland Club and those on the 5th floor, Alan, Melanie, Bill, John H., Reto, Talal and Dmitri but to name a few, I shall always have fond (if rather blurred) memories of our cultural visits to different areas of London. Also thanks to Andy, Alex, Rhys, Pete and Jason for fine golfing (I'll win one of these days) and rugby weekends. Thanks to Duncan and Charlie and all the other guys for the entertaining times we have had together, long may they continue.

Further thanks to members of the section at Loughborough, Betty, Andy, Tuan, Antonio, Steve, Rob, John H., Gabi, Martin and of course Mark. Also the organic chemists Chris, Simon and Liz, and physical chemists Simon (shandyman) and Duds.

Thanks also go to John Campbell and Mike Charlton (+ cake eaters) for their help and proofreading and making my visits to Zeneca enjoyable (I apologise for the odours).

For determining my crystal structures I am most grateful to fellow wurzel Alex Slawin, and also to David Williams of IC. For mass spectrometry thanks go to John Barton at Imperial and for microanalysis thanks go to Alex M. For solution NMR I would like to thank Dick Sheppard, Paul Hammerton (IC) and John Kershaw

(LUT) and solid state NMR Dave Apperley (Durham). Furthermore for the cryoscopy work and his tremendous hospitality I wish to thank Matt Davidson (Durham).

Finally thanks go to the EPSRC and Zeneca Specialties for their financial support.

INDEX

Title	p. 1
Certificate of Originality	p. 2
Dedication	p. 3
Abstract	p. 4
Acknowledgements	p. 6
Index	p. 8
List of Figures	p. 9
List of Tables	p. 12
Abbreviations	p. 15
General Experimental Conditions	p. 17
1 Introduction	p. 18
2 Tetraisopropyldithioimidodiphosphinate and its coordination chemistry	p. 38
3 Tetrabutylthioimidodiphosphinates and their coordination chemistry	p. 55
4 Diethoxy-diphenyl-dithioimidodiphosphinate, its mixed sulfur / oxygen analogues and their coordination chemistry	p. 77
5 Molecular modelling studies and an investigation into molecular weights in solution through cryoscopy	p. 104
Appendix - Crystal Structure Data	p. 125
References	p. 130

LIST OF FIGURES

- | | | |
|-------|--|-------|
| 1.1. | Structure of $\text{Ph}_2\text{P}(\text{S})\text{NHP}(\text{S})\text{Ph}_2$ <i>trans</i> dimer. | p. 21 |
| 1.2. | Resonance forms of $\text{Ph}_2\text{P}(\text{S})\text{NHP}(\text{S})\text{Ph}_2$. | p. 21 |
| 1.3. | Structure of $\text{Ph}_2\text{P}(\text{O})\text{NHP}(\text{O})\text{Ph}_2$ observed as its tautomer. | p. 22 |
| 1.4. | Structure of $\text{Me}_2\text{P}(\text{S})\text{NHP}(\text{S})\text{Me}_2$. | p. 22 |
| 1.5. | $\text{Na}_6\{\text{N}[(\text{PhO})_2\text{PS}]_2\}_6$ hexamer, phenoxy groups have been omitted for clarity. | p. 23 |
| 1.6. | Tetrahedral $\text{MS}_2\text{P}_2\text{N}$ ring conformation. | p. 25 |
| 1.7. | Square planar $\text{AS}_2\text{P}_2\text{N}$ (A = Se, Te, Au) ring conformations. | p. 26 |
| 1.8. | Differing $\text{MS}_2\text{P}_2\text{N}$ ring boat conformations for different geometries. | p. 26 |
| 1.9. | Octahedral $\text{Ph}_2\text{P}(\text{S})\text{NP}(\text{S})\text{Ph}_2^-$ complexes of tin and rhenium. | p. 27 |
| 1.10. | Structure of $\text{Cu}_4[\text{N}(\text{Ph}_2\text{PS})_2]_3$ with phenyls omitted for clarity. | p. 28 |
| 1.11. | Square based pyramidal structures of $\text{Ph}_2\text{P}(\text{E})\text{NP}(\text{E})\text{Ph}_2^-$ (E = S, O). | p. 28 |
| 1.12. | Octahedral tin complexes of $\text{Ph}_2\text{P}(\text{O})\text{NP}(\text{O})\text{Ph}_2^-$. | p. 29 |
| 1.13. | Structure of $\text{SnR}_2[\text{Ph}_2\text{P}(\text{S})\text{NP}(\text{O})\text{Ph}_2]_2$ for R = Me, Ph. | p. 30 |
| 1.14. | Coordination of mixed tetraphenoxy ligand. | p. 31 |
| 1.15. | Structures of $\text{Sn}[\text{N}(\text{Ph}_2\text{PE})_2]_2$ for E = Se, O. | p. 31 |
| 1.16. | Structure of tetrakis(tetraphenylimidodiphosphinato)di(3-phenylpropionato)dipraseodymium complex with phenyls on the ligands omitted for clarity. | p. 34 |
| 1.17 | Diagram of a metal extraction plant. | p. 36 |
| 1.18 | Schematic mixer / settler. | p. 37 |
| 2.1. | Crystal structure of ${}^i\text{Pr}_2\text{P}(\text{S})\text{NHP}(\text{S}){}^i\text{Pr}_2$. | p. 40 |
| 2.2. | Hydrogen-bonded chain of ${}^i\text{Pr}_2\text{P}(\text{S})\text{NHP}(\text{S}){}^i\text{Pr}_2$. | p. 41 |
| 2.3. | Crystal structures of $\text{M}[\text{}^i\text{Pr}_2\text{P}(\text{S})\text{NP}(\text{S}){}^i\text{Pr}_2]_2$ for M = Zn, Cd. | p. 43 |
| 2.4. | Crystal structures of $\text{M}[\text{}^i\text{Pr}_2\text{P}(\text{S})\text{NP}(\text{S}){}^i\text{Pr}_2]_2$ for M = Pd, Pt. | p. 46 |
| 2.5. | Crystal structure of $\{\text{Pd}[\text{L}][\text{HL}]\}^+$ for $\text{HL} = {}^i\text{Pr}_2\text{P}(\text{S})\text{NHP}(\text{S}){}^i\text{Pr}_2$. | p. 48 |
| 2.6. | Variable temperature NMR spectra of $\text{Pt}[\text{}^i\text{Pr}_2\text{P}(\text{S})\text{NP}(\text{S}){}^i\text{Pr}_2]_2$. | p. 50 |
| 3.1. | ${}^{31}\text{P}$ solid state NMR spectra of $\text{R}_2\text{P}(\text{S})\text{NHP}(\text{S})\text{R}_2$ for R = ${}^n\text{Bu}$, ${}^i\text{Bu}$ | p. 59 |

	and ^s Bu.	
3.2.	Crystal structure of ⁿ Bu ₂ P(S)NHP(S) ⁿ Bu ₂ dimer.	p. 61
3.3.	Crystal structure of ⁱ Bu ₂ P(S)NHP(S) ⁱ Bu ₂ .	p. 62
3.4.	Crystal structure of ^s Bu ₂ P(S)NHP(S) ⁱ Bu ₂ <i>trans</i> dimer.	p. 63
3.5.	³¹ P NMR AX type spectrum of Zn[ⁿ Bu ₂ P(S)NP(S) ⁱ Bu ₂] ₂ .	p. 66
4.1.	Crystal structure of (EtO) ₂ P(S)NHP(S)Ph ₂ dimer.	p. 79
4.2.	Crystal structure of (EtO) ₂ P(O)NHP(S)Ph ₂ dimer.	p. 80
4.3.	Crystal structure of (EtO) ₂ P(S)NHP(O)Ph ₂ .	p. 81
4.4.	Crystal structure of Zn[(EtO) ₂ P(O)NP(S)Ph ₂] ₂ .	p. 85
4.5.	Crystal structure of Pd[(EtO) ₂ P(S)NP(S)Ph ₂] ₂ .	p. 87
4.6.	Crystal structure of Pt[(EtO) ₂ P(S)NP(S)Ph ₂] ₂ .	p. 89
4.7.	Crystal structure of {Pt(PMe ₃) ₂ [(EtO) ₂ P(S)NP(S)Ph ₂]} ⁺ .	p. 91
4.8.	Phosphorus atoms labelled for {Pt(PMe ₃) ₂ [(EtO) ₂ P(S)NP(S)Ph ₂]} ⁺ .	p. 92
4.9.	³¹ P- ¹ H NMR spectrum of Pt(PMe ₃) ₂ [(EtO) ₂ P(S)NP(S)Ph ₂] ⁺ .	p. 93
4.10.	³¹ P- ¹ H VT NMR spectra of Pd[(EtO) ₂ P(S)NP(S)Ph ₂] ₂	p. 95
4.11.	Proposed structures of Pd[(EtO) ₂ P(O)NP(S)Ph ₂] ₂ .	p. 96
5.1.	Differing types of compound structure in the solid state.	p. 105
5.2.	Comparison of the MNDO modelled structure with the observed crystal structure of ⁱ Pr ₂ P(S)NHP(S) ⁱ Pr ₂ .	p. 106
5.3.	Comparison of the MNDO modelled structure with the observed crystal structure of ⁿ Bu ₂ P(S)NHP(S) ⁿ Bu ₂ .	p. 108
5.4.	Comparison of the MNDO modelled structure with the observed crystal structure of (EtO) ₂ P(S)NHP(S)Ph ₂ .	p. 110
5.5.	Comparison of the MNDO modelled structure with the observed crystal structure of ⁱ Bu ₂ P(S)NHP(S) ⁱ Bu ₂ .	p. 112
5.6.	Comparison of the MNDO modelled structure with the observed crystal structure of Zn[ⁱ Pr ₂ P(S)NP(S) ⁱ Pr ₂] ₂ .	p. 115
5.7.	Comparison of the MNDO modelled structure with the observed crystal structure of Zn[(EtO) ₂ P(O)NP(S)Ph ₂] ₂ .	p. 116
5.8.	Comparison of the ADF modelled structure with the observed crystal structure of Pd[ⁱ Pr ₂ P(S)NP(S) ⁱ Pr ₂] ₂ .	p. 118
5.9.	Plot of $\nu_{\text{solution}} - \nu_{\text{solid}}$ (x axis, cm ⁻¹) versus S ^{...} H (y axis, Å) for	p. 120

disulfur (S,S) and mixed sulfur / oxygen (S,O) compounds.

5.10. The cryoscopy apparatus.

p. 122

LIST OF TABLES

- | | | |
|------|---|-------|
| 1.1. | Coordination chemistry of imidodiphosphinates studied by infra-red ²²⁻²⁴ . | p. 24 |
| 1.2. | Summary of infra-red assignments for $R_2P(E)NHP(S)R_2$ ($R = Me, Ph; E = S, O$) and their metal complexes. | p. 25 |
| 1.3. | Bond lengths (\AA) and angles ($^\circ$) of $Bi[N(Ph_2PS)_2]_3$, $Fe[N(Ph_2PO)_2]_3$, $ReNCI[N(Ph_2PS)_2](PPh_3)$ and $VO[N(Ph_2PO)_2]_2$. | p. 29 |
| 1.4. | Bond lengths (\AA) and angles ($^\circ$) of $Me_2Sn[N(Ph_2PS)_2]_2$, ${}^nBu_2Sn[N(Ph_2PO)_2]_2$ and $Me_2Sn[Ph_2P(S)NP(O)Ph_2]_2$ with $E = S, O$. | p. 30 |
| 1.5. | Bond lengths (\AA) and angles ($^\circ$) of $Sn[N(Ph_2PE)_2]_2$ for $E = Se, O$. | p. 32 |
| 1.6. | A comparison of selected bond lengths (\AA) and angles ($^\circ$) for $Ph_2P(O)NHP(O)Ph_2$, $Mo(Cl)_2(O)_2[(OPPh_2)_2NH]$ and ${}^nBu_2Sn[(OPPh_2)_2N]_2$. | p. 32 |
| 2.1. | IR assignments for $M[{}^iPr_2P(S)NP(S){}^iPr_2]_2$ ($M = Zn, Cd, Ni, Co$ / cm^{-1}). | p. 41 |
| 2.2. | Selected bond lengths (\AA) and angles ($^\circ$) for ${}^iPr_2P(S)NHP(S){}^iPr_2$ and $M[{}^iPr_2P(S)NP(S){}^iPr_2]_2$ ($M = Zn, Cd, Ni$). | p. 42 |
| 2.3. | IR assignments for $M[{}^iPr_2P(S)NP(S){}^iPr_2]_2$ ($M = Pd, Pt$ / cm^{-1}). | p. 45 |
| 2.4. | Selected bond lengths (\AA) and angles ($^\circ$) for $M[{}^iPr_2P(S)NP(S){}^iPr_2]_2$ ($M = Zn, Pt, Pd$) and $\{Pd[L][HL]\}^+$ for $HL = {}^iPr_2P(S)NHP(S){}^iPr_2$. | p. 47 |
| 2.5. | Chemical shifts and [Pt-P] coupling for $Pt[{}^iPr_2P(S)NP(S){}^iPr_2]_2$ in CD_2Cl_2 at 233 K together with tentative assignments. | p. 49 |
| 3.1. | Chemical shifts and [P-P] coupling constants in ${}^{31}P$ NMR ($CDCl_3$) for tetrabutylthioimidodiphosphinate compounds. | p. 58 |
| 3.2. | ${}^{31}P$ solid state NMR for $R_2P(E)NHP(S)R_2$ ($R = {}^nBu, {}^iBu, {}^sBu$ and iPr). Chemical shifts and coupling constants. | p. 58 |
| 3.3. | Solid state (KBr disc) and solution (dichloromethane, CsI cell) FTIR of $R_2P(E)NHP(S)R_2$ ($R = {}^nBu, {}^iBu, {}^sBu, {}^iPr$ / cm^{-1}) and crystallographic S...H hydrogen bond lengths of $R_2P(E)NHP(S)R_2$ ($R = {}^nBu, {}^iBu, {}^iPr$) for comparison. | p. 60 |
| 3.4. | Selected bond lengths (\AA) and angles ($^\circ$) for $R_2P(E)NHP(S)R_2$ | p. 64 |

- (R = ⁿBu, ⁱBu), ^sBu₂P(S)NHP(S)ⁱBu₂ and Me₂P(S)NHP(S)Me₂ ²⁷.
- 3.5. Chemical shifts and coupling constants in ³¹P NMR (CDCl₃) for coordination complexes of R₂P(E)NHP(S)R'₂ (R = ⁿBu, ⁱBu, ^sBu; R' = ⁿBu, ⁱBu, ^sBu). p. 67
 - 3.6. FTIR assignments (cm⁻¹) for the coordination complexes of R₂P(E)NHP(S)R'₂ (R = ⁿBu, ⁱBu, ^sBu; R' = ⁿBu, ⁱBu, ^sBu). p. 68
 - 4.1. Chemical shifts and [P-P] coupling constants in ³¹P NMR (CDCl₃) for (EtO)₂P(E)NHP(S)Ph₂ (E = S/O) and (EtO)₂P(S)NHP(O)Ph₂. p. 78
 - 4.2. Selected bond lengths (Å) and angles (°) for (EtO)₂P(E)NHP(S)Ph₂ (E = S/O) and (EtO)₂P(S)NHP(O)Ph₂. p. 82
 - 4.3. FTIR assignments for Zn[(EtO)₂P(E)NHP(S)Ph₂]₂ (E = S/O) and Zn[(EtO)₂P(S)NHP(O)Ph₂]₂ (cm⁻¹). p. 83
 - 4.4. Chemical shifts and [P-P] coupling constants in ³¹P NMR (CDCl₃) for Zn[(EtO)₂P(E)NHP(S)Ph₂]₂ (E = S/O) and Zn[(EtO)₂P(S)NHP(O)Ph₂]₂. p. 83
 - 4.5. Chosen bond lengths (Å) and angles (°) for (EtO)₂P(O)NHP(S)Ph₂, Zn[(EtO)₂P(O)NHP(S)Ph₂]₂ and Zn[ⁱPr₂P(S)NP(S)ⁱPr₂]. p. 84
 - 4.6. Selected bond lengths (Å) and angles (°) for M[(EtO)₂P(S)NHP(S)Ph₂]₂ (M = Pd, Pt). p. 88
 - 4.7. Selected bond lengths (Å) and angles (°) for {Pt(PMe₃)₂[(EtO)₂P(S)NP(S)Ph₂]}⁺. p. 90
 - 4.8. ³¹P NMR data for {Pt(PMe₃)₂[(EtO)₂P(S)NP(S)Ph₂]}⁺BPh₄⁻. p. 92
 - 4.9. Chemical shifts and phosphorus-phosphorus coupling constants in ³¹P NMR (CDCl₃) for M[(EtO)₂P(E)NHP(S)Ph₂]₂ (M = Pd, Pt; E = S/O) and M[(EtO)₂P(S)NHP(O)Ph₂]₂ (M = Pd, Pt). p. 94
 - 4.10. Chemical shifts and phosphorus-phosphorus coupling constants in ³¹P VT NMR of Pd[(EtO)₂P(S)NP(S)Ph₂]₂. p. 96
 - 5.1. Comparing bond lengths (Å) and angles (°) of the crystal structures and MNDO modelled structures of ⁱPr₂P(S)NHP(S)ⁱPr₂ and (EtO)₂P(S)NHP(O)Ph₂. p. 105
 - 5.2. Comparing bond lengths (Å) and angles (°) of the crystal structures p. 107

- and MNDO modelled structures of ${}^n\text{Bu}_2\text{P}(\text{S})\text{NHP}(\text{S}){}^n\text{Bu}_2$ and ${}^s\text{Bu}_2\text{P}(\text{S})\text{NHP}(\text{S}){}^i\text{Bu}_2$.
- 5.3. Comparing bond lengths (Å) and angles (°) of the crystal structures p. 109 and MNDO modelled structures of $(\text{EtO})_2\text{P}(\text{S})\text{NHP}(\text{S})\text{Ph}_2$ and $(\text{EtO})_2\text{P}(\text{O})\text{NHP}(\text{S})\text{Ph}_2$.
 - 5.4. Heats of formation values for the modelled crystal (ΔH_{F1}) and p. 109 constrained (ΔH_{F2}) structures of the *trans* dimer type compounds (kcal / mol).
 - 5.5. Comparing bond lengths (Å) and angles (°) of the crystal structure p. 111 with the MNDO and the ADF modelled structures of ${}^i\text{Bu}_2\text{P}(\text{S})\text{NHP}(\text{S}){}^i\text{Bu}_2$.
 - 5.6. Monomer (ΔH_{FM}) and dimer (ΔH_{FD}) heats of formation for p. 113 *transoid* compounds (kcal / mol).
 - 5.7. Monomer (ΔH_{FM}) and dimer (ΔH_{FD}) heats of formation for p. 113 *transoid* compounds in solution in cyclohexane (kcal / mol).
 - 5.8. Comparing bond lengths (Å) and angles (°) of the crystal p. 114 structures and MNDO modelled structures of $\text{Zn}[{}^i\text{Pr}_2\text{P}(\text{S})\text{NP}(\text{S}){}^i\text{Pr}_2]_2$ and $\text{Zn}[(\text{EtO})_2\text{P}(\text{O})\text{NP}(\text{S})\text{Ph}_2]_2$.
 - 5.9. Comparing bond lengths (Å) and angles (°) of the crystal structure p. 117 and ADF modelled structure of $\text{Pd}[{}^i\text{Pr}_2\text{P}(\text{S})\text{NP}(\text{S}){}^i\text{Pr}_2]_2$.
 - 5.10. Comparison of the shifts in ν (NH) vibrations from solution and p. 119 solid state FTIR (cm^{-1}) with S...H hydrogen bond lengths in the crystal structures (Å).
 - 5.11. Cryoscopic results in benzene. p. 123
 - 5.12. Cryoscopic results in cyclohexane. p. 123

ABBREVIATIONS

Å	Angstrom Unit, 10^{-10} m
ADF	Amsterdam density function
ⁿ Bu	n-butyl, $-(\text{CH}_2)_3\text{CH}_3$
ⁱ Bu	i-butyl, $-\text{CH}_2\text{CH}(\text{CH}_3)(\text{CH}_3)$
^s Bu	s-butyl, $-\text{CH}(\text{CH}_2\text{CH}_3)(\text{CH}_3)$
^t Bu	t-butyl, $-\text{C}(\text{CH}_3)_3$
cm^{-1}	wavenumber
COD	cycloocta-1,5-diene, C_8H_{12}
COSMO	conductor-like screening of molecular orbitals
ΔH_{F1}	heat of formation of a MNDO modelled structure
ΔH_{F2}	heat of formation of a MNDO modelled structure with constraints
ΔH_{FD}	heat of formation of a MNDO modelled dimer structure
ΔH_{FM}	heat of formation of a MNDO modelled monomer structure
$\Delta H_{\text{FD}}'$	heat of formation of a MNDO modelled dimer structure in solution in cyclohexane
$\Delta H_{\text{FM}}'$	heat of formation of a MNDO modelled monomer structure in solution in cyclohexane
°	degrees
°C	degrees centigrade
DCM	dichloromethane, CH_2Cl_2
DMSO	dimethyl sulfoxide, $(\text{CH}_3)_2\text{SO}$
Et	ethyl, $-\text{C}_2\text{H}_5$
EtO	ethoxy, $-\text{OC}_2\text{H}_5$
Et_2O	diethyl ether
FAB +ve	fast atom bombardment (Cs^+ ions)
FT	Fourier transform (for NMR or IR)
Hz	Hertz
IR	infra-red
J	coupling constant, Hz

kcal mol ⁻¹	kilocalories per mole
K	Kelvin
Me	methyl, -CH ₃
MNDO	modified neglect of diatomic overlap
MOPAC	molecular orbital package
<i>m/z</i>	mass-to-charge ratio
NMR	nuclear magnetic resonance
Ph	phenyl, -C ₆ H ₅
ppm	parts per million
ⁱ Pr	i-propyl, -CH(CH ₃) ₂
THF	tetrahydrofuran, C ₄ H ₈ O

GENERAL EXPERIMENTAL CONDITIONS

Unless stated otherwise, all reactions were performed under an atmosphere of oxygen-free nitrogen using standard Schlenk procedures. All glassware was oven dried at 100 °C or flame dried under vacuum before use.

All solvents and reagents were purchased from Aldrich, BDH or Fisons and used as received. In addition toluene, THF, Et₂O and petroleum ether (60-80) were distilled from sodium-benzophenone under nitrogen, and CH₂Cl₂ from CaH₂. CDCl₃ (99+ atom % D), CD₂Cl₂ (99.6+ atom % D) and d₆-DMSO (99.5+ atom % D) were as supplied.

³¹P (36.2, 109.4, 101.25, 161.97 MHz) and ¹⁹⁵Pt solution NMR (53.6 MHz) were recorded on JEOL FX90Q, JEOL JNM EX270, BRUKER AC250 and BRUKER DPX400 FT spectrometers. ³¹P (121.4 MHz) and ¹⁵N solid state NMR (30.40 MHz) were recorded on a Varian Unity Plus FT spectrometer. Chemical shifts are reported relative to 85 % H₃PO₄ on the JEOL spectrometers and (MeO)₃P on the Bruker spectrometers for ³¹P and Na₂[PtCl₆] (aq) for ¹⁹⁵Pt solution NMR. For the solid state NMR, shifts are reported relative to 85 % H₃PO₄ (aq.) for ³¹P and the NO₃⁻ signal in solid NH₄NO₃ for ¹⁵N NMR. Infra-red spectra were recorded as KBr discs and dichloromethane solutions in CsI cells on a Perkin Elmer 1720X FT and a Perkin Elmer System 2000 FTIR spectrometer. Raman spectra were recorded on a Perkin Elmer 1700X FT spectrometer with a Systems Nd/YAG laser (1064 nm) and a Perkin Elmer System 2000 FT spectrometer with a diode pumped Nd/YAG laser. Microanalyses were carried out by the respective microanalytical services of Imperial College, Loughborough University and Zeneca Specialties Research Centre. FAB +ve mass spectra were recorded on a Vacuum Generators Autospec Q machine at Imperial College and by the EPSRC mass spectrometry service at Swansea and the mass spectrometry service at the Zeneca Specialties Research Centre.

I am grateful to Johnson Matthey PLC for the loan of platinum and palladium salts.

CHAPTER 1:

INTRODUCTION

1.1 *An Introduction to the Chemistry of Diphosphine Ligands.*

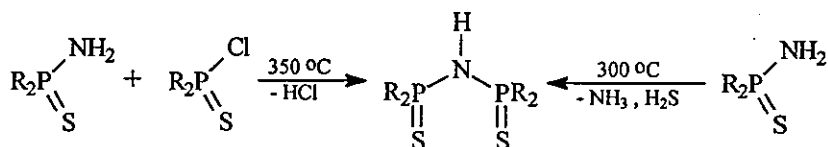
Throughout inorganic and organometallic chemistry few ligands have been as widely used as diphosphines¹⁻⁴. It is still perhaps true to say the most commonly used diphosphine to date has been bis(diphenylphosphino)ethane, $\text{Ph}_2\text{PCH}_2\text{CH}_2\text{PPh}_2$ (dppe), a molecule capable of forming five membered chelate rings. Over the last twenty years its homologue bis(diphenylphosphino)methane, $\text{Ph}_2\text{PCH}_2\text{PPh}_2$ (dppm), has become a popular ligand⁵⁻⁷. The versatility of dppm arises from its readiness to coordinate to metal centres through the lone pair of electrons at one or both of the phosphorus atoms. The oxidised compounds $\text{Ph}_2\text{PCH}_2\text{P(E)Ph}_2$ and $\text{Ph}_2\text{P(E)CH}_2\text{P(E)Ph}_2$ (E = chalcogen) prepared either by oxidation of dppm^{8,9} or from condensation of smaller fragments^{10,11} were found to be excellent ligands through the coordination *via* the lone pairs of E to the metal⁹⁻¹¹.

Compared with the great amount of work that has been carried out on diphosphines in which the phosphorus atoms are linked by a carbon atom or chain, far less has been done on ligands where the backbone of the molecule comprises a heteroatom, or in our particular area of interest, fully oxidised diphosphinoamines, $\text{R}_2\text{P(E)NHP(E)R}_2$ (E = S, Se, O). A review of work in this area has recently been published¹². Zeneca have great interest in this hitherto relatively undeveloped field of oxidised diphosphinoamines (particularly dithioimidodiphosphinates) for potential use as metal extraction reagents in a bid to find a more efficient, economical and environmentally friendly alternative to smelting for the metal mining industry.

1.2 *Synthetic Aspects.*

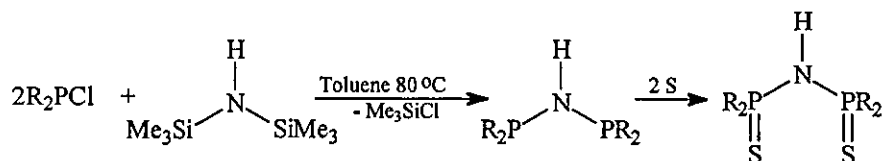
The first reported synthesis of a fully oxidised diphosphinoamine was that of tetraphenyldithioimidodiphosphinate¹³, $\text{Ph}_2\text{P(S)NHP(S)Ph}_2$ in 1966. Both this and its methyl analogue¹⁴, $\text{Me}_2\text{P(S)NHP(S)Me}_2$ were made via an HCl elimination reaction (Equation 1.1) between the dialkylaminothiophosphine and its corresponding

dialkylchlorothiophosphine. The reaction was performed as a melt, with temperatures up to 350 °C, and the product which crystallised on cooling was extracted into water



Eqn 1.1.

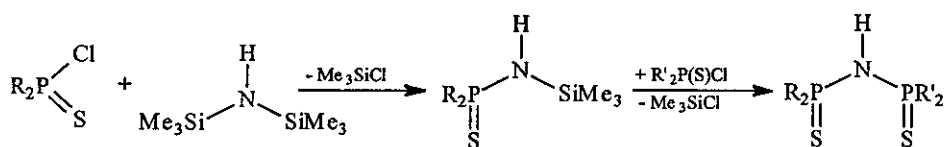
and precipitated out as a clean solid. A second method¹⁵ in a melt involved merely reacting $\text{Ph}_2\text{P}(\text{S})\text{NH}_2$ with itself at 300 °C (Equation 1.1) with by-products of ammonia and hydrogen sulfide. A further synthesis of $\text{Ph}_2\text{P}(\text{S})\text{NHP}(\text{S})\text{Ph}_2$ was reported (Equation 1.2) in the form of the condensation of hexamethyldisilazane with chlorodiphenylphosphine followed by the simple oxidation of the resulting



Eqn 1.2.

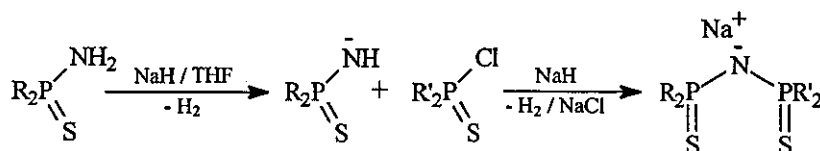
bis(diphenylphosphino)amine with sulfur¹⁶. The driving force of the condensation is the loss of trimethylsilyl chloride so the reaction needs to be carried out at a constant temperature of 80 °C. Conversion is clean and this synthesis produces far better yields (60 - 90 %). Furthermore by adding hydrogen peroxide instead of sulfur, the dioxygen species¹⁶ or the mono-oxygen species¹⁷ can be produced, and by adding selenium the diseleno¹⁸ species can be made, all in good yields.

In contrast hexamethyldisilazane can be used to produce ligands with mixed R-groups on the phosphorus centres by reacting it with one equivalent of $\text{R}_2\text{P}(\text{S})\text{Cl}$, then the product is further reacted with another equivalent of a different species¹⁹, $\text{R}'_2\text{P}(\text{S})\text{Cl}$ (Equation 1.3). Another route in which ligands with mixed R-groups may be made is a modified version of the HCl elimination reaction²⁰, carried out under



Eqn 1.3.

less extreme conditions in dimethylsulfoxide using potassium hydroxide as a base to help clip the two halves together resulting in reasonable yields (30 - 50 %). This synthetic route has subsequently been modified and improved²¹ by using a more aggressive base in sodium hydride (Equation 1.4) and changing the solvent to tetrahydrofuran giving better yields (50 - 90 %). In many respects the driving force of the step which clips the two halves together is the formation of the sodium salt of the



Eqn 1.4.

ligand. A further advantage of this synthesis is that the effervescence of the hydrogen being given off is an indication of how successfully the reaction is working. In addition, this route can be used to make mixed sulfur oxygen ligands as long as the halide rather than the amine contains the phosphine oxide. If an amine with a phosphorus-oxygen double bond is deprotonated with sodium hydride, the negative charge resides on the oxygen as opposed to the nitrogen.

1.3 Imidodiphosphinate Ligands.

The crystal structure of $\text{Ph}_2\text{P(S)NHP(S)Ph}_2$ has been reported on three separate occasions²²⁻²⁴. In each case the sulfur atoms in the structure were observed to be *trans* to one another. However only one of the papers reported hydrogen bonds between the

sulfur *cis* to the N-H proton and the N-H proton of another molecule²³, hence forming a *trans* dimer (Figure 1.1). In principle this compound may adopt a number of

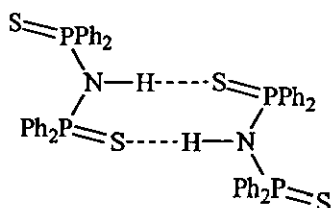


Figure 1.1. Structure of $\text{Ph}_2\text{P}(\text{S})\text{NHP}(\text{S})\text{Ph}_2$ *trans* dimer.

resonance forms. The proton bonded to the nitrogen is only 0.17 Å below the PNP plane indicating a tendency toward sp^2 hybridization of the nitrogen. The three possible resonance forms could then be I-III with I dominating (Figure 1.2). The positive charge on the nitrogen will increase the acidity of the hydrogen attached to it and enhance its ability to hydrogen bond. In addition the P-S bond of 1.950(1) Å for an hydrogen-bonded sulfur is greater than for the other sulfur {1.937(1) Å} indicating III is prevalent over II.

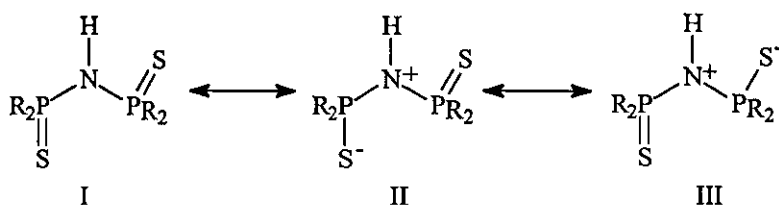


Figure 1.2. Resonance forms of $\text{Ph}_2\text{P}(\text{S})\text{NHP}(\text{S})\text{Ph}_2$.

In contrast to these resonance forms the structure of $\text{Ph}_2\text{P}(\text{O})\text{NHP}(\text{O})\text{Ph}_2$ ²² is very interesting as it is *trans* but it exists as the $\text{Ph}_2\text{P}(\text{O})\text{NP}(\text{OH})\text{Ph}_2$ tautomer in an H-bonding chain with $\text{OH}\cdots\text{O}$ bridging (Figure 1.3).

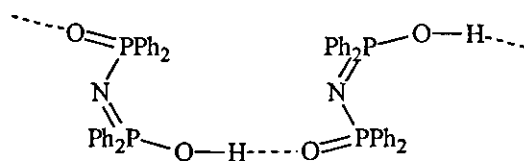


Figure 1.3. Structure of $\text{Ph}_2\text{P}(\text{O})\text{NHP}(\text{O})\text{Ph}_2$ observed as its tautomer.

However the related compound $(\text{PhO})_2\text{P}(\text{O})\text{NHP}(\text{O})(\text{OPh})_2$ exists as a *trans* dimer²⁵ isostructural with the compound in Figure 1.1, the hydrogen bonding observed *via* the N-H proton. Evidently the different electronic effects of the more electronegative phenoxy substituents on the phosphorus centres are responsible for this. Its disulfur analogue²⁶ predictably has the same structure though as would be expected the $\text{NH}\cdots\text{O}$ hydrogen bond is far stronger, demonstrated by the fact that $(\text{PhO})_2\text{P}(\text{O})\text{NHP}(\text{O})(\text{OPh})_2$ remains as a dimer when in solution in benzene whereas $(\text{PhO})_2\text{P}(\text{S})\text{NHP}(\text{S})(\text{OPh})_2$ is a monomer.

Phenyl and phenoxy substituted compounds comprise the majority of crystallographic data published on imidodiphosphinates until recently when the tetramethyl analogue $\text{Me}_2\text{P}(\text{S})\text{NHP}(\text{S})\text{Me}_2$ was reported²⁷. Again a *trans* conformation was observed, however instead of seeing a dimer, a hitherto unobserved hydrogen bonded ladder was found (Figure 1.4).

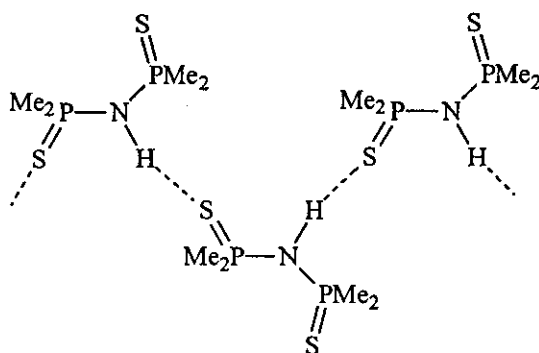


Figure 1.4. Structure of $\text{Me}_2\text{P}(\text{S})\text{NHP}(\text{S})\text{Me}_2$.

Salts of imidodiphosphate ligands have also yielded some interesting and unexpected structures. There are two reported structures^{28,29} for the potassium salt of $\text{Ph}_2\text{P}(\text{S})\text{NHP}(\text{S})\text{Ph}_2$, one with the cation in 18-crown-6 ether, $[\text{K}(\text{18-crown-6})]^+ [\text{Ph}_2\text{P}(\text{S})\text{NP}(\text{S})\text{Ph}_2]^-$ and $\text{K}^+ [\text{Ph}_2\text{P}(\text{S})\text{NP}(\text{S})\text{Ph}_2]^-$. In $[\text{K}(\text{18-crown-6})]^+$

$[\text{Ph}_2\text{P}(\text{S})\text{NP}(\text{S})\text{Ph}_2]^-$ the sulfur atoms are of *gauche* orientation which is in agreement with the structure of $[\text{K}^+[\text{Ph}_2\text{P}(\text{S})\text{NP}(\text{S})\text{Ph}_2]^-]$ which shows the sulfur atoms to be *gauche* also, with sulfur-potassium contacts around 3.20 Å. The two structures significantly differ in the crystal packing, $[\text{K}^+[\text{Ph}_2\text{P}(\text{S})\text{NP}(\text{S})\text{Ph}_2]^-]$ can be described as possessing an inorganic core which is a ladder structure comprised of K_2S_2 rings contained within the organic substituents (phenyl rings). In contrast a third salt, $(\text{Ph}_3\text{PNPPH}_3)^+[\text{Ph}_2\text{P}(\text{S})\text{NP}(\text{S})\text{Ph}_2]^-$ ³⁰ is very different. The PNP bond angle of the anion is $180.0(1)^\circ$ in comparison with the two above salts (PNP angle $128 - 33^\circ$), giving an *anti* orientation of the sulfurs. This may be due to the fact the anion is “free” and there are no interactions between the sulfurs and the cation.

Finally the most unexpected of all salt structures is the sodium salt of $(\text{PhO})_2\text{P}(\text{O})\text{NHP}(\text{O})(\text{OPh})_2$, which was observed to be a hexamer³¹ with a Na_6O_{12} core (Figure 1.5). The PNP angle is 132° and the orientation of the sulfurs are *gauche*.

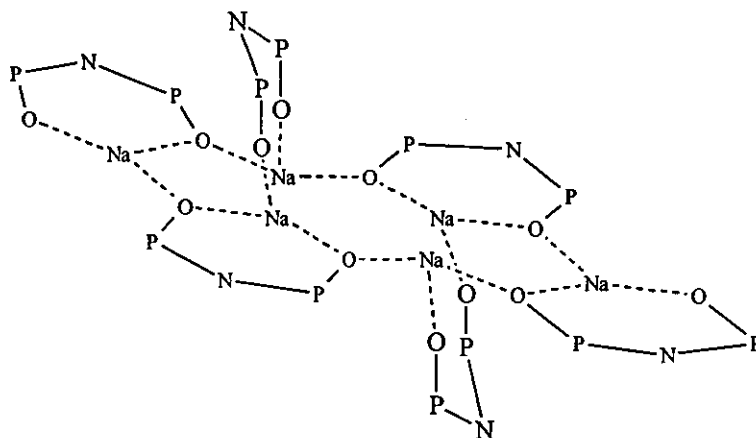
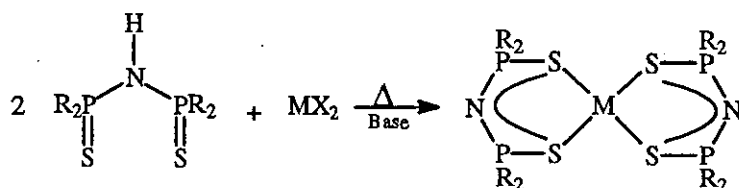


Figure 1.5. $\text{Na}_6\{\text{N}[(\text{PhO})_2\text{PS}]_2\}_6$ hexamer, phenoxy groups have been omitted for clarity.

1.4 Coordination Chemistry of Imidodiphosphinates.

The first substantial investigation into the coordination chemistry of imidodiphosphinates³² was reported in 1978 and the ligand studied was $\text{Ph}_2\text{P}(\text{S})\text{NHP}(\text{S})\text{Ph}_2$. The main forms of characterisation were elemental analyses and

infra-red spectroscopy. The typical preparation for all metal dithioimidodiphosphinate complexes involved refluxing the free ligand or its salt with a metal dihalide (Equation 1.5), though interestingly neutral complexes were produced in mild conditions. They could be converted to anionic complexes under reflux. Two further pieces of work^{33,34}



Eqn. 1.5.

were published studying infra-red analysis on complexes of $\text{Ph}_2\text{P}(\text{S})\text{NP}(\text{S})\text{Ph}_2^-$ (summary of work presented in Table 1.1). Of particular interest were copper complexes which in the presence of water underwent substitution of one sulfur for oxygen producing a mixed sulfur/oxygen species. This published data

Table 1.1. Coordination chemistry of imidodiphosphinates studied by infra-red

22-24

Ligand	Metal complex
$\text{Ph}_2\text{P}(\text{S})\text{NHP}(\text{S})\text{Ph}_2 = \text{HL}$	HLCox_2 (X=Cl,Br,I), $\text{HLCO}(\text{ClO}_4)_2$, HLZnCl_2 , HLCuBr , HLPdBr_2
$(\text{Ph}_2\text{PS})_2\text{N}^- = \text{L}$	CoL_2 , LHgCl , HgL_2 , CuL_2 , Cu_3L_3 , Cu_4L_3 , PdL_2 , PtL_2 , FeL_2
$[\text{Ph}_2\text{P}(\text{S})\text{NP}(\text{O})\text{Ph}_2]^- = \text{L}'$	CuL'_2 , NiL'_2
$(\text{Me}_2\text{PS})_2\text{N}^- = \text{L}''$	CoL''_2

formed the basis of infra-red assignments of complexes in this work (typical values characteristic of the neutral ligand and its complexed anion are presented in Table 1.2).

The bands indicative of the anion are PNP which increase by around 300 cm^{-1} due to the change in bond order as the negative charge is delocalised over the whole anion and the P-N bonds are significantly shortened. As expected there is also a difference for the PS vibration which decreases by 60 cm^{-1} again due to the

Table 1.2. Summary of infra-red assignments for $R_2P(E)NHP(S)R_2$ ($R = \text{Me}, \text{Ph}; E = \text{S}, \text{O}$) and their metal complexes (cm^{-1}).

	N-H	PNP	PS	PO	NPS
HL	3250, 1325	930, 900, 780	650, 620	1200	-
M^+L^-		1250 - 1190, 1160, 780	600, 560	1070	420

change in bond order where the P-S bond is lengthened through delocalisation.

These changes in bond length are highlighted by the tetrahedral $\text{Ni}[\text{N}(\text{Ph}_2\text{PS})_2]_2$ complex¹⁸ where P-N and P-S bonds are approximately 1.59 Å and 2.02 Å respectively, compared to $\text{Ph}_2\text{P}(\text{S})\text{NHP}(\text{S})\text{Ph}_2$ where the P-N and P-S bonds are approximately 1.70 Å and 1.92 Å respectively. The geometry of $\text{NiS}_2\text{P}_2\text{N}$ ring is puckered (or it could be seen as a distorted boat conformation, Figure 1.6) with no four adjacent atoms coplanar, isostructural to that published for the tetrahedral $\text{Mn}[\text{N}(\text{Ph}_2\text{PS})_2]_2$ complex³⁵. Three tetrahedral complexes of $\text{Me}_2\text{P}(\text{S})\text{NHP}(\text{S})\text{Me}_2$



Figure 1.6. Tetrahedral $\text{MS}_2\text{P}_2\text{N}$ ring conformation.

have also been reported^{27,36,37}, one of which is a nickel complex whose structure is compared to that of $\text{Ni}[\text{N}(\text{Ph}_2\text{PS})_2]_2$. There do not appear to be any significant differences between the structures which might be attributed to steric effects. The PNP angles are much the same ($127 - 130^\circ$) as are the NPS ($115 - 118^\circ$) and NiSP angles ($101 - 107^\circ$). The P-N and P-S bond lengths are also in good agreement, the only slight difference is in the Ni-S bonds, 2.27 - 2.30 Å for the tetramethyl complex compared to 2.29 - 2.32 Å for the tetraphenyl complex. It is possible the steric bulk of the phenyl groups involved prevent the bonds from being any shorter.

A far more interesting area of coordination chemistry is that of square planar complexes which exhibit some fascinating behaviour. The first reported were square

planar complexes of selenium³⁸ and tellurium³⁹ (Figure 1.7) with $\text{Ph}_2\text{P}(\text{S})\text{NHP}(\text{S})\text{Ph}_2$, the $\text{SeS}_2\text{P}_2\text{N}$ ring being a slightly distorted chair as opposed to the $\text{TeS}_2\text{P}_2\text{N}$ ring which is a near perfect chair conformation, in stark contrast to the puckered ring observed for the tetrahedral complexes. However a square planar

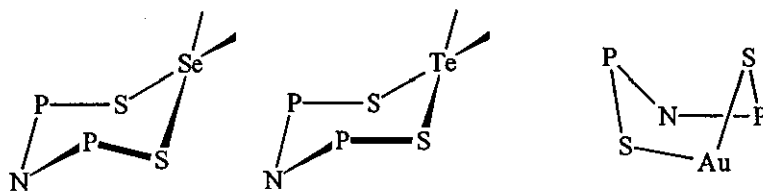


Figure 1.7. Square planar $\text{AS}_2\text{P}_2\text{N}$ (A = Se, Te, Au) ring conformations.

species was soon observed with a puckered ring conformation (distorted boat, $\text{Cl}_2\text{Au}[\text{N}(\text{Ph}_2\text{PS})_2]$ ⁴⁰, Figure 1.7 and $\text{Pd}[\text{N}((\text{PhO})_2\text{PS})_2]$ ²¹), similar to the $\text{MS}_2\text{P}_2\text{N}$ ring observed for tetrahedral complexes. This anomaly of seemingly unpredictable ring conformations was investigated through the syntheses and single crystal analyses of the $\{(\text{Me}_3\text{P})_2\text{Pt}[\text{N}(\text{Ph}_2\text{PS})_2]\}^+$ and $\{(\text{Me}_3\text{P})_2\text{Pt}[\text{N}((\text{PhO})_2\text{PS})_2]\}^+$ cationic complexes⁴¹. The tetraphenyl complex was observed to be distorted boat and the tetraphenoxy complex was chair conformation. There do not appear to be any steric factors which favour either geometry in this case so the difference in the electron-withdrawing ability of the substituent groups could be significant. It is also possible of course that the difference in conformations may simply be a result of crystal packing.

The $\text{MS}_2\text{P}_2\text{N}$ ring adopts the boat conformation for the tris octahedral complex⁴² $\text{Bi}[\text{N}(\text{Ph}_2\text{PS})_2]_3$, with the metal and the nitrogen at the highest points, in contrast to the distorted boat conformations observed for other geometries (Figure 1.8).

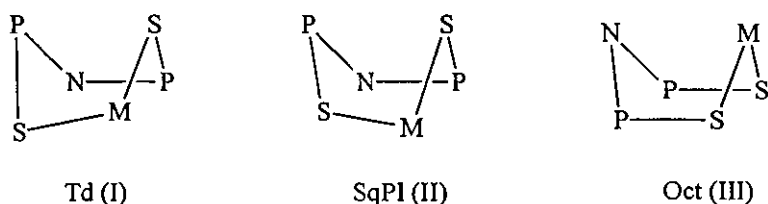


Figure 1.8. Differing $\text{MS}_2\text{P}_2\text{N}$ ring boat conformations for different geometries.

However in the dimethyltin octahedral complex ⁴³, $\text{Me}_2\text{Sn}[\text{N}(\text{Ph}_2\text{PS})_2]_2$ the ligands approximate to a square planar geometry so the form of boat conformation observed is equivalent to II, as is the case for the rhenium compounds ⁴⁴ $\text{ReOCl}_2[\text{N}(\text{Ph}_2\text{PS})_2] (\text{PPh}_3)$, $\text{ReO}(\text{OEt})[\text{N}(\text{Ph}_2\text{PS})_2]_2$ (Figure 1.9) and $\text{Mn}(\text{CO})_4[\text{N}(\text{Ph}_2\text{PS})_2]^{45}$ where II is also observed.

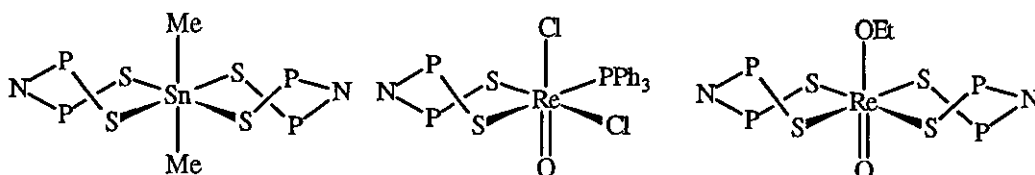


Figure 1.9. Octahedral $\text{Ph}_2\text{P}(\text{S})\text{NP}(\text{S})\text{Ph}_2^-$ complexes of tin and rhenium.

As expected there are differences in typical S-M-S bond angles within the $\text{MS}_2\text{P}_2\text{N}$ ring for I (110 - 113 °), II (96 - 100 °) and III (84 - 93 °), these give an interesting comparison to the chair conformation where the S-M-S angle is 86 - 88 °, more closely matching those angles found in a tris octahedral complex with near perfect chair $\text{MS}_2\text{P}_2\text{N}$ ring conformation than the square planar complex with distorted boat conformation. These different angles may produce differing ν (MS) bond vibrations in the infra-red ³². For typical tetrahedral complexes of $\text{Ph}_2\text{P}(\text{S})\text{NP}(\text{S})\text{Ph}_2^-$ values observed are 270 - 300 cm^{-1} . However for platinum and palladium complexes of $\text{Ph}_2\text{P}(\text{S})\text{NP}(\text{S})\text{Ph}_2^-$ there are values between 300 - 330 cm^{-1} tentatively assigned to ν (MS).

A further complex of $[\text{Ph}_2\text{P}(\text{S})\text{NP}(\text{S})\text{Ph}_2]^-$ with differing geometry is $\text{Cu}_4[\text{N}(\text{Ph}_2\text{PS})_2]_3$ ⁴⁶, a very unusual structure where each sulfur is bound to two copper atoms and the $\text{MS}_2\text{P}_2\text{N}$ ring adopts the chair conformation (Figure 1.10). The Cu-S bond lengths (2.25 - 2.30 Å) and P-N-P (135 - 143 °), M-S-P (102 - 103 °), S-P-N (117 - 119 °) bond angles are all in good agreement with other $\text{Ph}_2\text{P}(\text{S})\text{NP}(\text{S})\text{Ph}_2^-$ complexes. However the S-Cu-S angles within the $\text{MS}_2\text{P}_2\text{N}$ rings are 123 - 124 °, much larger than any S-M-S angle for a typical tetrahedral (110-113 °) or even square planar (91 - 101 °) complex.

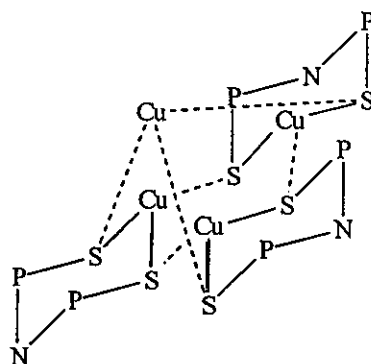


Figure 1.10. Structure of $\text{Cu}_4[\text{N}(\text{Ph}_2\text{PS})_2]_3$ with phenyls omitted for clarity.

Furthermore the square based pyramidal $\text{ReNCl}[\text{N}(\text{Ph}_2\text{PS})_2](\text{PPh}_3)$ complex⁴⁷ in which the $\text{MS}_2\text{P}_2\text{N}$ ring adopts conformation II (Figure 1.8), in contrast to its dioxygen analogue $\text{VO}[\text{N}(\text{Ph}_2\text{PO})_2]_2$ ⁴⁸ (Figure 1.11) where the ring is nearly planar. As expected the V-O (1.98 - 1.99 Å) and P-O (1.52 - 1.53 Å) bond lengths are significantly shorter than Re-S (2.38 - 2.45 Å) and P-S (2.02 - 2.06 Å) distances (Table 1.3). The P-N-P (124 °) and the O-V-O (88 - 89 °) bond angles are smaller than those for the rhenium complex, P-N-P (126 °) and S-Re-S (96 °). The greatest difference is found in the V-O-P angle (135 - 137 °) *versus* Re-S-P (105 - 113 °) or indeed any M-S-P angle (97 - 115 °). This is probably due to the near planarity of the

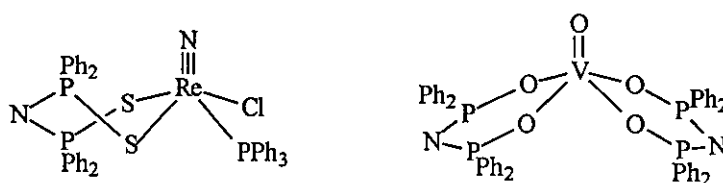


Figure 1.11. Square based pyramidal structures of $\text{Ph}_2\text{P}(\text{E})\text{NP}(\text{E})\text{Ph}_2^-$ (E = S, O).

$\text{MO}_2\text{P}_2\text{N}$ ring through the presence of oxygen instead of sulfur as the donor atom. The O-P-N (115 - 117 °) and S-P-N (117 - 118 °) angles are in good agreement.

Further comparison can be made with $\text{Fe}[\text{N}(\text{Ph}_2\text{PO})_2]_3$ ⁴⁹, the octahedral dioxygen analogue of $\text{Bi}[\text{N}(\text{Ph}_2\text{PS})_2]_3$. Again the main differences are the Fe-O (1.99 - 2.04 Å) and P-O (1.50 - 1.52 Å) bond distances are notably shorter than the Bi-S (2.73

- 2.85 Å) and P-S (2.00 - 2.03 Å) distances, and the Fe-O-P bond angle of 128 - 132 ° is far greater than the 99 - 107 ° found for Bi-S-P. The difference in angles between

Table 1.3. Bond lengths (Å) and angles (°) of Bi[N(Ph₂PS)₂]₃, Fe[N(Ph₂PO)₂]₃, ReNCI[N(Ph₂PS)₂](PPh₃) and VO[N(Ph₂PO)₂]₂.

E = S, O	Bi[N(Ph ₂ PS) ₂] ₃	Fe[N(Ph ₂ PO) ₂] ₃	Re[N(Ph ₂ PS) ₂] NCI(PPh ₃)	VO[N(Ph ₂ PO) ₂] ₂
M-E	2.73 - 2.85	1.99 - 2.04	2.38 - 2.45	1.98 - 1.99
P-E	2.00 - 2.03	1.50 - 1.52	2.02 - 2.06	1.52 - 1.53
P-N	1.59 - 1.60	1.57 - 1.60	1.57 - 1.60	1.59
E-M-E	84 - 93	89 - 90	96	88 - 89
M-E-P	99 - 107	128 - 132	105 - 113	135 - 137
E-P-N	117 - 120	116 - 117	117 - 118	115 - 117
P-N-P	133 - 137	124 - 126	126	124

Fe-O-P and V-O-P is probably due to the greater steric strain in the octahedral complex preventing the MO₂P₂N ring from being so near to planar. Further octahedral structures Sn(I₂)[N(Ph₂PO)₂]₂⁵⁰ and Sn(ⁿBu)₂[N(Ph₂PO)₂]₂⁵¹ (Figure 1.12) contain equatorial MO₂P₂N rings which compare well with Fe[N(Ph₂PO)₂]₃. It is interesting to note the ⁿBu groups occupy the two axial positions of the octahedron in Sn(ⁿBu)₂[N(Ph₂PO)₂]₂ as opposed to Sn(I₂)[N(Ph₂PO)₂]₂ where the iodines occupy both an axial and equatorial position. The MO₂P₂N ring with oxygens occupying both equatorial and axial positions also shows good agreement with other values except for the P-N-P angle (123 °) in contrast to values in Table 1.3 and the P-N-P angle (130 °) for the axial ring.

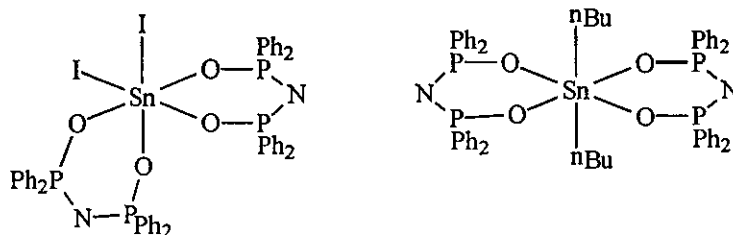


Figure 1.12. Octahedral tin complexes of Ph₂P(O)NP(O)Ph₂.

Further comparison can be made with the octahedral tin complexes of the mixed chalcogen ligand⁵², $\text{Ph}_2\text{P}(\text{S})\text{NP}(\text{O})\text{Ph}_2^-$ (Figure 1.13). When one oxygen is replaced by a sulfur the planarity of the $\text{ME}_2\text{P}_2\text{N}$ ring ($\text{E} = \text{S}, \text{O}$) is lost and a boat

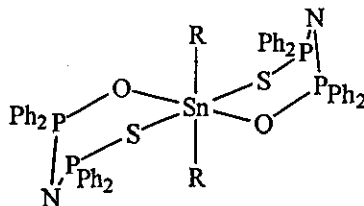


Figure 1.13. Structure of $\text{SnR}_2[\text{Ph}_2\text{P}(\text{S})\text{NP}(\text{O})\text{Ph}_2]_2$ for $\text{R} = \text{Me}, \text{Ph}$.

conformation is observed. The bond lengths and angles are in good agreement (Table 1.4). It is interesting to note the isomer in which the sulfur and oxygen are *trans* to one another is preferred. This may be explained by the fact that the M-S and P-S bonds are generally 0.5 Å longer than M-O and P-O bonds, and the Sn-O-P angle is almost 30° greater than the Sn-S-P angle. The *trans* geometry probably reduces steric hinderance and any ring strain.

Table 1.4. Bond lengths (Å) and angles (°) of $\text{Me}_2\text{Sn}[\text{N}(\text{Ph}_2\text{PS})_2]_2$,

${}^n\text{Bu}_2\text{Sn}[\text{N}(\text{Ph}_2\text{PO})_2]_2$ and $\text{Me}_2\text{Sn}[\text{Ph}_2\text{P}(\text{S})\text{NP}(\text{O})\text{Ph}_2]_2$ with $\text{E} = \text{S}, \text{O}$.

	$\text{Me}_2\text{Sn}[\text{N}(\text{Ph}_2\text{PS})_2]_2$	${}^n\text{Bu}_2\text{Sn}[\text{N}(\text{Ph}_2\text{PO})_2]_2$	$\text{Me}_2\text{Sn}[\text{Ph}_2\text{P}(\text{S})\text{NP}(\text{O})\text{Ph}_2]_2$
Sn-S	2.73 - 2.74	-	2.76
Sn-O	-	2.20	2.20
P-S	2.10 - 2.02	-	2.02
P-O	-	1.52 - 1.53	1.52
P-N	1.58	1.58 - 1.60	1.58 - 1.60
E-Sn-E	98	89	91
Sn-S-P	106	-	105
Sn-O-P	-	103 - 131	132
S-P-N	119	-	118
O-P-N	-	118	116
P-N-P	136	130	132

The palladium complex of the mixed sulfur/oxygen tetraphenoxy compound⁵³ (Figure 1.14) is of significant interest. With the strong electron withdrawing effect of the phenoxy groups, the phosphoryl groups become too “hard” to coordinate to the metal, instead four membered PdSPN rings are observed.

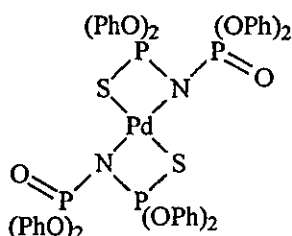


Figure 1.14. Coordination of mixed tetraphenoxy ligand.

When the $\text{Ph}_2\text{P}(\text{O})\text{NP}(\text{O})\text{Ph}_2^-$ ligand is reacted with tin (II) acetate⁵⁰ the resulting structure is a trigonal bipyramid (Figure 1.15) which is distorting towards a square pyramid, with all angles at the tin reduced by a lone pair effect. The selenium

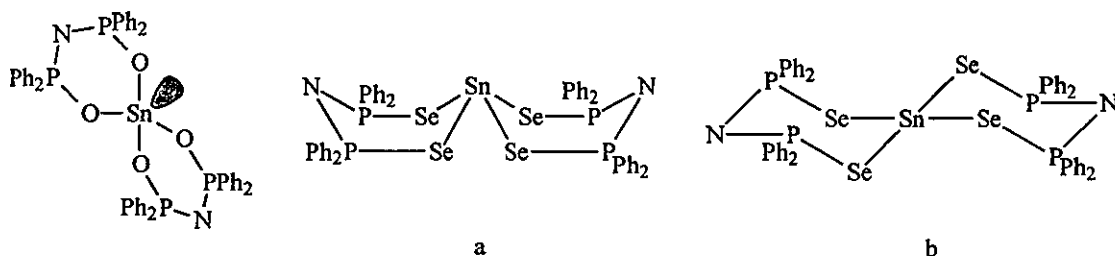


Figure 1.15. Structures of $\text{Sn}[\text{N}(\text{Ph}_2\text{PE})_2]_2$ for $\text{E} = \text{Se}, \text{O}$.

analogue⁵⁴ exists in two forms, a distorted square (tetragonal) pyramid with the $\text{MSe}_2\text{P}_2\text{N}$ ring adopting the boat conformation ($\{a\}$, red crystals), and a square planar complex with the the $\text{MSe}_2\text{P}_2\text{N}$ ring adopting the chair conformation ($\{b\}$, yellow crystals). The two isomers crystallised from the same yellow chloroform/hexane solution of $\text{Sn}[\text{N}(\text{Ph}_2\text{PSe})_2]_2$, suggesting the difference in energy between the two conformers is very little. Selected bond lengths and angles (Table 1.5) reveal again the large difference in Sn-E-P angles, again the $\text{MO}_2\text{P}_2\text{N}$ ring is far more planar. Furthermore the P-N-P angles for the diseleno compounds (129° , 136°) are respectively less and greater than those of the neutral ligand.

Table 1.5. Bond lengths (Å) and angles (°) of $\text{Sn}[\text{N}(\text{Ph}_2\text{PE})_2]_2$ for E = Se, O.

E = O, Se	$\text{Sn}[\text{N}(\text{Ph}_2\text{PO})_2]_2$	a $\text{Sn}[\text{N}(\text{Ph}_2\text{PSe})_2]_2$	b $\text{Sn}[\text{N}(\text{Ph}_2\text{PSe})_2]_2$
Sn-E	2.13 - 2.38	2.80 - 2.94	2.64 - 2.66
P-E	1.51 - 1.53	2.16 - 2.19	2.17 - 2.18
E-Sn-E	86	89	88
Sn-E-P	127 - 134	-	97
P-N-P	125 - 128	129	136

A further dioxygen complex of particular interest is $\text{MoCl}_2(\text{O})_2[\text{HN}(\text{Ph}_2\text{PO})_2]$, the only reported structure of a protonated ligand complex⁵⁵. The structural data made for an interesting comparison with the fully deprotonated octahedral complex⁵¹ and the free neutral ligand²² (Table 1.6). In the free neutral ligand the proton is in exchange between the two oxygens rather than being bound to the nitrogen, thus the P-O bond lengths are equal (1.52 Å) compared to $\text{Ph}_2\text{P}(\text{S})\text{NHP}(\text{S})\text{Ph}_2$ where the P-S bond lengths are different as one sulfur is pendant and the other is involved in hydrogen bonding. This may explain why, although bound to a molybdenum atom, the P-O bond lengths are so similar for the free neutral ligand and the protonated ligand complex. However it is somewhat surprising that the M-O bonds (2.20 Å) are

Table 1.6. A comparison of selected bond lengths (Å) and angles (°) for $\text{Ph}_2\text{P}(\text{O})\text{NHP}(\text{O})\text{Ph}_2$, $\text{Mo}(\text{Cl})_2(\text{O})_2[(\text{OP Ph}_2)_2\text{NH}]$ and ${}^n\text{Bu}_2\text{Sn}[(\text{OPPh}_2)_2\text{N}]_2$.

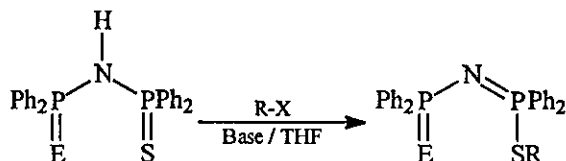
	$\text{Ph}_2\text{P}(\text{OH})\text{NP}(\text{O})\text{Ph}_2$	$\text{Mo}(\text{Cl})_2(\text{O})_2[(\text{OP Ph}_2)_2\text{NH}]$	${}^n\text{Bu}_2\text{Sn}[(\text{OPPh}_2)_2\text{N}]_2$
P-O	1.52	1.50	1.52 - 1.53
P-N	1.54	1.66	1.58 - 1.60
M-O	-	2.20 - 2.21	2.20
O-P-N	117	110 - 111	118
P-N-P	180	123	130
M-O-P	-	139 - 141	103 - 131
O-M-O	-	78	89

also equal. The P-N bonds for the molybdenum complex are considerably longer at 1.66 Å than in both other structures, probably due to the fact that they are truly single bonds as opposed to the free neutral ligand where the exchange of the proton between

the two oxygens increases the P-N bond order, and the tin complex where deprotonation of the ligand produces a change in bond order due to the delocalisation of the negative charge over the ligand. There is a degree of distortion in the molybdenum octahedron as the O-M-O angle (78°) falls well short of the right angle observed for the tin complex. However the M-O-P angles are significantly greater (140°) than those for the tin compound ($103 - 131^\circ$) ensuring the planarity of the MO_2P_2N ring. In contrast the O-P-N angle (110°) is 7° less than both the free ligand and the anionic complex. Finally its P-N-P angle (123°) again is smaller by 7° than the octahedral complex, but cannot be compared with the neutral ligand which has a linear P-N-P backbone.

1.5 Uses of Imidodiphosphinates.

Compounds tested of the general formula $Ph_2P(E)NP(SR)Ph_2$ (for E = S, O; R = alkyl; Equation 1.6) were unsuccessful as fungicides⁵⁶. The tetraphenyl dioxygen complex



Eqn. 1.6

tris(tetraphenylimidodiphosphinato) praseodymium⁵⁷ was considered to possibly be a new method for determining the enantiomeric purity of carboxylic acids by reacting it with salts of carboxylic acids to give dinuclear dicarboxylato complexes (Figure 1.16).

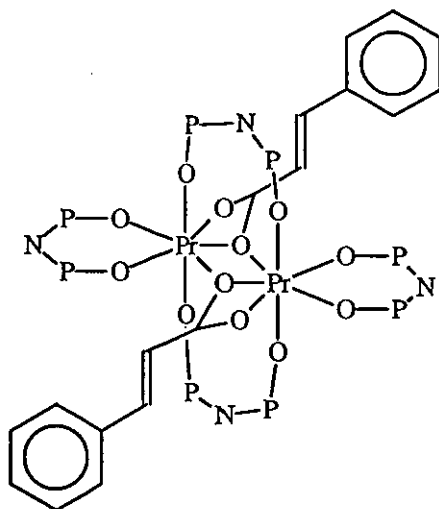


Figure 1.16. Structure of tetrakis(tetraphenylimidodiphosphinato)di(3-phenylpropionato)dipraseodymium complex with phenyls on the ligands omitted for clarity.

The ability of the ligands $\text{Ph}_2\text{P}(\text{S})\text{NHP}(\text{S})\text{Ph}_2$, $\text{Ph}_2\text{P}(\text{S})\text{NHP}(\text{O})\text{Ph}_2$ and $\text{Ph}_2\text{P}(\text{O})\text{NHP}(\text{O})\text{Ph}_2$ to extract the metals Ag, Au, Hg, Yb, Hf, Pd and Sc, and their stability to gamma radiation has been reported⁵⁸. All the ligands and their complexes underwent decomposition when exposed to gamma radiation.

Aqueous acidified solutions of salts of the metals were stirred with benzene solutions of the above ligands. $\text{Ph}_2\text{P}(\text{S})\text{NHP}(\text{S})\text{Ph}_2$ was more selective than $\text{Ph}_2\text{P}(\text{S})\text{NHP}(\text{O})\text{Ph}_2$, which again was more selective than the dioxygen ligand, in fact Sc and other rare earth metal extraction was suppressed and the uptake of Ag and Hg was better for $\text{Ph}_2\text{P}(\text{S})\text{NHP}(\text{S})\text{Ph}_2$. The best ligand for Sc extraction was $\text{Ph}_2\text{P}(\text{O})\text{NHP}(\text{O})\text{Ph}_2$. Starting concentration of the ligand solutions of $\text{Ph}_2\text{P}(\text{S})\text{NHP}(\text{S})\text{Ph}_2$ and $\text{Ph}_2\text{P}(\text{S})\text{NHP}(\text{O})\text{Ph}_2$ were found to affect the efficiency of extraction, whereas $\text{Ph}_2\text{P}(\text{O})\text{NHP}(\text{O})\text{Ph}_2$ remained reasonably constant. Evidently scandium prefers hard donor atoms in the oxygens to the soft sulfurs. However there is possibly a more subtle factor that may contribute to the reduced efficiency at higher concentration. Considering the main structural difference in the solid state between the ligands is the acidic proton sits on one of the oxygens instead of the nitrogen for $\text{Ph}_2\text{P}(\text{OH})\text{NP}(\text{O})\text{Ph}_2$, and the ligand does not exist as a *trans* dimer but as an hydrogen bonded chain, in contrast to the other ligands which are *trans* dimers. It is likely that

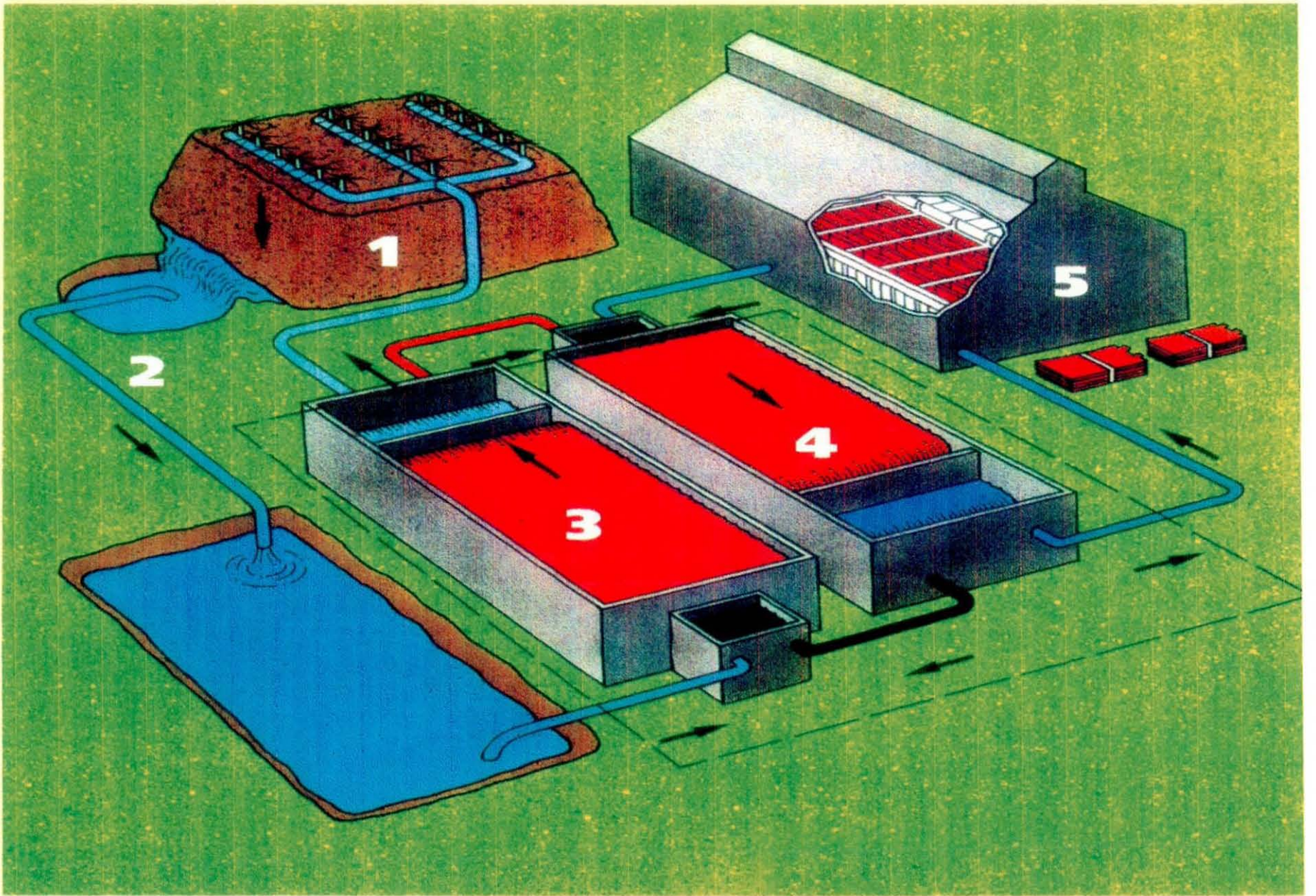
in a reasonably non-polar solvent such as benzene at increasing concentrations the compounds $\text{Ph}_2\text{P}(\text{S})\text{NHP}(\text{S})\text{Ph}_2$ and $\text{Ph}_2\text{P}(\text{S})\text{NHP}(\text{O})\text{Ph}_2$ may form *trans* dimers in solution, thus reducing their ability to coordinate to a metal.

1.6. *Metal Extraction Technology.*

As a result of the research at Zeneca into metal extraction technology, the technique that was developed for copper is now tried and tested and very efficient. There are five principal stages (Figure 1.17).

1. The metal ore is taken straight from the mine and fashioned into a heap.
2. The heap of ore is leached with aqueous acid producing a solution containing a mixture of metal ions.
3. The acidic solution is combined with an organic solution of the extractant reagent and stirred (Figure 1.18). The two phases are subsequently separated, the aqueous phase with some or all of the desired metal ions removed and returned to the heap to leach more metal.
4. The organic phase containing solely the desired metal in the form of a complex with the extraction reagent is combined with more aqueous acid to strip the metal back into the aqueous acidic phase. The organic phase containing the extraction reagent is then returned to stage 3.
5. The aqueous solution of pure metal ions is piped into electrolytic cells and pure metal is collected at the cathode. The remaining acid is then returned to stage 4.

At every stage there is no waste as the reagents involved are recycled making this method of metal extraction far more environmentally friendly than smelting.



Recovery of copper by solvent extraction

Figure 1.17. Diagram of a metal extraction plant.

SCHMATIC MIXER/SETTLER

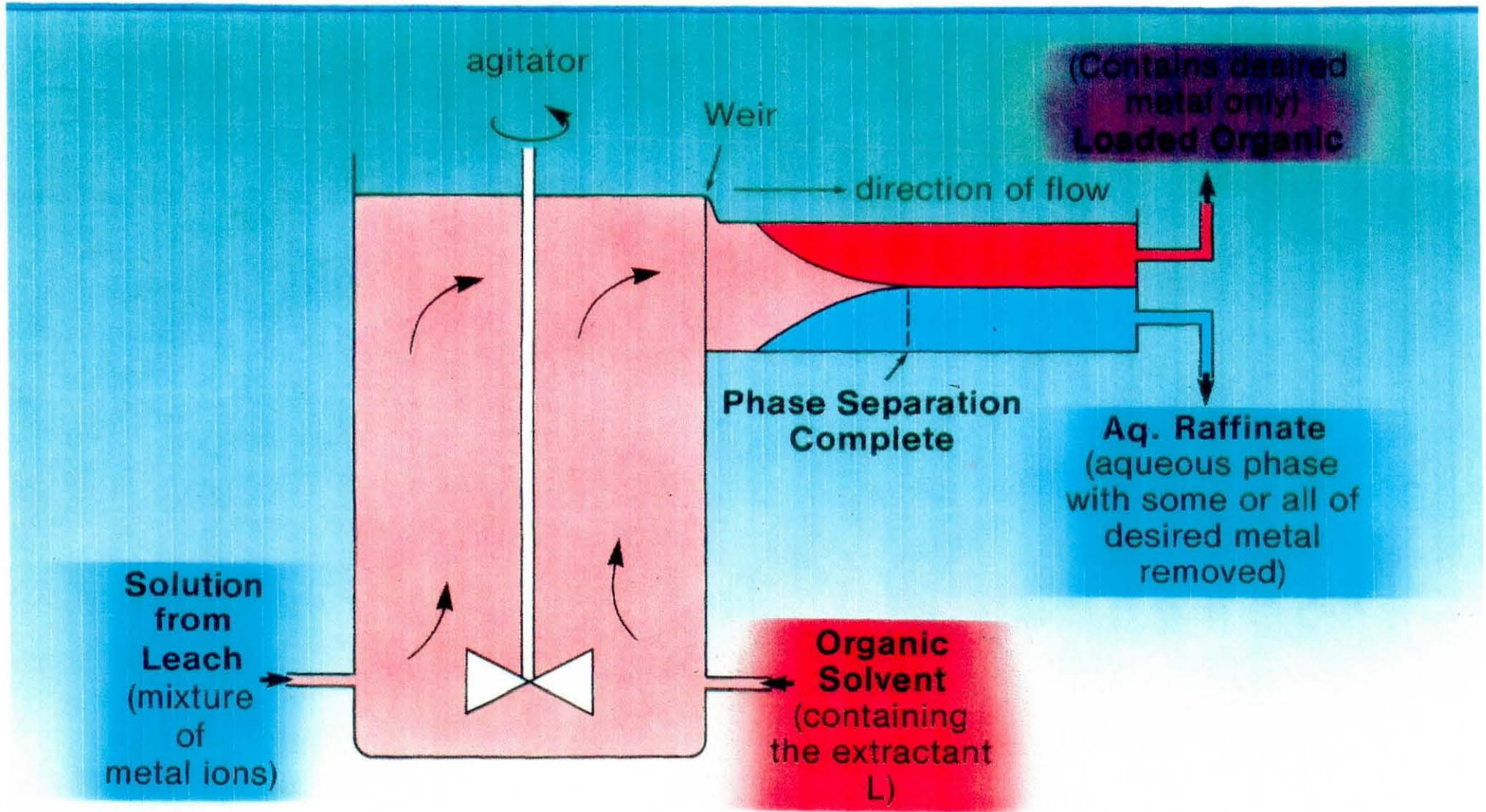


Figure 1.18. Schematic mixer/settler.

CHAPTER 2:
TETRAISOPROPYLDITHIOIMIDODIPHOSPHINATE
AND ITS COORDINATION CHEMISTRY

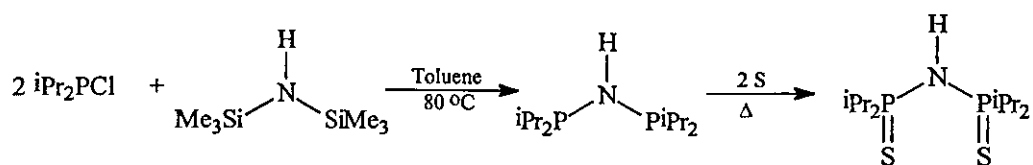
2.1 Introduction

There have been several studies^{18,32-35,38-40} into the coordination chemistry of $\text{Ph}_2\text{P}(\text{S})\text{NHP}(\text{S})\text{Ph}_2$ since this type of ligand is readily prepared and provides an inorganic analogue of β -diketonates. There is rather less work on alkyl analogues of $\text{R}_2\text{P}(\text{S})\text{NHP}(\text{S})\text{R}_2$ although some studies on $\text{Me}_2\text{P}(\text{S})\text{NHP}(\text{S})\text{Me}_2$ and its complexes have been reported^{27,36,37}. In addition the remarkable conformational differences that have been observed for $\text{MS}_2\text{P}_2\text{N}$ rings^{38-40,42,43} have therefore prompted us to investigate the synthesis and coordination chemistry of ${}^i\text{Pr}_2\text{P}(\text{S})\text{NHP}(\text{S}){}^i\text{Pr}_2$ (**1**). Structurally **1** adopts a uniquely *gauche* arrangement of sulfur atoms in contrast to those reported for the phenyl^{5,21,22} and methyl¹⁵ analogues both of which have *anti* conformations of the sulfur atoms. In addition the platinum and palladium complexes reveal contrasting square planar structures where the six membered $\text{MS}_2\text{P}_2\text{N}$ ring adopts “*chair*” and distorted “*boat*” conformations. Indeed fluxional behaviour was observed for the platinum complex and was investigated by variable temperature NMR. Where possible products were characterised by NMR, FTIR, FT Raman, FAB⁺ mass spectroscopy, microanalyses and X-ray crystallography.

RESULTS AND DISCUSSION

2.2 Ligand Synthesis.

The synthesis of **1** was based on a literature preparation of related compounds¹⁶ involving the reaction of diisopropylchlorophosphine with hexamethyldisilazane, followed by oxidation with sulfur (Equation 2.1). **1** precipitated analytically pure upon cooling of the toluene solution and crystals were grown from the diffusion of hexane into a dichloromethane solution of **1**.



Eqn. 2.1.

A signal was observed in the solution ^{31}P NMR (CDCl_3) at 91.2 ppm, contrasting with the solid state ^{31}P NMR where a doublet was observed (91.0, 89.2 ppm, $^2J(^{31}\text{P}-^{31}\text{P})$ 213.6 Hz) indicating two different phosphorus environments were present. However ^{15}N solid state NMR gave one peak at -322.0 ppm indicating only one conformation of **1** exists in the solid state. It is likely the two different phosphorus environments are caused by the hydrogen bonding array observed in the crystal structure, where one phosphorus is pendant and the other is bound to the sulfur involved in the hydrogen bonding. This data is supported by FTIR, the ν (N-H) vibration in the solution (3320 cm^{-1}) and solid state (3243 cm^{-1}) of **1** indicates a significant decrease in hydrogen bonding in solution. Other characteristic bands found in the FTIR, were ν (PNP) 936, 906, 776 and ν (PS) 646 cm^{-1} . FAB +ve mass spectra revealed the expected parent ion (314 m/z) and a dimer ion (627 m/z).

1 has a *gauche* arrangement (Figure 2.1) of the sulfur atoms with the S-P...P-S ‘torsion angle’ being 79° ; P(1)-S(1) and P(2)-S(2) are rotated by 36° and 43° (in opposite directions) with respect to the P-N-P plane. The geometries about each phosphorus centre are essentially the same; there are noticeable distortions from tetrahedral with a slight enlargement of the S-P-C angle and a marked asymmetry in the N-P-(S/ ^iPr) angles with the N-P-C angles being contracted and the N-P-S angles being enlarged from ideal tetrahedral. The angle at nitrogen [$131.6(1)^\circ$] is enlarged somewhat from trigonal but comparable to that observed in the methyl and phenyl analogues. The P-N bond lengths are equivalent and similar to those reported for related systems. The molecules in **1** pack (Figure 2.2) to form H-bonded chains that extend in the crystallographic *a* direction [S(2)...N 3.57, S(2)...H 2.60 Å, S...H-N 170°].

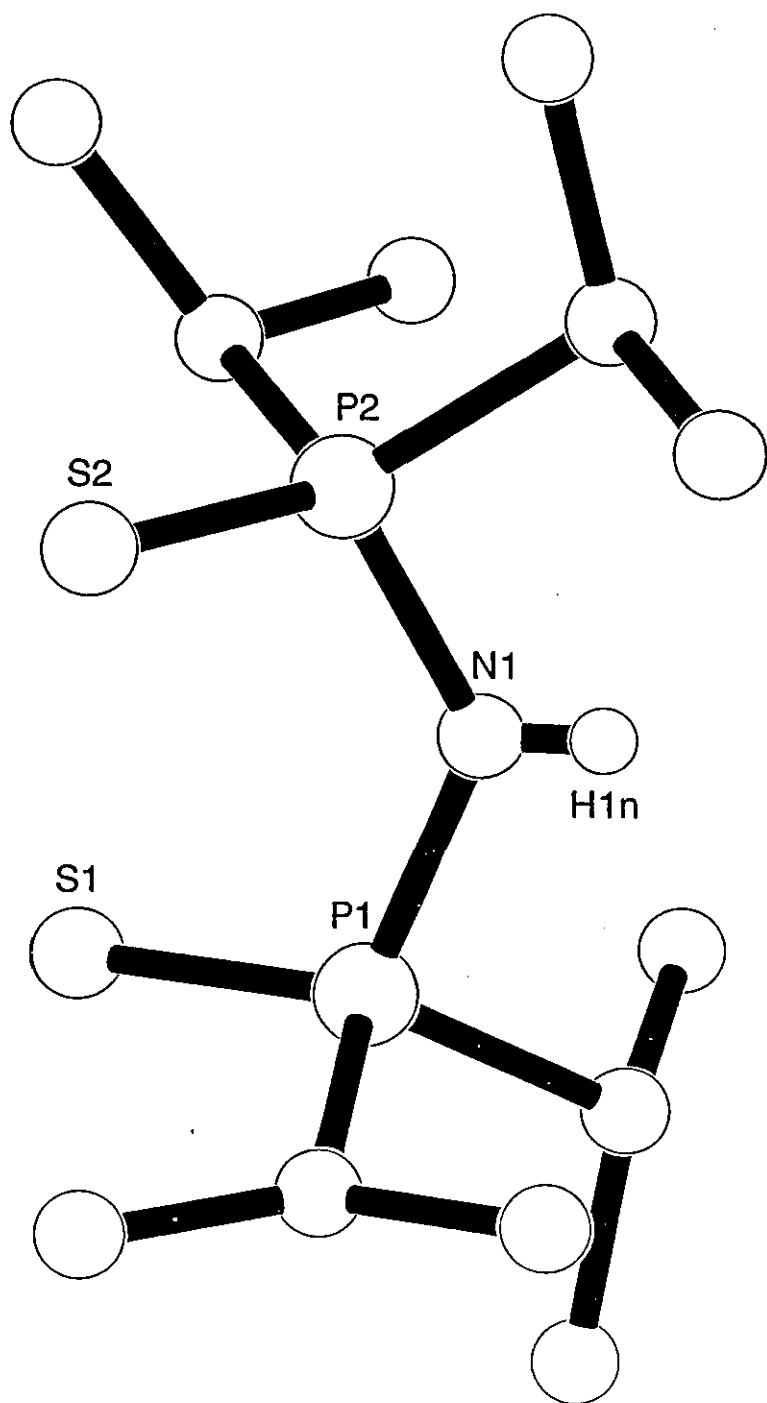


Figure 2.1. Crystal structure of ${}^i\text{Pr}_2\text{P}(\text{S})\text{NHP}(\text{S}){}^i\text{Pr}_2$.

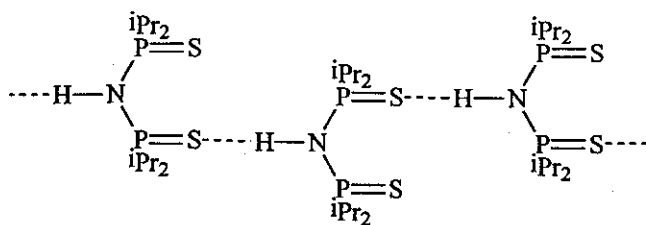


Figure 2.2. Hydrogen-bonded chain observed for **1**.

This arrangement, which is similar to the methyl analogue is in contrast to the phenyl analogue which is known to form dimer pairs. Although the difference in P=S bond lengths is small [1.949(1) cf. 1.941(1) Å] and at the margin of significance the longer bond is associated with the H-bonded sulfur atom.

2.3.1 Tetrahedral Complexes of **1**.

Reaction of **1** with zinc, nickel and cadmium carbonates and cobalt dichloride gave $M[\text{}^i\text{Pr}_2\text{P}(\text{S})\text{NP}(\text{S})\text{}^i\text{Pr}_2]_2$ {M = Zn (**2**), Ni (**3**), Cd (**4**) and Co (**5**)} in good yields. In each case reflux was required to produce coordination except for the zinc complex which was approximately 70% reacted (by ^{31}P NMR) merely upon stirring for 1 hour. All of the compounds gave satisfactory elemental analyses and display the expected spectroscopic properties. FAB +ve mass spectra revealed the expected parent ions.

Deprotonation/complexation of **1** to give **2**, **3** and **5** resulted in a coordination shift of the phosphorus nuclei of approximately 30 ppm. In addition there is a marked increase in the frequency of the ν_{as} (PNP) vibration (Table 2.1) for **2**, **3**, **4** and **5** coupled with a decrease in the frequency of the ν (PS) vibration compared to the free

Table 2.1. IR assignments for $M[\text{}^i\text{Pr}_2\text{P}(\text{S})\text{NP}(\text{S})\text{}^i\text{Pr}_2]_2$ (M = Zn, Cd, Ni, Co / cm^{-1}).

	ν (NH)	ν (PNP)	ν (PS)	ν (NPS)
1	3243, 1322	936, 906, 776	646	-
2	-	1226, 775	563	-
3	-	1230, 765	548	408
4	-	1225, 783	558	400
5	-	1228, 779	560	417

ligand, as has been previously observed in related systems³²⁻³⁴. These observations are indicative of changes in bond order upon removal of the amine proton, higher for P-N and lower for P-S bonds due to the delocalisation of the negative charge over the ligand. This agrees with the crystallographic data of the neutral ligand and its metal complexes (Table 2.2).

Table 2.2. Selected bond lengths (Å) and angles (°) for ${}^i\text{Pr}_2\text{P}(\text{S})\text{NHP}(\text{S}){}^i\text{Pr}_2$ and $\text{M}[{}^i\text{Pr}_2\text{P}(\text{S})\text{NP}(\text{S}){}^i\text{Pr}_2]_2$ (M = Zn, Cd, Ni).

	LH	M = Zn 2	M = Cd 3	M = Ni 4
P(1)-S(1)	1.941(1)	2.032(1)	2.018(2)	2.027(1)
P(2)-S(2)	1.949(1)		2.032(2)	
P(3)-S(3)			2.023(2)	
P(4)-S(4)			2.022(2)	
P(1)-N(1)	1.682(3)	1.581(2)	1.585(3)	1.581(2)
P(2)-N(1)	1.684(2)		1.580(3)	
P(3)-N(3)			1.573(3)	
P(4)-N(3)			1.592(3)	
M-S(1)		2.345(1)	2.526(2)	2.2844(9)
M-S(2)			2.516(2)	
M-S(3)			2.531(2)	
M-S(4)			2.514(2)	
S(1)-P(1)-N(1)	114.14(9)	118.5(1)	119.0(1)	118.0(1)
S(2)-P(2)-N(1)	114.76(10)		118.5(1)	
S(3)-P(3)-N(3)			119.2(1)	
S(4)-P(4)-N(3)			119.2(1)	
P(1)-N(1)-P(2)	131.6(1)	140.5(3)	143.2(2)	137.1(2)
P(3)-N(3)-P(4)			141.0(2)	
M-S(1)-P(1)		107.1(1)	103.4(1)	111.00(4)
M-S(2)-P(2)			103.8(1)	
M-S(3)-P(3)			104.2(1)	
M-S(4)-P(4)			103.8(1)	
S(1)-M-S(2)		112.4(1)	110.6(1)	109.86(2)
S(3)-M-S(4)			109.4(1)	
S(1)M-S(4)		108.0(1)	108.1(1)	108.69(4)
S(2)-M-S(3)			107.3(1)	
S(1)-M-S(3)			111.8(1)	
S(2)-M-S(4)			109.5(1)	

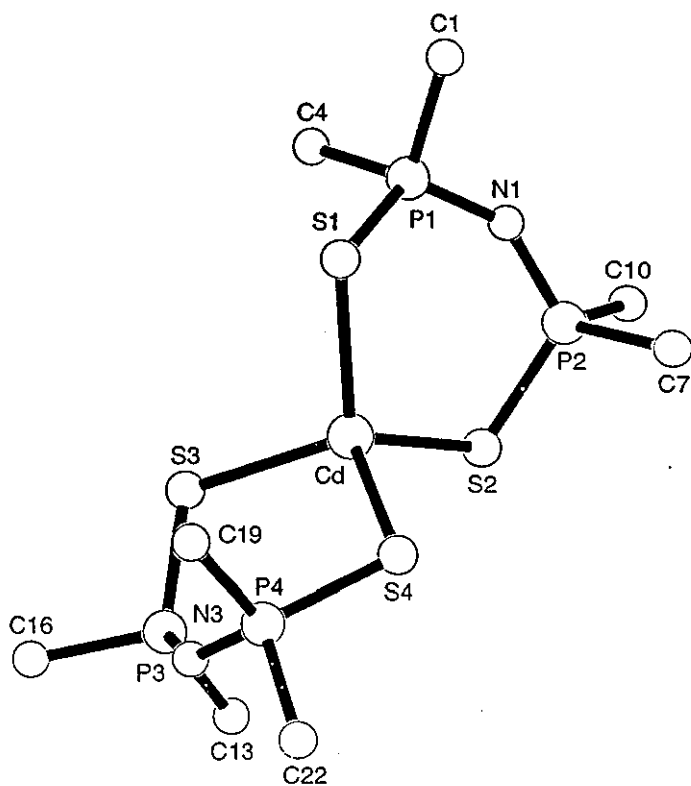
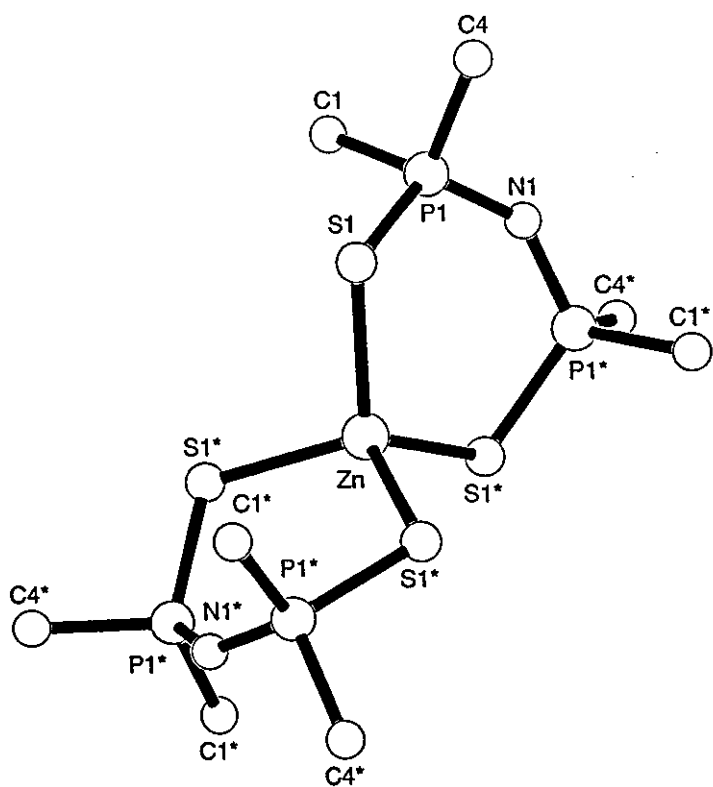
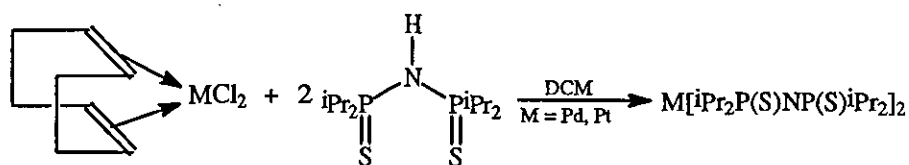


Figure 2.3. Crystal structures of $M[\text{Pr}_2\text{P}(\text{S})\text{NP}(\text{S})\text{Pr}_2]_2$ for $M = \text{Zn}, \text{Cd}$.

2, **3**, **4** are essentially isostructural (Figure 2.3) indeed the zinc and nickel compounds are isomorphous. **2** has crystallographic S_4 symmetry, the Zn-S distance being 2.345(1) Å. The S-Zn-S bite angle is 112.4(1)° and the other S-Zn-S angle is 108.0(1)°. The ZnS_2P_2N rings have puckered geometries with a pseudo boat conformation. This conformation appears to be the most commonly adopted for complexes containing $[R_2P(S)NP(S)R_2]$ ligands although other conformations have been reported^{13,14}. The P-S bond lengths in **2** are enlarged and the P-N bond lengths reduced with respect to **1** reflecting the increased electronic delocalisation as a consequence of deprotonation. The distortions in the geometries at phosphorus that were observed in the free ligand (angles ranging from 101-115°) are also present in **2** with angles in the range 104.9-118.5°; the largest distortions are associated with N-P-S in both cases. On complexation the P-N-P angle is substantially increased [140.5(3) in **2** versus 131.6(1) in **1**] which is in striking contrast to the change in geometry upon complexation to cobalt for the methyl analogue¹⁵ [128.0(3)° $Co\{SPMe_2\}_2N\}_2$ versus 133.2(2)° for $Me_2P(S)NHP(S)Me_2$]. The reasons for this difference are not immediately apparent and cannot be attributed simply to steric interactions associated with the ⁱPr substituents. As mentioned above, **2**, **3** and **4** are essentially isostructural with **2** and **4** being isomorphous. A least squares fit of the core atoms in **2** and **3** reveals only very minor differences. Inspection of the packing of the three complexes does not reveal any significant intermolecular approaches to either the sulfur or nitrogen atoms.

2.3.2 Square Planar Complexes of **1**.

Reactions of **1** with the cycloocta-1,5-diene metal dichlorides (Equation 2.2) gave $M[{}^iPr_2P(S)NP(S) {}^iPr_2]_2$ {M = Pd (**6**) and Pt (**8**)} in good yields. **6** and **8** have satisfactory microanalyses and reasonable spectroscopic properties with the exception of the NMR spectrum of **8** which, with a trace of **1** present appears to behave in a fluxional manner, we speculate that this is probably due to the PtS_2P_2N ring changing



Eqn. 2.2

between the “chair” and the “boat” conformation in the solution phase and some sort of protonation/deprotonation exchange. This would explain the broad peak at 59.7 ppm.

Again the infra-red shows the expected changes in ν (PNP) and ν (PS) bond vibrations (presented in Table 2.3) due to the changes in bond order.

Table 2.3. IR assignments for $M[iPr_2P(S)NP(S)iPr_2]_2$ ($M = Pd, Pt / cm^{-1}$).

	ν (PNP)	ν (PS)	ν (NPS)
6	1200	543	408
8	1221	583	414

The structures of **6** and **8** (Figure 2.4) are of particular interest, **6** shows the more common pseudo “boat” conformation for the PdS_2P_2N ring whereas the “chair” formation is observed for the PtS_2P_2N ring in **8**. The structures make for an interesting comparison between the two conformations (comparative bond lengths and angles for **2**, **6**, **7**, **8** are presented in Table 2.4). M-S distances are almost equal, P-S bonds are slightly longer and P-N bonds slightly shorter for **8**. The most substantial differences are found in the S-M-S and M-S-P angles which are around 10° smaller in both cases for the “chair” conformation. The M-S-P angles for the different conformations will become important later in judging the amount of *s* orbital character that can be attributed to these bonds. The S-P-N bond angles are nearly equal and the P-N-P angle is 5° smaller for **6**. The structures compare favourably with that of **2** with the exception of S-M-S and P-N-P bond angles which are smaller for the square planar complexes.

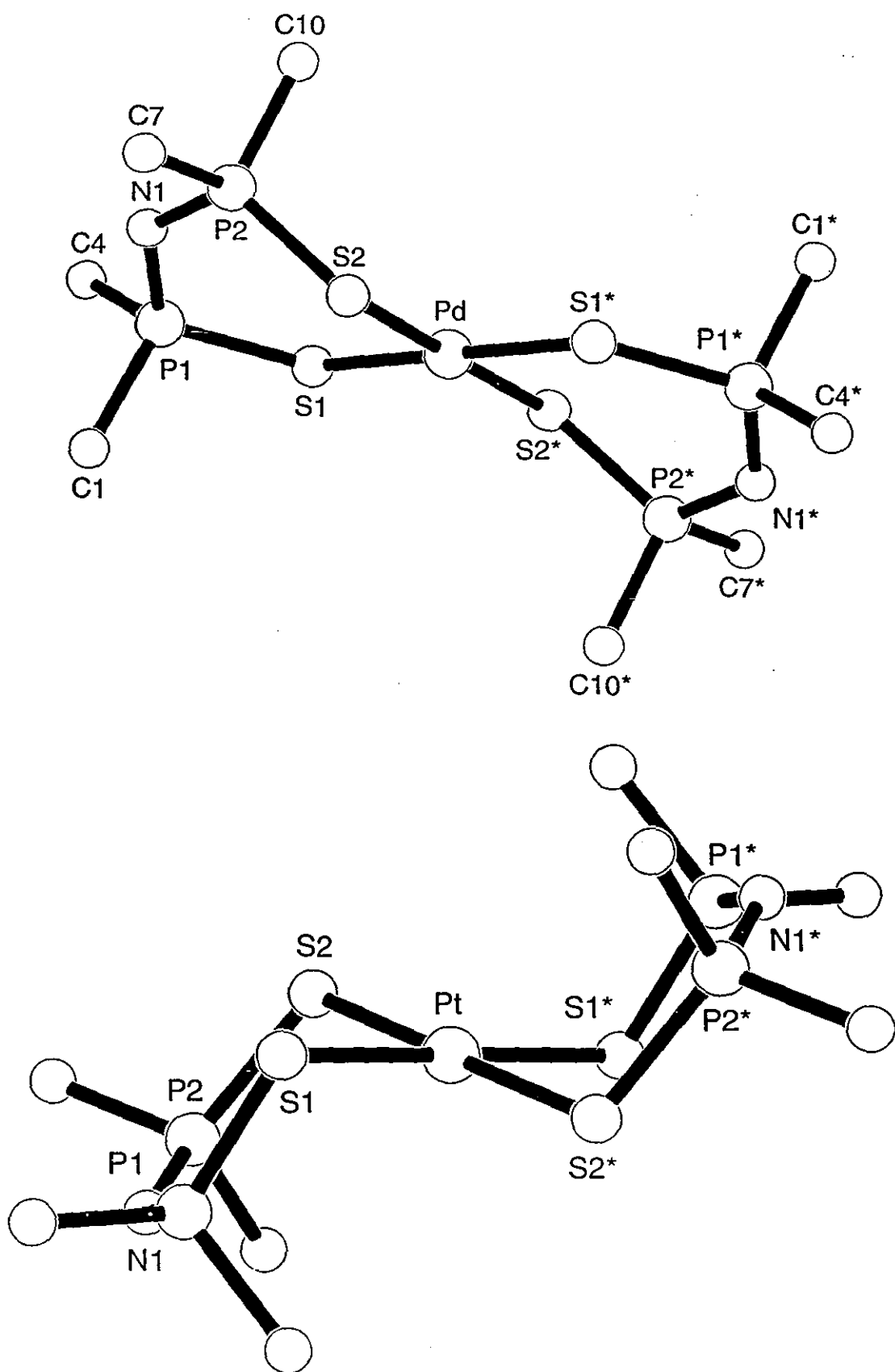


Figure 2.4. Crystal structures of $M[{}^i\text{Pr}_2\text{P}(\text{S})\text{NP}(\text{S}){}^i\text{Pr}_2]_2$ for $M = \text{Pd}, \text{Pt}$.

The crystallisation of $[\text{Pd}(\text{}^i\text{Pr}_2\text{P}(\text{S})\text{NP}(\text{S})\text{}^i\text{Pr}_2)(\text{}^i\text{Pr}_2\text{P}(\text{S})\text{NHP}(\text{S})\text{}^i\text{Pr}_2)]^+\text{Cl}^-$ (7) from a dichloromethane solution of 6 and its resulting structure (Figure 2.5) allows us the opportunity to compare coordinated neutral and anionic ligands. Structurally, the bond angles are all fairly similar, the differences as expected are in the bond lengths, for the protonated $\text{PdS}_2\text{P}_2\text{N}$ ring the M-S (2.35-2.36 Å) and P-N (1.64-1.65 Å) bonds

Table 2.4. Selected bond lengths (Å) and angles (°) for $\text{M}[\text{}^i\text{Pr}_2\text{P}(\text{S})\text{NP}(\text{S})\text{}^i\text{Pr}_2]_2$

(M = Zn, Pt, Pd) and $\{\text{Pd}[\text{L}][\text{HL}]\}^+$ for HL = $\text{}^i\text{Pr}_2\text{P}(\text{S})\text{NHP}(\text{S})\text{}^i\text{Pr}_2$.

	ZnL ₂ 2	PtL ₂ 8	PdL ₂ 6	[Pd(L)(HL)] ⁺ 7	
				Ring (1) ^a	Ring (2) ^b
M-S(1)	2.345(1)	2.338(3)	2.341(1)	2.359(3)	2.329(3)
M-S(2)		2.334(2)	2.347(1)	2.353(4)	2.314(3)
S(1) - P(1)	2.032(1)	2.034(3)	2.030(2)	2.008(5)	2.045(4)
P(1) - N(1)	1.581(2)	1.586(4)	1.597(4)	1.65(1)	1.587(10)
N(1) - P(2)	1.581(2)	1.575(4)	1.588(4)	1.64(1)	1.590(10)
P(2) - S(2)	2.032(1)	2.038(2)	2.023(2)	1.976(5)	2.040(5)
S(1) - M - S(2)	112.4(1)	90.9(1)	100.7(1)	99.2(1)	100.5(1)
M- S(1) - P(1)	107.1(1)	99.6(1)	114.0(1)	103.4(2)	110.6(1)
S(1) - P(1) - N(1)	118.3(1)	116.5(1)	119.1(2)	111.6(4)	114.0(4)
P(1) - N(1) - P(2)	140.5(3)	135.0(2)	130.2(2)	128.7(6)	128.2(7)
N(1) - P(2) - S(2)	118.5(1)	118.3(1)	117.1(1)	115.8(4)	117.1(4)
P(2) - S(2) - M	107.1(1)	104.1(1)	108.6(1)	115.5(2)	110.5(2)

^a Ring (1) is protonated ^b Ring (2) is sequentially numbered, *i.e.* S(3) corresponds to S(1) in Ring (1)

are longer and the P-S bonds (1.98-2.01 Å) are shorter than those of the deprotonated $\text{PdS}_2\text{P}_2\text{N}$ ring (M-S 2.31-2.33; P-N 1.59; P-S 2.04-2.05 Å) in agreement with the absence of delocalisation of a negative charge.

Having observed both the “chair” and “boat” conformations and seemingly straightforward protonation of square planar complexes, these two topics were investigated by variable temperature $^{31}\text{P}\{-^1\text{H}\}$ NMR (Figure 2.6). A sample of 8 in CD_2Cl_2 with a trace of 1 present was cooled from 298 K down to 193 K, with spectra

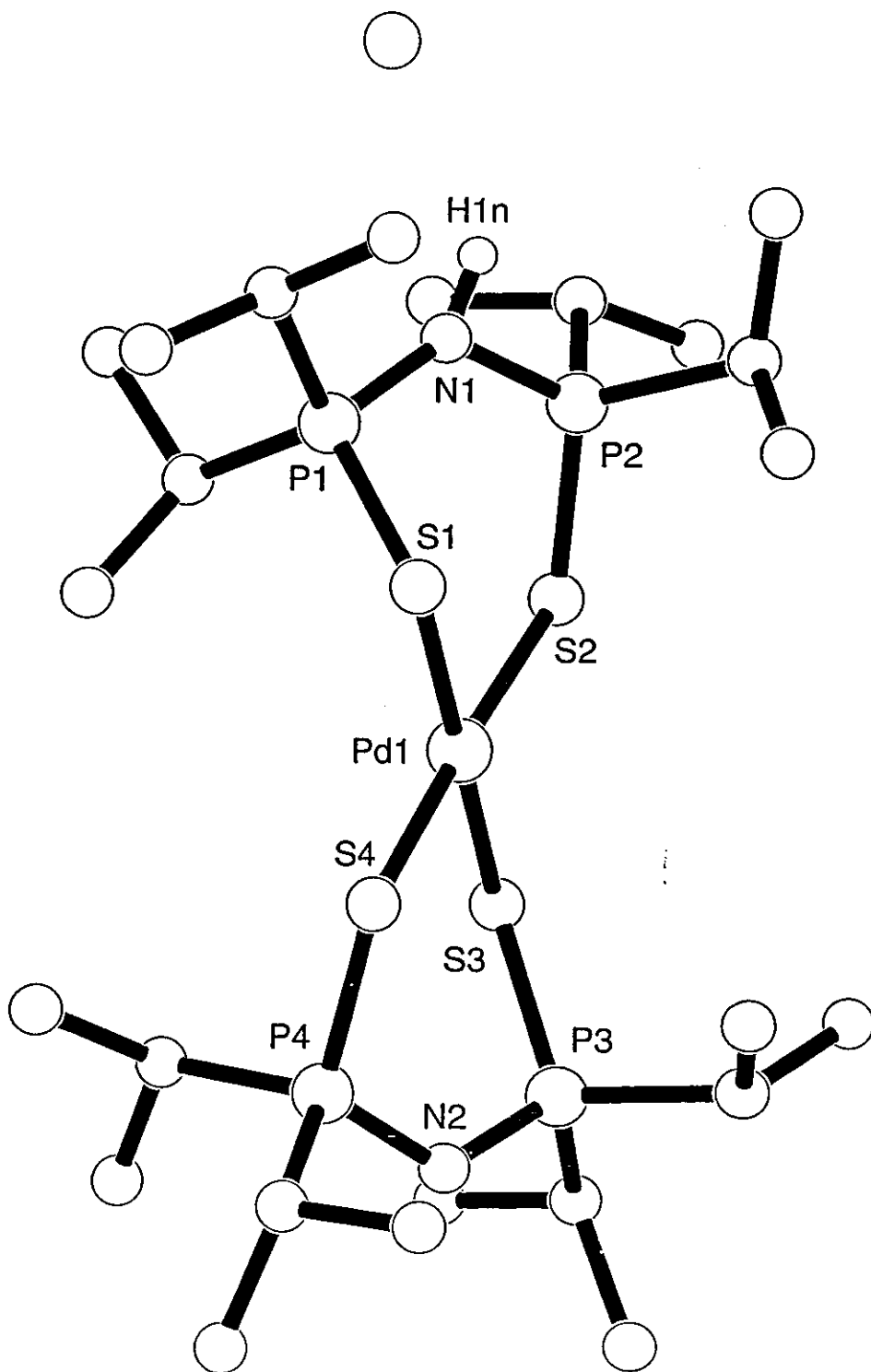


Figure 2.5. Crystal structure of $\{Pd[L][HL]\}^+Cl^-$ for $HL = iPr_2P(S)NHP(S)iPr_2$.

being taken at increments of 10 K from 293 K downwards. The coalescence temperature appeared to be 273 K where the broad peak separated into two singlets of near equal intensity at 59.5 ppm [$^2J(^{31}\text{P}-^{195}\text{Pt})$ 86.6 Hz] and 58.8 ppm [$^2J(^{31}\text{P}-^{195}\text{Pt})$ 71.5 Hz]. On further cooling more peaks emerged and their satellites were observed at 233 K (Figure 2.6, Table 2.5).

Table 2.5. Chemical shifts and [Pt-P] coupling constants for $\text{Pt}[\text{}^i\text{Pr}_2\text{P}(\text{S})\text{NP}(\text{S})\text{}^i\text{Pr}_2]_2$ in CD_2Cl_2 at 233 K together with tentative assignments.

	δ / ppm	$^2J(^{31}\text{P}-^{195}\text{Pt}) / \text{Hz}$
$\text{Pt}[\text{N}(\text{}^i\text{Pr}_2\text{PS})_2]_2$ “chair”	58.2	72.0
$\text{Pt}[\text{N}(\text{}^i\text{Pr}_2\text{PS})_2]_2$ “boat”	59.5	84.8
$[\text{HN}(\text{}^i\text{Pr}_2\text{PS})_2]\text{Pt}[\text{N}(\text{}^i\text{Pr}_2\text{PS})_2] +$	62.4	88.5
$[\text{HN}(\text{}^i\text{Pr}_2\text{PS})_2]\text{Pt}[\text{N}(\text{}^i\text{Pr}_2\text{PS})_2] +$	81.5	104.1

The “chair” and “boat” isomers of the fully deprotonated complex, $\{\text{Pt}[\text{N}(\text{}^i\text{Pr}_2\text{PS})_2]_2\}$ are at lower frequency than any of the other peaks (59.5 and 58.2 ppm). The two geometries have significantly different M-S-P bond angles with those of the “boat” geometry in **6** (108.6-114.0°) being greater than the “chair” **8** (99.6-104.1°). The larger angle may imply a greater proportion of *s* character in the hybridised sulfur. This greater proportion of *s* character is likely to increase the magnitude of the platinum-phosphorus coupling⁵⁹, therefore it can be deduced that the peak at 59.5 ppm with the larger coupling corresponds to a complex exhibiting the distorted “boat” geometry and the peak at 58.4 ppm is its isomer in the “chair” conformation.

The other resonances observed (62.4 and 81.5 ppm) are assigned as being due to protonation of the complexed ligand by the free ligand which acts as a proton donor. It is likely the signal at 81.5 ppm of the highest frequency and closest to the neutral ligand peak (89.1 ppm) is that of the protonated ligand complexed, $\{\text{Pt}[\text{HN}(\text{}^i\text{Pr}_2\text{PS})_2][\text{N}(\text{}^i\text{Pr}_2\text{PS})_2]\}^+$, and the signal at 62.4 ppm is that of the deprotonated ligand co-ordinated to the platinum, $\{\text{Pt}[\text{HN}(\text{}^i\text{Pr}_2\text{PS})_2][\text{N}(\text{}^i\text{Pr}_2\text{PS})_2]\}^+$, respectively in the platinum analogue of **7**. In addition, a solution of **8** in CDCl_3 was treated with a few drops of 85% HBF_4 solution in ether at room temperature,

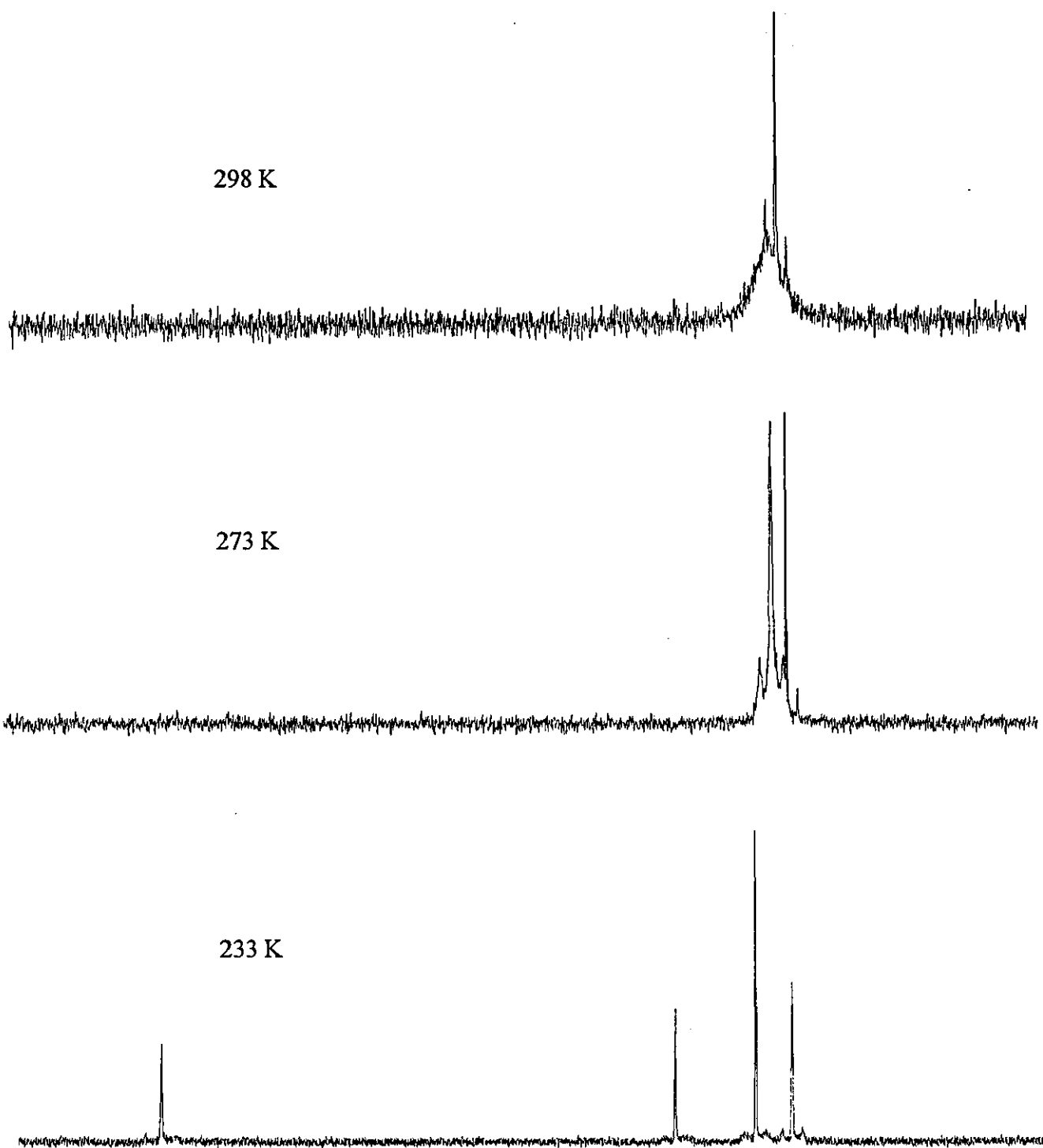
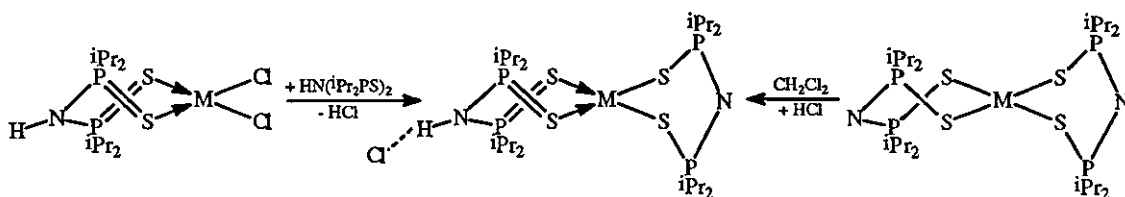


Figure 2.6. Variable temperature ^{31}P NMR spectra of $\text{Pt}[\text{}^1\text{Pr}_2\text{P}(\text{S})\text{NP}(\text{S})\text{}^1\text{Pr}_2]_2$.

the only signal observed in $^{31}\text{P}\text{-}\{^1\text{H}\}$ NMR was a very broad peak at 85ppm, consistent with a doubly protonated complex $\{\text{Pt}[\text{HN}(\text{iPr}_2\text{PS})_2]_2\}^{2+}$.

With the knowledge that these complexes can be protonated by acid, it is possible a trace of HCl in dichloromethane behaved as a proton donor while **6** was being crystallised such that a very small proportion of the crystals grown were **7**. However, assuming that the mechanism by which the neutral ligand coordinates to the metal involves initially replacing the cycloocta-1,5-diene, the possibility that on the coordination and deprotonation of the second ligand to replace the chlorines, the previously coordinated ligand failed to deprotonate cannot be discounted (Equation 2.3).



Eqn. 2.3.

A further square planar complex was formed from the reaction of **1** with bis(trimethylphosphine)platinum dichloride to give $\{\text{Pt}(\text{PMe}_3)_2[\text{N}(\text{iPr}_2\text{PS})_2]\}^+ \text{BPh}_4^-$ (**9**) in reasonable yield and with satisfactory elemental analysis. Notably the ^{31}P NMR showed no ^3J phosphorus-phosphorus coupling between the trimethylphosphines and the phosphorus centres in the ligand, merely two singlets with satellites at 59.0 ppm $\{^2\text{J}(^{31}\text{P}\text{-}^{195}\text{Pt}) 70.4 \text{ Hz}\}$ for the ligand and -21.9 ppm $\{^1\text{J}(^{31}\text{P}\text{-}^{195}\text{Pt}) 3053 \text{ Hz}\}$ for the trimethylphosphines were recorded.

2.4. Experimental.

${}^i\text{Pr}_2\text{P}(\text{S})\text{NHP}(\text{S}){}^i\text{Pr}_2$ **1**. This method is based on a literature preparation of related compounds ¹⁶, the reaction was performed under nitrogen. A solution of ${}^i\text{Pr}_2\text{PCl}$ (4.87 g, 5.0 ml, 32 mmol) in toluene (100 ml) was added dropwise to a solution of $\text{HN}(\text{SiMe}_3)_2$ (2.58 g, 3.4 ml, 16.0 mmol) in hot (50 °C) toluene (50 ml) over 30 minutes. Heating and stirring was continued for 3 hours after which time the reaction was cooled to room temperature and sulfur was added (1.0 g, 31 mmol). The reaction was then refluxed for a further 6 hours and cooled to 0°C. The resulting white precipitate was filtered off and washed with CS_2 (2 x 10ml) and light petroleum ether (2 x 10 ml). The crude product was recrystallised from CH_2Cl_2 and hexane (2.90 g, 9.27 mmol, 58 % yield, mp 165-6 °C). Microanalysis calculated for $\text{C}_{12}\text{H}_{29}\text{NP}_2\text{S}_2$: C 46.0; H 9.3; N 4.4; S 20.5; P 19.8 %. Observed: C 45.9; H 8.5; N 4.5; S 20.4; P 20.9 %. ${}^{31}\text{P}$ - $\{^1\text{H}\}$ NMR (CDCl_3): 91.2 ppm. FTIR (dichloromethane solution, CsI plates at 100 microns): ν (N-H) 3320 cm^{-1} ; (KBr disc): ν (N-H) 3243; δ (N-H) 1322; ν (PNP) 936, 906, 776; ν (PS) 646 cm^{-1} . FT Raman (capillary sample): ν (N-H) 3245; ν (PNP) 944; ν (PS) 656 cm^{-1} . FAB +ve MS: m/z 314 corresponds to $\{\text{HN}({}^i\text{Pr}_2\text{PS})_2\}^+$; m/z 627 corresponds to $\{[\text{HN}({}^i\text{Pr}_2\text{PS})_2]_2\}^+$.

$\text{Zn}[\text{N}({}^i\text{Pr}_2\text{PS})_2]_2$ **2**. $\text{ZnCO}_3 \cdot 2\text{Zn}(\text{OH})_2 \cdot \text{H}_2\text{O}$ (0.10 g, 0.29 mmol) was added to a solution of **1** (0.30 g, 0.96 mmol) in dichloromethane (20 ml), and the mixture was refluxed for two hours. The cloudy/white mixture was filtered and the filtrate was reduced by two thirds and cooled overnight to give the product as clear crystals (0.30 g, 0.43 mmol, 90% yield, mp 144 °C). Microanalysis calculated for $\text{C}_{24}\text{H}_{56}\text{N}_2\text{P}_4\text{S}_4\text{Zn}$: C 41.9; H 8.2; N 4.1; S 18.6; P 18.0 %. Observed: C 42.6; H 7.4; N 4.4; S 18.6; P 18.7 %. ${}^{31}\text{P}$ - $\{^1\text{H}\}$ NMR (CDCl_3): 64.4 ppm. FTIR (KBr disc): ν (PNP) 1226, 775; ν (PS) 563, 541. FT Raman (capillary sample): ν (PNP) 1254, 1167, 776; δ (NPS) 508, 443; ν (MS) 257 cm^{-1} . FAB +ve MS: m/z 689 corresponds to $[\text{Zn}\{\text{N}({}^i\text{Pr}_2\text{PS})_2\}_2]^+$.

$\text{Cd}[\text{N}({}^i\text{Pr}_2\text{PS})_2]_2$ **3**. CdCO_3 (0.10 g, 0.58 mmol) was added to a solution of **1** (0.363 g, 1.16 mmol) in dichloromethane (30 ml), and the mixture was refluxed for two hours.

Again the mixture was cloudy white and it was filtered, the filtrate being evaporated to dryness as a white solid, then colourless crystals were obtained from dichloromethane/light petroleum ether (0.368 g, 0.50 mmol, 86% yield, mp 161 °C). Microanalysis calculated for $C_{24}H_{56}N_2P_4S_4Cd$: C 39.2; H 7.7; N 3.8; S 17.4; P 16.9 %. Observed: C 38.7; H 6.5; N 3.8; S 17.0; P 18.0 %. ^{31}P - $\{^1H\}$ NMR ($CDCl_3$): 63.09 ppm, $J(^{31}P$ - $^{111/113}Cd)$ 25 Hz. FTIR (KBr disc): ν (PNP) 1230, 1157, 765; ν (PS) 548; δ (NPS) 408 cm^{-1} . FT Raman (capillary sample): ν (PNP) 768; δ (NPS) 500, 438; ν (MS) 256 cm^{-1} . FAB⁺ MS: m/z 739 corresponds to $[Cd\{N(^iPr_2PS)_2\}_2]^+$.

$Ni[N(^iPr_2PS)_2]_2$ **4**. $2NiCO_3 \cdot 3Ni(OH)_2 \cdot 4H_2O$ (0.10 g, 0.17 mmol) was added to a solution of **1** (0.16 g, 0.51 mmol) in dichloromethane (30 ml), and the green mixture was refluxed for two hours then filtered. The filtrate was evaporated to a green solid, then green crystals were obtained from dichloromethane/light petroleum ether (0.144 g, 0.21 mmol, 83% yield, mp 126 °C). Microanalysis calculated for $C_{24}H_{56}N_2P_4S_4Ni$: C 42.3; H 8.3; N 4.1; S 18.8; P 18.2 %. Observed: C 42.6; H 7.9; N 4.1; S 18.7; P 19.3 %. FTIR (KBr disc): ν (PNP) 1253, 1225, 783; ν (PS) 558; δ (NPS) 400 cm^{-1} . FAB +ve MS: m/z 683 corresponds to $[Ni\{N(^iPr_2PS)_2\}_2]^+$.

$Co[N(^iPr_2PS)_2]_2$ **5**. **1** (0.10 g, 0.319 mmol) was added to a blue solution of $CoCl_2$ (0.02g, 0.154 mmol) in dichloromethane (30 ml). The mixture was refluxed for 1 hour. The solution was then evaporated to dryness and recrystallized from dichloromethane (0.102 g, 0.149 mmol, 97% yield). Microanalysis calculated for $C_{24}H_{56}N_2P_4S_4Co$: C 42.2; H 8.3; N 4.1 %. Observed: C 39.7; H 7.7; N 4.1 %. FTIR (KBr disc): ν (PNP) 1254, 1228, 779; ν (PS) 560, 541; δ (NPS) 417 cm^{-1} . FAB +ve MS: m/z 684 corresponds to $[Co\{N(^iPr_2PS)_2\}_2]^+$.

$Pd[N(^iPr_2PS)_2]_2$ **6**. **1** (0.220 g, 0.703 mmol) was added to a solution of $PdCl_2COD$ (0.1g, 0.350 mmol) in dichloromethane (30 ml), which immediately turned from yellow to red/orange. The mixture was stirred for a further thirty minutes. The solution was then evaporated to dryness then recrystallized from dichloromethane, giving red/orange needles (0.245 g, 0.336 mmol, 96% yield, mp 138 °C). Microanalysis calculated for $C_{24}H_{56}N_2P_4S_4Pd$: C 39.5; H 7.7; N 3.8 %. Observed: C 38.3; H 6.9; N

3.6 %. $^{31}\text{P}\{-^1\text{H}\}$ NMR (CDCl_3): 64.8 ppm. FTIR (KBr disc): ν (PNP) 1200, 1159; ν (PS) 543; δ (NPS) 408 cm^{-1} . FAB +ve MS: m/z 731 corresponds to $[\text{Pd}\{\text{N}(\text{Pr}_2\text{PS})_2\}_2]^+$.

$[\text{Pd}\{\text{N}(\text{Pr}_2\text{PS})_2\}\{\text{HN}(\text{Pr}_2\text{PS})_2\}]^+\text{Cl}^-$ **7**. From crystals grown from the dichloromethane solution of **6**, the first crystal selected for X-ray single crystal diffraction studies gave the unexpected structure of the mono-protonated complex **7**. This compound has only been characterised by single crystal analysis.

$\text{Pt}[\text{N}(\text{Pr}_2\text{PS})_2]_2$ **8**. **1** (0.084 g, 0.268 mmol) was added to a solution of PtCl_2COD (0.05 g, 0.134 mmol) in dichloromethane (30 cm^3), which was stirred for 2h, after which the solution had turned from clear to yellow. The solution was evaporated to dryness and recrystallized from acetone, giving yellow plates (0.10 g, 0.122 mmol, 90 % yield, mp $145\text{ }^\circ\text{C}$). Microanalysis calculated for $\text{C}_{24}\text{H}_{56}\text{N}_2\text{P}_4\text{S}_4\text{Pt}$: C 35.2; H 6.9; N 3.4 %. Observed: C 34.5; H 6.7; N 2.8 %. $^{31}\text{P}\{-^1\text{H}\}$ NMR (CD_2Cl_2): 61.3 ppm, ^2J ($^{195}\text{Pt}\text{-}^{31}\text{P}$) 71.7 Hz. FTIR (KBr disc): ν (PNP) 1221; ν (PS) 583; δ (NPS) 414 cm^{-1} . FAB +ve MS: m/z 819 corresponds to $[\text{Pt}\{\text{N}(\text{Pr}_2\text{PS})_2\}_2]^+$.

$[\text{Pt}(\text{PMe}_3)_2\{\text{N}(\text{Pr}_2\text{PS})_2\}]^+\text{Cl}^-$ **9**. KO^tBu (0.013 g, 0.118 mmol) and **1** (0.037 g, 0.118 mmol) was added to a solution of *cis* $\text{Pt}(\text{PMe}_3)_2\text{Cl}_2$ (0.050 g, 0.120 mmol) and NaBPh_4 (0.040 g, 0.117 mmol) in THF (20 ml) and stirred overnight. The mixture was evaporated to dryness, washed thoroughly with dichloromethane and filtered. The filtrate was evaporated to dryness giving a white solid (0.049 g, 0.071 mmol, 60 % yield). Microanalysis calculated for $\text{C}_{42}\text{H}_{66}\text{NP}_4\text{S}_2\text{BPt}$: C 51.5; H 6.8; N 1.4 %. Observed: C 51.2; H 6.7; N 1.6 %. $^{31}\text{P}\{-^1\text{H}\}$ NMR (CDCl_3): 59.0 ppm, ^2J ($^{31}\text{P}\text{-}^{195}\text{Pt}$) 70.4 Hz, -21.9 ppm, ^1J ($^{31}\text{P}\text{-}^{195}\text{Pt}$) 3053 Hz. FTIR (KBr disc): ν (PNP) 1260, 1226, 1152; ν (PS) 624, 534; δ (NPS) 412 cm^{-1} .

CHAPTER 3:
TETRABUTYLDITHIOIMIDODIPHOSPHINATES
AND THEIR COORDINATION CHEMISTRY

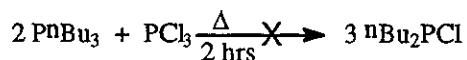
3.1 Introduction.

The results of the work on ${}^i\text{Pr}_2\text{P}(\text{S})\text{NHP}(\text{S}){}^i\text{Pr}_2$ prompted us to look in more detail at tetraalkyldithioimidodiphosphinates and how differing steric bulk produced by α and β branching in the alkyl substituents might affect the neutral ligand structures and their coordination complexes, in particular the $\text{MS}_2\text{P}_2\text{N}$ ring conformations. Consequently the ligands ${}^n\text{Bu}_2\text{P}(\text{S})\text{NHP}(\text{S}){}^n\text{Bu}_2$ (**10**), ${}^i\text{Bu}_2\text{P}(\text{S})\text{NHP}(\text{S}){}^i\text{Bu}_2$ (**11**), ${}^s\text{Bu}_2\text{P}(\text{S})\text{NHP}(\text{S}){}^s\text{Bu}_2$ (**12**), ${}^n\text{Bu}_2\text{P}(\text{S})\text{NHP}(\text{S}){}^i\text{Bu}_2$ (**13**), ${}^n\text{Bu}_2\text{P}(\text{S})\text{NHP}(\text{S}){}^s\text{Bu}_2$ (**14**) and ${}^i\text{Bu}_2\text{P}(\text{S})\text{NHP}(\text{S}){}^s\text{Bu}_2$ (**15**) were all synthesised and coordinated to Zn, Pd and the symmetrical compounds coordinated to Pt.

RESULTS AND DISCUSSION

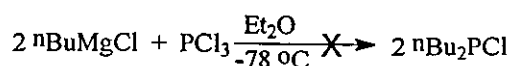
3.2.1. Attempted Ligand Syntheses.

A variety of different synthetic routes were attempted to make **10**. Having observed the high yield of the synthesis of **1** from reacting ${}^i\text{Pr}_2\text{PCl}$ with $\text{HN}(\text{SiMe}_3)_2$ the synthesis of ${}^n\text{Bu}_2\text{PCl}$ was attempted. The first route investigated was refluxing PCl_3 with $\text{P}{}^n\text{Bu}_3$ under anaerobic conditions hoping for a rearrangement of substituents to give ${}^n\text{Bu}_2\text{PCl}$ (Equation 3.1). On cooling the mixture was distilled



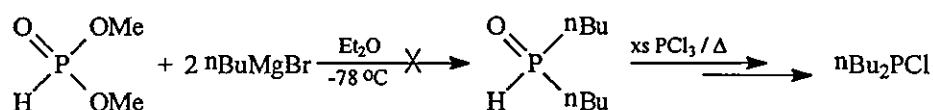
Eqn. 3.1

under vacuum, the distillate giving a signal in the ${}^{31}\text{P}$ NMR at 110 ppm ($\delta\{{}^n\text{Bu}_2\text{PCl}\}$ 50 ppm). Another direct route was attempted by adding the stoichiometric amount of Grignard reagent to PCl_3 at low temperature (Equation 3.2), however we were unable to control the stoichiometry by using low temperatures or concentrations and as a result the reaction consistently followed through to $\text{P}{}^n\text{Bu}_3$. Another approach was to



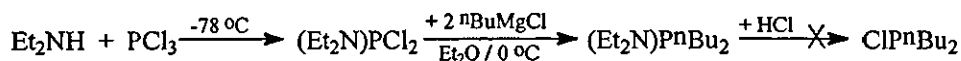
Eqn. 3.2

replace substituent groups on a phosphine oxide with Grignard reagent and then reflux with a tenfold excess of PCl_3 to produce the dialkylchlorophosphine (Equation 3.3). This route produced at least fifteen products on the first stage and was therefore not pursued.



Eqn. 3.3

It was evident there was no control over the stoichiometry if PCl_3 was used so in order to exert some control one of the chlorines was replaced by diethylamine (Equation 3.4). $\text{Cl}_2\text{P}(\text{NEt}_2)$ could then be reacted with Grignard under stoichiometric control to form ${}^n\text{Bu}_2\text{P}(\text{NEt}_2)$ in excellent yield. However the amine group then proved



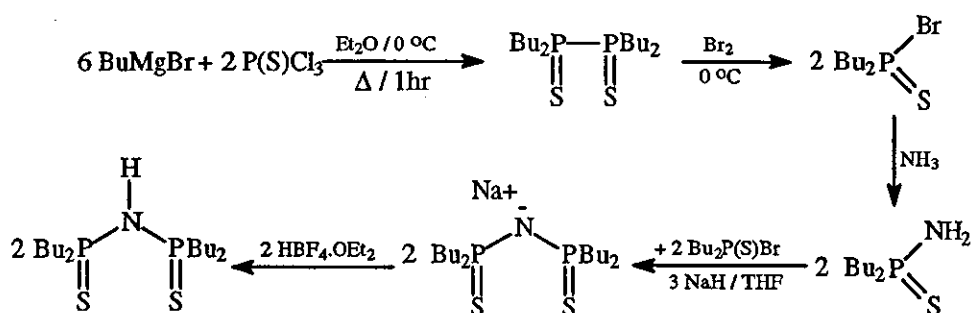
Eqn. 3.4

very difficult to replace with a halide and ${}^n\text{Bu}_2\text{P}(\text{NEt}_2)$ would not react with $\text{HN}(\text{SiMe}_3)_2$. Indeed on addition of HCl solution in ether an unknown air sensitive product formed in good yield (^{31}P NMR 110 ppm), evidently the same as that formed by refluxing PCl_3 with P^nBu_3 .

3.2.2. Ligand Synthesis.

10 was eventually made via a different approach. Instead of attempting to produce ${}^n\text{Bu}_2\text{PCl}$, the alternative synthetic strategy of making ${}^n\text{Bu}_2\text{P}(\text{S})\text{NH}_2$ and ${}^n\text{Bu}_2\text{P}(\text{S})\text{Br}$ and “clipping” the two halves together in the presence of NaH via an HBr elimination reaction was adopted (Equation 3.5). An excess of 3 moles of ${}^n\text{BuMgBr}$

was reacted with P(S)Cl_3 to give the dithiodiphosphine ${}^n\text{Bu}_2\text{P(S)P(S)}{}^n\text{Bu}_2$ (40 % yield) which was then cleaved with Br_2 and distilled under vacuum to give ${}^n\text{Bu}_2\text{P(S)Br}$ ⁶⁰ (90 % yield). This was then reacted with NH_3 to give ${}^n\text{Bu}_2\text{P(S)NH}_2$ (100 % yield). This



Eqn. 3.5

process was repeated to make the ${}^i\text{Bu}$ and ${}^s\text{Bu}$ analogues. The tert-butyl analogue would not react with NH_3 due to steric hindrance. The amine and halide were then reacted with a 3 mole excess of NaH , the driving force of the reaction being the formation of the sodium salt, $\text{Na}^+[\text{Bu}_2\text{P(S)NP(S)Bu}_2]^-$ (60 % yield). The salt could then be protonated with $\text{HBF}_4 \cdot \text{OEt}_2$ to give the neutral ligand in overall yield of 22 %. Whilst all ligands emerged as oils, they crystallised from the minimum amount of dichloromethane in a freezer.

Signals observed in the ${}^{31}\text{P}$ NMR in CDCl_3 (Table 3.1) show the shift of **12** at 87.0 ppm is at a significantly higher frequency than those for **10** and **11**, 71.0 and 68.3 ppm respectively. Whilst one might expect some difference with the increased steric bulk, such as 3 ppm for the difference between n-butyl and iso-butyl substituted ligands, 16 ppm is an unexpectedly large variance in comparison. In addition the ${}^2\text{J}({}^{31}\text{P}-{}^{31}\text{P})$ coupling observed in the AX type spectra for the mixed substituent ligands also reflects the effect of the sec-butyl group, **14** and **15** having a coupling 4 Hz greater than **13**. It is also interesting to note the reduction in frequency of the signal for the sec-butyl substituted phosphorus in **14** (84.7 ppm) and **15** (87.8 ppm) in

Table 3.1. Chemical shifts and [P-P] coupling constants in ^{31}P NMR (CDCl_3) for tetrabutylthioimidodiphosphate compounds.

	δ / ppm			$^2J(^{31}\text{P}-^{31}\text{P})$ / Hz
	P ₁	P ₂	P ₃	
$^n\text{Bu}_2\text{P}(\text{S})\text{NHP}(\text{S})^n\text{Bu}_2$	71.0	-	-	-
$^i\text{Bu}_2\text{P}(\text{S})\text{NHP}(\text{S})^i\text{Bu}_2$	-	68.3	-	-
$^s\text{Bu}_2\text{P}(\text{S})\text{NHP}(\text{S})^s\text{Bu}_2$	-	-	87.0	-
$^n\text{Bu}_2\text{P}(\text{S})\text{NHP}(\text{S})^i\text{Bu}_2$	72.3	70.4	-	26.4
$^n\text{Bu}_2\text{P}(\text{S})\text{NHP}(\text{S})^s\text{Bu}_2$	79.0	-	84.7	30.8
$^i\text{Bu}_2\text{P}(\text{S})\text{NHP}(\text{S})^s\text{Bu}_2$	-	76.1	82.8	30.8

P₁ denotes the n-butyl, P₂ the iso-butyl and P₃ the sec-butyl substituted phosphorus atoms.

comparison to the shift for **12** (87.0 ppm) of around 4 ppm is significantly less than the increase observed for the n-butyl and iso-butyl substituted phosphorus centres in **14** and **15** (79.0, 76.1 ppm) of 8 ppm in comparison to **10** (71.0 ppm) and **11** (68.3 ppm).

In contrast doublets were observed in the ^{31}P solid state NMR spectra of **10** and **11** (c.f. **1**), though the 2J phosphorus coupling was far greater than **1** (Table 3.2, Figure 3.1). The implication is hydrogen bonding in **10** and **11** is significantly stronger than in **1** thus making the difference between the pendant and the “bound” phosphorus centres much greater. **12** gave an unexpected spectrum of three main

Table 3.2. ^{31}P solid state NMR for $\text{R}_2\text{P}(\text{E})\text{NHP}(\text{S})\text{R}_2$ (R = ^nBu , ^iBu , ^sBu and ^iPr). Chemical shifts and coupling constants. * denotes tentatively assigned coupling constants.

	δ / ppm	$^2J(^{31}\text{P}-^{31}\text{P})$ / Hz
$^n\text{Bu}_2\text{P}(\text{S})\text{NHP}(\text{S})^n\text{Bu}_2$	77.8, 67.8	1214.7
$^i\text{Bu}_2\text{P}(\text{S})\text{NHP}(\text{S})^i\text{Bu}_2$	75.0, 64.3	1294.0
$^s\text{Bu}_2\text{P}(\text{S})\text{NHP}(\text{S})^s\text{Bu}_2$	89.7, 88.3, 86.7, 84.9	170.8, 219.8*
$^i\text{Pr}_2\text{P}(\text{S})\text{NHP}(\text{S})^i\text{Pr}_2$	91.0, 89.2	213.6

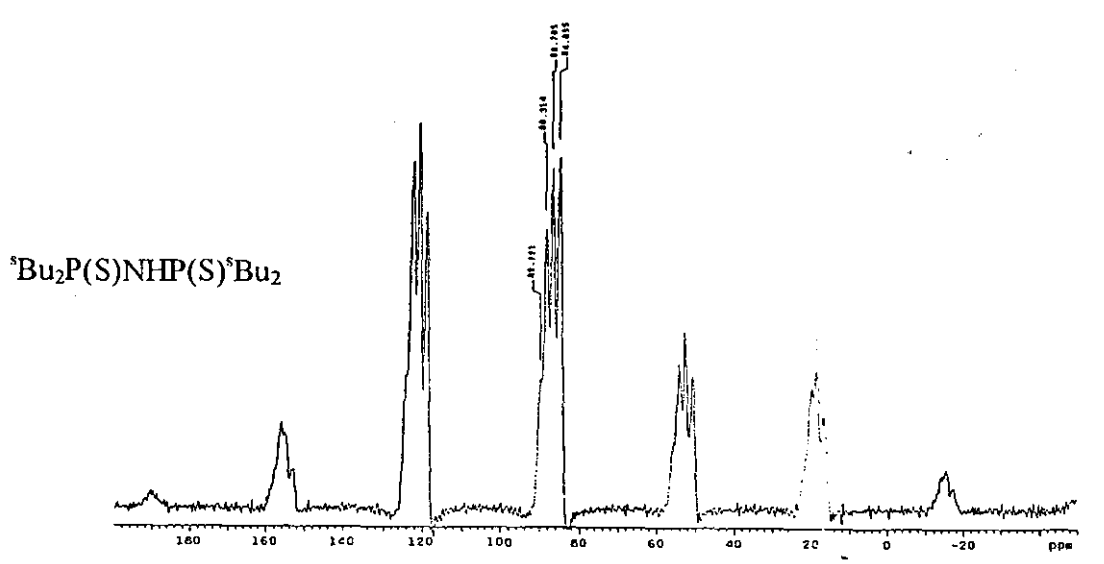
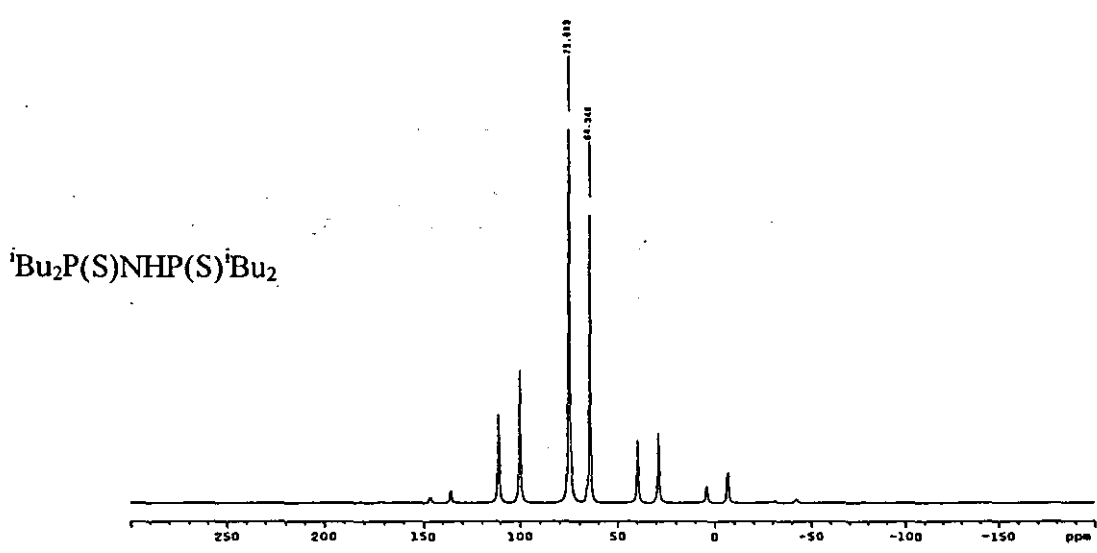
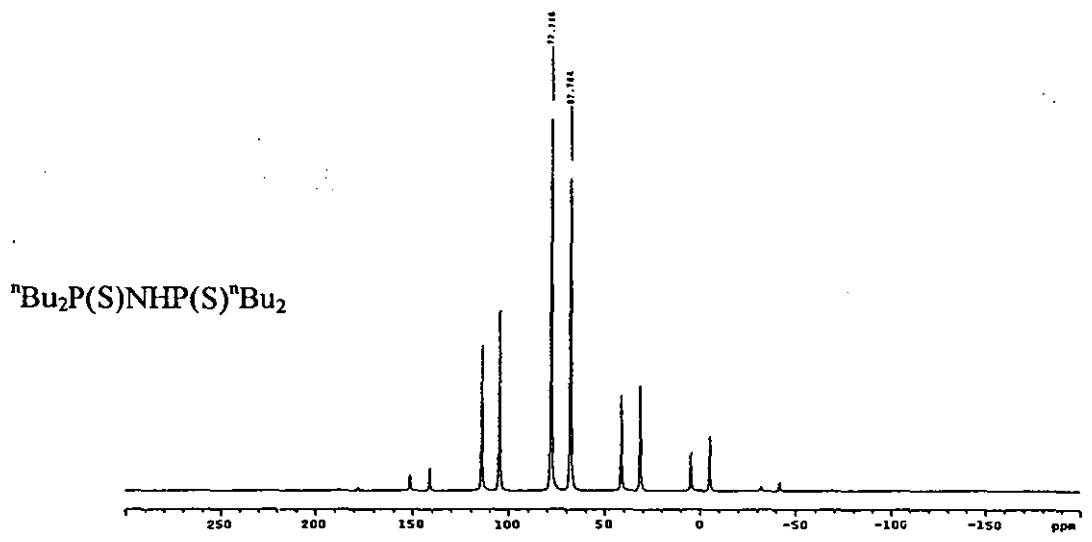


Figure 3.1. ${}^{31}\text{P}$ solid state NMR spectra of $\text{R}_2\text{P}(\text{S})\text{NHP}(\text{S})\text{R}_2$ for $\text{R} = {}^n\text{Bu}, {}^i\text{Bu}, {}^s\text{Bu}$.

peaks and a shoulder, implying the compound exists in the solid state in two independent forms. This was confirmed by the solid state ^{15}N NMR which showed two distinct peaks at - 322 and - 325 ppm. However the [P-P] coupling is low so again the implication is weaker hydrogen bonding within the solid state forms of **12**. There is supporting evidence from solution and solid state FTIR (Table 3.3). Once in solution the ν (NH) band is observed around 3320 cm^{-1} for all four compounds. Therefore the fact the ν (NH) band is $50 - 70\text{ cm}^{-1}$ lower for **10** and **11** in the solid state implies there is a significantly higher degree of hydrogen bonding which is in agreement with the hydrogen bond lengths, **10** (2.44 Å) and **11** (2.51 Å) being significantly shorter than **1** (2.60 Å).

Table 3.3. Solid state (KBr disc) and solution (dichloromethane, CsI cell) FTIR of $\text{R}_2\text{P}(\text{E})\text{NHP}(\text{S})\text{R}_2$ ($\text{R} = {}^n\text{Bu}, {}^i\text{Bu}, {}^s\text{Bu}, {}^i\text{Pr} / \text{cm}^{-1}$) and crystallographic S...H hydrogen bond lengths of $\text{R}_2\text{P}(\text{E})\text{NHP}(\text{S})\text{R}_2$ ($\text{R} = {}^n\text{Bu}, {}^i\text{Bu}, {}^i\text{Pr}$) for comparison.

	ν (NH) solid	ν (NH) solution	$\nu_{\text{solution}} - \nu_{\text{solid}}$	S...H (Å)
${}^n\text{Bu}_2\text{P}(\text{S})\text{NHP}(\text{S}){}^n\text{Bu}_2$	3172	3325	153	2.44
${}^i\text{Bu}_2\text{P}(\text{S})\text{NHP}(\text{S}){}^i\text{Bu}_2$	3180	3323	143	2.51
${}^s\text{Bu}_2\text{P}(\text{S})\text{NHP}(\text{S}){}^s\text{Bu}_2$	3225	3319	94	-
${}^i\text{Pr}_2\text{P}(\text{S})\text{NHP}(\text{S}){}^i\text{Pr}_2$	3243	3320	77	2.60

The characteristic ν (PNP) bands³²⁻³⁴ were also observed in the FTIR, $782 - 768\text{ cm}^{-1}$ and tentative assignments at $744 - 753\text{ cm}^{-1}$. However no ν (PS) vibrations were observed that could be confidently assigned. All of the compounds gave satisfactory elemental analyses and FAB +ve mass spectra revealed the expected parent ions ($\text{M} + \text{H}$ 370 m/z). Of the crystals obtained only those of **10**, **11** and **15** were suitable for single crystal analysis. **10** was observed to be a *trans* dimer (Figure 3.2) similar to $\text{Ph}_2\text{P}(\text{S})\text{NHP}(\text{S})\text{Ph}_2$ ²³ with an S-P...P-S torsion angle of 179.0° indicating the planarity of the SPNPS backbone. The P(1)-S(1) bond length at $1.941(2)\text{ Å}$ is significantly longer than that for P(2)-S(2) at $1.929(2)\text{ Å}$. This maybe because the S(1) is hydrogen bonded to the NH proton of the molecule that forms the other half of the dimer whereas the S(2) atom is pendant. The P-N bonds were

1.681(4) and 1.686(3) Å and the P-N-P bond angle was 132.1(2)° as expected. The S...H hydrogen bond is very strong at 2.439(4) Å.

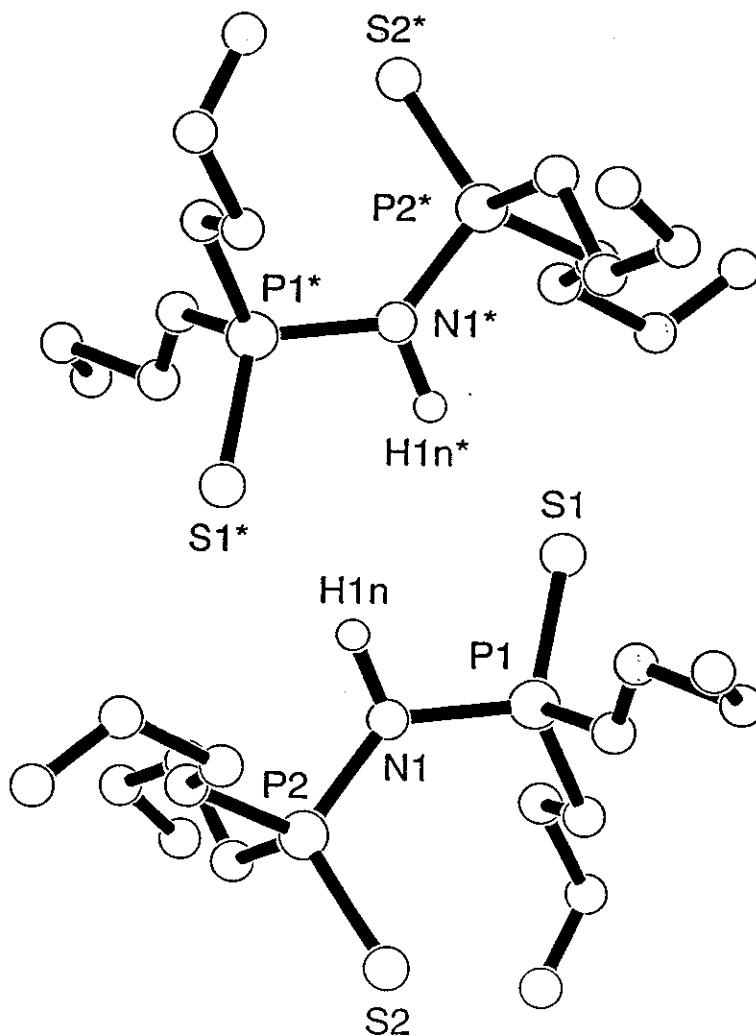


Figure 3.2. Crystal structure of $n\text{Bu}_2\text{P}(\text{S})\text{NHP}(\text{S})n\text{Bu}_2$ dimer.

In contrast **11** has the structure of a *trans* hydrogen bonded chain (Figure 3.3) which has previously been observed for $\text{Me}_2\text{P}(\text{S})\text{NHP}(\text{S})\text{Me}_2$ ²⁷. The S-P...P-S torsion angle is 179.8° again indicating the planarity of the SPNPS backbone. The P(2)-S(2)

bond length at 1.948(3) Å is very much longer than the P(1)-S(1) bond length of 1.931(3) Å, again due to the fact the S(2) sulfur is involved in the hydrogen bonding whereas the S(1) sulfur is pendant. Surprisingly the P(1)-N(1) bond length at 1.657(5) Å differs significantly from the P(2)-N(1) bond length which is 1.706(6) Å though the P-N-P bond angle is an expected 133.0(4)°. In addition the S[⋯]H hydrogen bond is quite short at 2.513(4) Å.

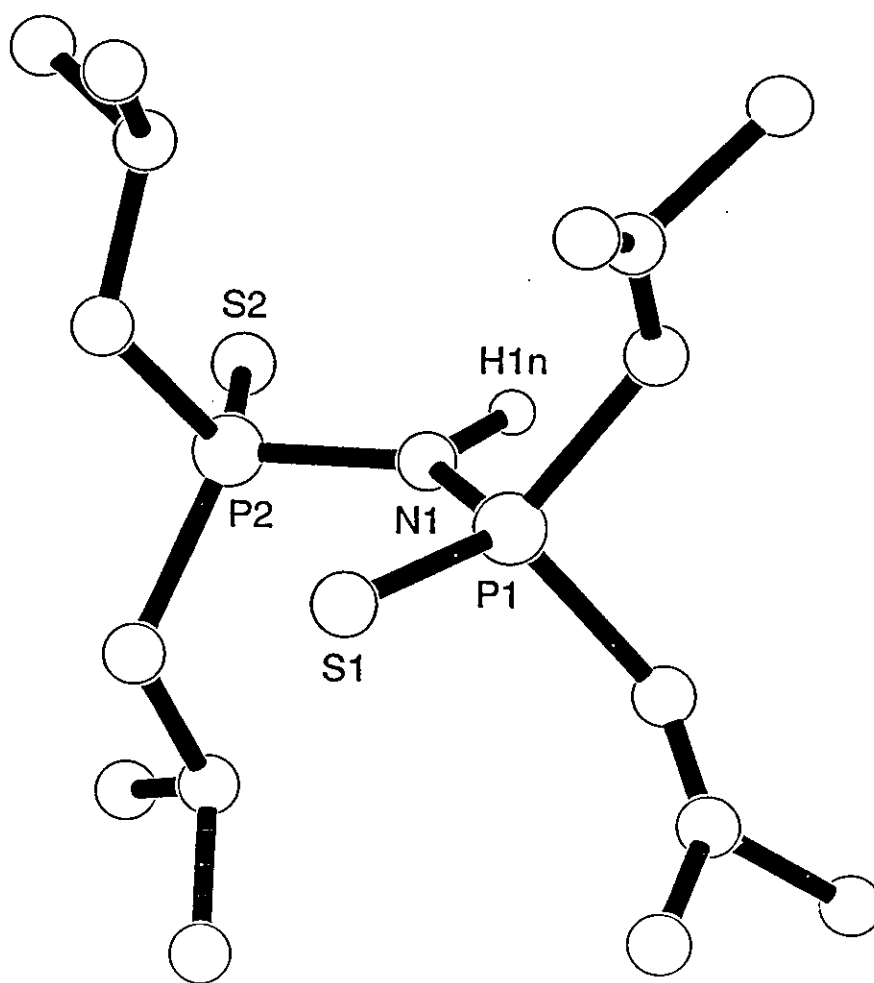


Figure 3.3. Crystal structure of ${}^i\text{Bu}_2\text{P}(\text{S})\text{NHP}(\text{S}){}^i\text{Bu}_2$.

15 is another *trans* dimer (Figure 3.4) with an SP...PS torsion angle of 179.4°. Again there is a difference between the P(1)-S(1) bond length of 1.943(1) Å and the

P(2)-S(2) bond length of 1.935(2) Å. The P-N bonds were 1.69-1.70 Å and the P-N-P angle was 133.1(2) ° as expected. The S[⋯]H hydrogen bond is 2.668(3) Å. It is interesting to note the phosphorus atom attached to the sulfur which is involved in the intermolecular hydrogen bond has iso-butyl substituents and the phosphorus with sec-butyl substituents is pendant, probably due to the higher degree of steric bulk.

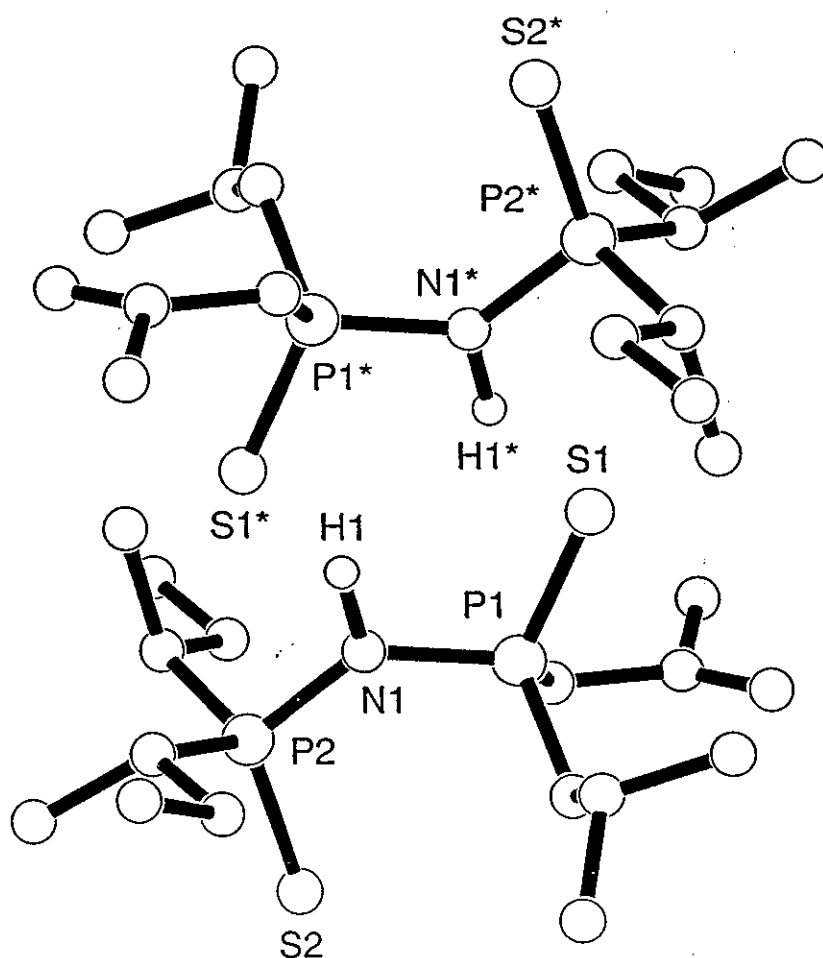


Figure 3.4. Crystal structure of ${}^i\text{Bu}_2\text{P}(\text{S})\text{NHP}(\text{S})^i\text{Bu}_2$ *trans* dimer.

A comparison of P-S bonds (Table 3.4) for the *trans* dimers **10** and **15** shows a difference between P(1)-S(1) and P(2)-S(2) of 0.008 - 0.013 Å due to the fact that one sulfur is pendant and the other is involved in intermolecular hydrogen bonding. This

difference is significantly greater for **11** and $\text{Me}_2\text{P}(\text{S})\text{NHP}(\text{S})\text{Me}_2$ ²⁷ (0.017 - 0.023 Å). The S...H distances for **11** and $\text{Me}_2\text{P}(\text{S})\text{NHP}(\text{S})\text{Me}_2$ are in excellent agreement at

Table 3.4. Selected bond lengths (Å) and angles (°) for $\text{R}_2\text{P}(\text{E})\text{NHP}(\text{S})\text{R}_2$ (R = ⁿBu, ⁱBu), ${}^s\text{Bu}_2\text{P}(\text{S})\text{NHP}(\text{S}){}^i\text{Bu}_2$ and $\text{Me}_2\text{P}(\text{S})\text{NHP}(\text{S})\text{Me}_2$ ²⁷.

	$\text{HN}({}^n\text{Bu}_2\text{PS})_2$ 10	${}^s\text{Bu}_2\text{P}(\text{S})\text{NHP}(\text{S}){}^i\text{Bu}_2$ 15	$\text{HN}({}^i\text{Bu}_2\text{PS})_2$ 11	$\text{HN}(\text{Me}_2\text{PS})_2$
P(1)-S(1)	1.941(2)	1.943(1)	1.931(3)	1.939(2)
P(2)-S(2)	1.929(2)	1.935(2)	1.948(3)	1.962(2)
P(1)-N(1)	1.681(4)	1.686(3)	1.657(5)	1.679(3)
P(2)-N(1)	1.686(3)	1.695(3)	1.706(6)	1.675(3)
S(1)-P(1)-N(1)	109.3(1)	107.5(1)	114.4(3)	114.0(1)
S(2)-P(2)-N(1)	114.6(1)	113.9(1)	107.1(2)	107.9(1)
P(1)-N(1)-P(2)	132.1(2)	133.1(2)	133.0(4)	133.2(2)
S(1)-P(1)...P(2)-S(2)	179.0	179.4	179.8	176.9
S...H(1n)	2.439(4)	2.668(3)	2.513(4)	2.513(5)
N(1)-H(1n)	1.070(3)	1.077(4)	1.243(5)	0.894(5)

2.513 Å and the two *trans* dimers differ at 2.439(4) and 2.668(3) Å, the closer contact being with the straight chain n-butyl substituted ligand, which has significantly less steric bulk and thus would allow the two halves of the dimer to approach more closely. The P-N-P bond angles (132 - 133 °) are all in good agreement as are the P-N bond lengths with the exception of **11** (1.657(5), 1.706(6) Å) where the difference between P-N bonds does not correlate in any way with those for $\text{Me}_2\text{P}(\text{S})\text{NHP}(\text{S})\text{Me}_2$. There is a common trend for S-P-N bond angles, the larger angle (113.9 - 114.6 °) refers to the pendant sulfur and the smaller angle (107.1 - 109.3 °) refers to the sulfur involved in the intermolecular hydrogen bonding. The S-P...P-S torsion angles (176.9 - 179.8 °) show just how planar the SPNPS backbone is in the *trans* conformation.

3.3. Coordination Complexes of **10**, **11**, **12**, **13**, **14** and **15**.

Two moles of each neutral ligand were refluxed in THF with two moles of KO^tBu and one mole of ZnCl₂ for 30 minutes, then on cooling the solutions were evaporated to dryness and the residue was dissolved in the minimum of dichloromethane and filtered. The filtrate was evaporated to dryness revealing a

colourless oil in every case. The complexes decompose on silica and alumina and are extremely soluble. Furthermore the potassium salts of the ligands are soluble in ether making product purification extremely difficult. Reasonable elemental analyses were observed except for **20** and the expected parent ion was observed in FAB +ve mass spectra ($M + H$ 801 m/z) for all the zinc complexes; $Zn[nBu_2P(S)NP(S)^nBu_2]_2$ (**16**), $Zn[iBu_2P(S)NP(S)^iBu_2]_2$ (**17**), $Zn[sBu_2P(S)NP(S)^sBu_2]_2$ (**18**), $Zn[nBu_2P(S)NP(S)^iBu_2]_2$ (**19**), $Zn[nBu_2P(S)NP(S)^sBu_2]_2$ (**20**) and $Zn[sBu_2P(S)NP(S)^iBu_2]_2$ (**21**).

Square planar complexes were produced by the same procedure. Two moles of each neutral ligand were reacted with one mole of $PdCl_2COD$ (**10**, **11** and **12** were also reacted with $PtCl_2COD$). Again the products proved to be impure oils, dark red for the palladium complexes and yellow for the platinum complexes, which readily decompose on silica and alumina. Reasonable elemental analyses were observed and the expected parent ion was observed in FAB +ve mass spectra (Pd complexes: $M + H$ 843 m/z ; Pt complexes: $M + H$ 931 m/z) for each complex; $Pd[nBu_2P(S)NP(S)^nBu_2]_2$ (**22**), $Pd[iBu_2P(S)NP(S)^iBu_2]_2$ (**23**), $Pd[sBu_2P(S)NP(S)^sBu_2]_2$ (**24**), $Pd[nBu_2P(S)NP(S)^iBu_2]_2$ (**25**), $Pd[nBu_2P(S)NP(S)^sBu_2]_2$ (**26**), $Pd[sBu_2P(S)NP(S)^iBu_2]_2$ (**27**), $Pt[nBu_2P(S)NP(S)^nBu_2]_2$ (**28**), $Pt[iBu_2P(S)NP(S)^iBu_2]_2$ (**29**) and $Pt[sBu_2P(S)NP(S)^sBu_2]_2$ (**30**).

Signals observed in ^{31}P NMR ($CDCl_3$, Figure 3.5) showed a decrease in frequency upon deprotonation/coordination to the metal centres of around 20 ppm (Table 3.5) as was the case with **1**. Generally the shifts of the zinc and palladium complexes are in good agreement though the platinum complexes all have a chemical shift 5 ppm lower than their corresponding palladium complexes (compared to **8** which is 3.5 ppm lower than **6**). In addition the 2J platinum phosphorus coupling constants are around 12 Hz greater than **8**.

It is interesting to note the [P-P] coupling of $Zn[nBu_2P(S)NP(S)^iBu_2]_2$ is a 7 Hz less than the mixed substituent ligand complexes involving the sec-butyl group and that such a variance is not observed for the palladium complexes. In addition the 2J phosphorus coupling of the palladium complexes of the mixed substituent ligands is generally of a lower value than the zinc complexes. Despite running the spectra at a higher field strength and using zero filling, no $^4J(^{31}P-^{31}P)$ *trans* or *cis* couplings were observed for these complexes.

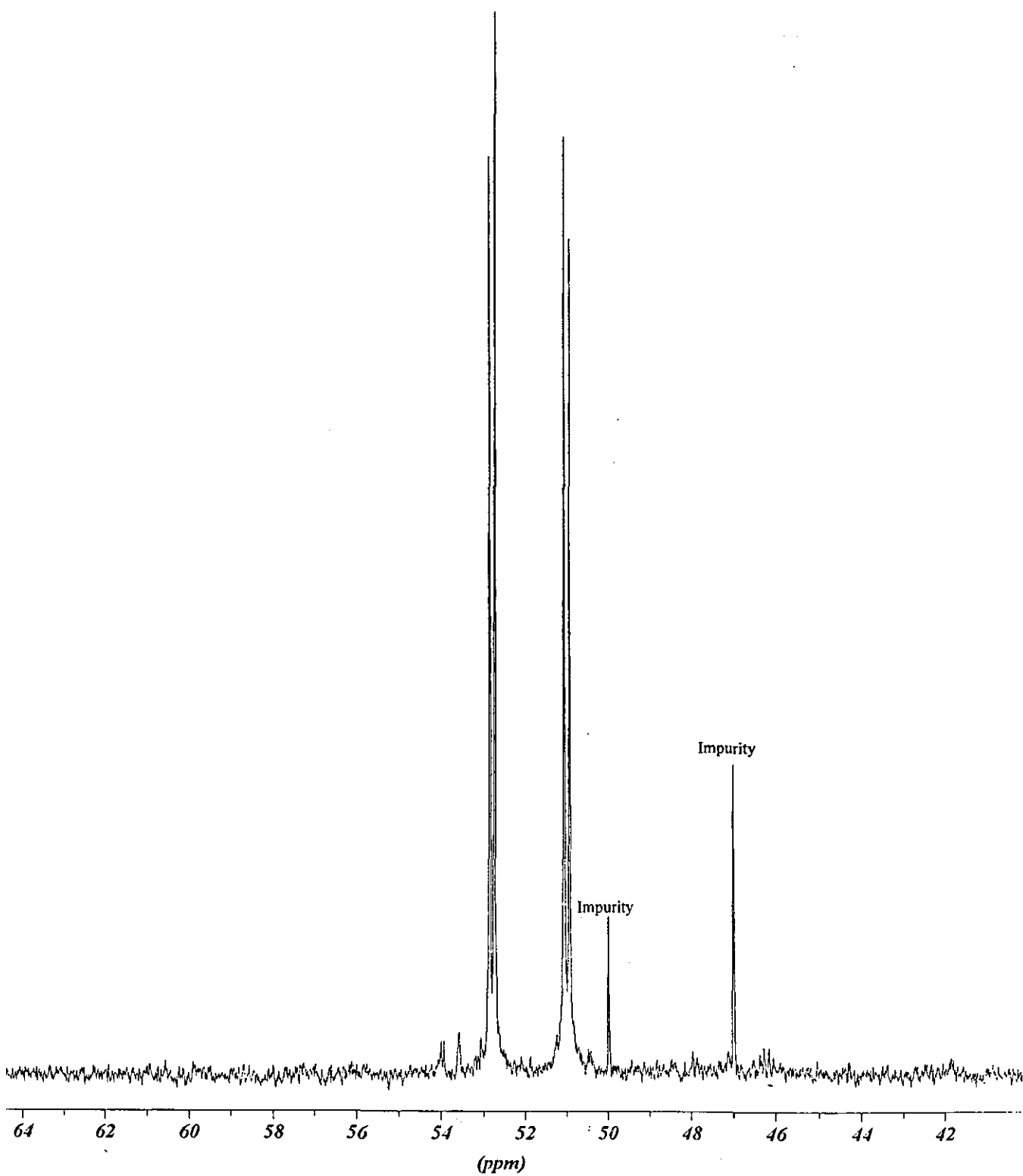


Figure 3.5. ^{31}P NMR AX type spectrum of $\text{Zn}[\text{nBu}_2\text{P}(\text{S})\text{NP}(\text{S})\text{Bu}_2]_2$.

Table 3.5. Chemical shifts and coupling constants in ^{31}P NMR (CDCl_3) for coordination complexes of $\text{R}_2\text{P}(\text{E})\text{NP}(\text{S})\text{R}'_2$ ($\text{R} = {}^n\text{Bu}, {}^i\text{Bu}, {}^s\text{Bu}$; $\text{R}' = {}^n\text{Bu}, {}^i\text{Bu}, {}^s\text{Bu}$). * denotes spectra run at 161.97 MHz, all others were run at 36.2 MHz.

	δ / ppm			${}^2J ({}^{31}\text{P}-{}^{31}\text{P}) / \text{Hz}$
	P_1	P_2	P_3	
$\text{Zn}[{}^n\text{Bu}_2\text{P}(\text{S})\text{NP}(\text{S}){}^n\text{Bu}_2]_2$ (16)	52.2	-	-	-
$\text{Zn}[{}^i\text{Bu}_2\text{P}(\text{S})\text{NP}(\text{S}){}^i\text{Bu}_2]_2$ (17)	-	49.1	-	-
$\text{Zn}[{}^s\text{Bu}_2\text{P}(\text{S})\text{NP}(\text{S}){}^s\text{Bu}_2]_2$ (18)	-	-	63.0	-
$\text{Zn}[{}^n\text{Bu}_2\text{P}(\text{S})\text{NP}(\text{S}){}^i\text{Bu}_2]_2$ (19)	51.5	49.6	-	19.8
$\text{Zn}[{}^n\text{Bu}_2\text{P}(\text{S})\text{NP}(\text{S}){}^s\text{Bu}_2]_2$ (20)	50.4	-	64.0	26.4
$\text{Zn}[{}^i\text{Bu}_2\text{P}(\text{S})\text{NP}(\text{S}){}^s\text{Bu}_2]_2$ (21)	-	48.7	63.4	26.4
$\text{Pd}[{}^n\text{Bu}_2\text{P}(\text{S})\text{NP}(\text{S}){}^n\text{Bu}_2]_2$ (22)	51.8	-	-	-
$\text{Pd}[{}^i\text{Bu}_2\text{P}(\text{S})\text{NP}(\text{S}){}^i\text{Bu}_2]_2$ (23)	-	49.7	-	-
$\text{Pd}[{}^s\text{Bu}_2\text{P}(\text{S})\text{NP}(\text{S}){}^s\text{Bu}_2]_2$ (24)	-	-	62.2	-
$\text{Pd}[{}^n\text{Bu}_2\text{P}(\text{S})\text{NP}(\text{S}){}^i\text{Bu}_2]_2^*$ (25)	52.0	50.2	-	16.8
$\text{Pd}[{}^n\text{Bu}_2\text{P}(\text{S})\text{NP}(\text{S}){}^s\text{Bu}_2]_2^*$ (26)	50.8	-	64.9	19.3
$\text{Pd}[{}^i\text{Bu}_2\text{P}(\text{S})\text{NP}(\text{S}){}^s\text{Bu}_2]_2^*$ (27)	-	49.1	64.3	18.2
-	-	-	-	${}^2J ({}^{31}\text{P}-{}^{195}\text{Pt}) / \text{Hz}$
$\text{Pt}[{}^n\text{Bu}_2\text{P}(\text{S})\text{NP}(\text{S}){}^n\text{Bu}_2]_2$ (28)	47.1	-	-	92.4
$\text{Pt}[{}^i\text{Bu}_2\text{P}(\text{S})\text{NP}(\text{S}){}^i\text{Bu}_2]_2$ (29)	-	43.8	-	88.0
$\text{Pt}[{}^s\text{Bu}_2\text{P}(\text{S})\text{NP}(\text{S}){}^s\text{Bu}_2]_2$ (30)	-	-	58.1	88.0

P_1 denotes the n-butyl, P_2 the iso-butyl and P_3 the sec-butyl substituted phosphorus atoms.

Characteristic bands in the FTIR ³²⁻³⁴ were observed indicating the change in bond order that occurs upon removal of the amine proton (Table 3.6), in particular the marked increase in the $\nu_{\text{as}}(\text{PNP})$ vibration to 1200 - 1230 cm^{-1} as the negative charge is delocalised over the ligand and the P-N bond lengths shorten. There is good agreement for the $\nu(\text{PS})$ vibration for all complexes. Two general observations are the $\nu(\text{PNP})$ values for the square planar complexes are slightly greater than those for the

Table 3.6. FTIR assignments (cm^{-1}) for the coordination complexes of $\text{R}_2\text{P}(\text{E})\text{NHP}(\text{S})\text{R}'_2$ ($\text{R} = {}^n\text{Bu}, {}^i\text{Bu}, {}^s\text{Bu}$; $\text{R}' = {}^n\text{Bu}, {}^i\text{Bu}, {}^s\text{Bu}$).

Zn complexes	ν (PNP)	ν (PS)	ν (NPS)
16	1227, 776	553	-
17	- , 782	558, 538	398
18	1211, 773	537	437
19	1225, 770	552	421, 401
20	1204, 780	550	432,401
21	1207, 780	525	438
Pd complexes			
22	1218	525	-
23	1258	544	401
24	1246	537	-
25	1220	542	-
26	1260	532	401
27	1248	531	-
Pt complexes			
28	1226	529	-
29	1246	541	400
30	1261	533	437

tetrahedral zinc complexes and the ν (NPS) bands seem to be observed more easily for the tetrahedral zinc complexes. These observations may well be due to the differing geometries of the complexes which were highlighted by the structures of 2, 3, 4, 6 and 8.

3.4. Experimental.

${}^n\text{Bu}_2\text{P}(\text{S})\text{Br}$, ${}^i\text{Bu}_2\text{P}(\text{S})\text{Br}$ and ${}^s\text{Bu}_2\text{P}(\text{S})\text{Br}$ were all synthesised by the same procedure illustrated here for ${}^n\text{Bu}_2\text{P}(\text{S})\text{Br}$. Under anhydrous conditions a solution of $\text{P}(\text{S})\text{Cl}_3$ (58.38 g, 35.0 ml, 0.34 M) in Et_2O (100 ml) was added dropwise at $0\text{ }^\circ\text{C}$ to a solution of BuMgBr (0.85M) in Et_2O agitated by an overhead stirrer. Upon completion of addition and warming to room temperature of the mixture it was refluxed for 2 hours. On cooling the mixture was quenched with aqueous 2M HCl (300 ml). The ether layer was then separated off and the aqueous layer washed with Et_2O (3 x 100ml). The ether layers were combined and evaporated to a very strongly smelling oily residue ($\text{Bu}_4\text{P}_2\text{S}_2$) which was subsequently dissolved in dichloromethane (200 ml). The solution was cooled to $0\text{ }^\circ\text{C}$ and a solution of Br_2 (27.92 g, 9 ml, 0.17 M) in dichloromethane (200 ml) was added dropwise with stirring turning the mixture a pink/brown colour. On warming to room temperature the now pungently smelling mixture was evaporated to dryness and the dark brown oily residue was distilled under vacuum (bp $118\text{-}125\text{ }^\circ\text{C}$ at 3-4 mmHg) to give ${}^n\text{Bu}_2\text{P}(\text{S})\text{Br}$, a faintly yellow coloured liquid, (34.3 g, 0.133 M, 39.2 % yield). ${}^{31}\text{P}\text{-}\{^1\text{H}\}$ NMR (CDCl_3): 92.0 ppm.

For ${}^i\text{Bu}_2\text{P}(\text{S})\text{Br}$, yellow/brown liquid (bp $116\text{-}120\text{ }^\circ\text{C}$ at 2-3 mmHg, 57.27 g, 0.223 M, 42.3 % yield). ${}^{31}\text{P}\text{-}\{^1\text{H}\}$ NMR (CDCl_3): 89.1 ppm.

For ${}^s\text{Bu}_2\text{P}(\text{S})\text{Br}$, yellow/brown liquid (bp $102\text{-}104\text{ }^\circ\text{C}$ at 0.5-1.5 mmHg, 34.64 g, 0.135 M, 37.3 % yield). ${}^{31}\text{P}\text{-}\{^1\text{H}\}$ NMR (CDCl_3): 124.5 ppm.

${}^n\text{Bu}_2\text{P}(\text{S})\text{NH}_2$, ${}^i\text{Bu}_2\text{P}(\text{S})\text{NH}_2$ and ${}^s\text{Bu}_2\text{P}(\text{S})\text{NH}_2$ were all synthesised by the same procedure illustrated here for ${}^n\text{Bu}_2\text{P}(\text{S})\text{NH}_2$. NH_3 gas was bubbled through a solution of ${}^n\text{Bu}_2\text{P}(\text{S})\text{Br}$ (10.0 g, 38.9 mmol) in Et_2O (200 ml) with stirring for 15-30 minutes. The mixture was then filtered and the NH_4Br solid residue was washed thoroughly with Et_2O (3 x 30 ml). The filtrate was then evaporated to dryness yielding a colourless oil (7.50 g, 38.9 mmol, 99.9 % yield). ${}^{31}\text{P}\text{-}\{^1\text{H}\}$ NMR (CDCl_3): 66.3 ppm.

For ${}^i\text{Bu}_2\text{P}(\text{S})\text{NH}_2$, white solid, (15.13 g, 78.4 mmol, 100 % yield). ${}^{31}\text{P}\text{-}\{^1\text{H}\}$ NMR (CDCl_3): 67.0 ppm.

For ${}^s\text{Bu}_2\text{P}(\text{S})\text{NH}_2$, faintly brown oil, (8.21 g, 42.5 mmol, 98.6 % yield). ${}^{31}\text{P}\text{-}\{^1\text{H}\}$ NMR (CDCl_3): 81.0 ppm.

ⁿBu₂P(S)NHP(S)ⁿBu₂ 10. A slurry of NaH (60% dispersion in paraffin oil 1.24 g, 31.0 mmol) in THF (10 ml) was added dropwise to a solution of ⁿBu₂P(S)NH₂ (2.00 g, 10.4 mmol) in THF (40 ml) at 0 °C with stirring. On warming to room temperature the mixture was left for a further 30 minutes, then it was cooled again to 0 °C and a solution of ⁿBu₂P(S)Br (2.66 g, 10.4 mmol) in THF (10 ml) was added dropwise. The mixture was then refluxed overnight. On cooling, MeOH (10 ml) was cautiously added dropwise to destroy off any excess NaH. An excess of 85 % HBF₄.OEt₂ in Et₂O (8 ml) was then added with stirring to protonate the Na⁺ [N(ⁿBu₂PS)₂]⁻ salt. The mixture was evaporated to dryness and washed with dichloromethane (3 x 20 ml). The resulting filtrate was evaporated to dryness giving a clear oily residue. This was then dissolved in the minimum of dichloromethane and cooled overnight in a freezer yielding colourless crystals (2.45 g, 6.63 mmol, 64 % yield, mp 61 °C). Microanalysis calculated for C₁₆H₃₇NP₂S₂: C 52.0; H 10.1; N 3.8 %. Observed: C 52.1; H 10.4; N 3.5 %. ³¹P-¹H NMR (CDCl₃): 71.0 ppm; ¹H NMR (CDCl₃): 3.15 ppm NH proton. FTIR (dichloromethane solution, CsI cell at 100 microns): ν (N-H) 3325 cm⁻¹; (KBr disc): ν (N-H) 3172; δ (N-H) 1319; ν (PNP) 930, 907, 767 cm⁻¹. FT Raman (capillary sample): ν (N-H) 3166; δ (N-H) 1344; ν (PNP) 971; ν (PS) 587 cm⁻¹. CI +ve MS: m/z 370 corresponds to {HN(ⁿBu₂PS)₂}⁺.

Zn[N(ⁿBu₂PS)₂]₂ 16. A solution of **10** (0.080 g, 0.217 mmol), ZnCl₂ (0.015 g, 0.109 mmol) and KO^tBu (0.024 g, 0.214 mmol) in THF (20 ml) was refluxed for 1 hour. On cooling the mixture was evaporated to dryness and dichloromethane added. The mixture was then filtered and the filtrate evaporated to dryness, giving a colourless oil. Microanalysis calculated for C₃₂H₇₂N₂P₄S₄Zn: C 47.9; H 9.0; N 3.5 %. Observed: C 48.2; H 8.8; N 3.4 %. ³¹P-¹H NMR (CDCl₃): 52.0 ppm. FTIR (KBr disc): ν (PNP) 1227, 1186, 775; ν (PS) 553 cm⁻¹. FAB +ve MS: m/z 801 corresponds to {Zn[N(ⁿBu₂PS)₂]₂}⁺.

Pd[N(ⁿBu₂PS)₂]₂ 22. A solution of **10** (0.10 g, 0.271 mmol), PdCl₂COD (0.039 g, 0.137 mmol) and KO^tBu (0.030 g, 0.271 mmol) in THF (20 ml) was refluxed for 1 hour changing colour from yellow to red/orange. On cooling the mixture was evaporated to dryness and dichloromethane added. The mixture was then filtered and

the filtrate evaporated to dryness, giving a dark red oil. Microanalysis calculated for $C_{32}H_{72}N_2P_4S_4Pd$: C 45.6; H 8.6; N 3.3 %. Observed : C 48.9; H 9.2; N 3.3 %. ^{31}P - $\{^1H\}$ NMR ($CDCl_3$): 51.8 ppm. FTIR (KBr disc): ν (PNP) 1218, 1151; ν (PS) 606, 525 cm^{-1} . FAB +ve MS: m/z 843 corresponds to $\{Pd[N(^nBu_2PS)_2]_2\}^+$.

$Pt[N(^nBu_2PS)_2]_2$ **28**. A solution of **10** (0.083 g, 0.225 mmol), $PtCl_2COD$ (0.042 g, 0.112 mmol) and KO^tBu (0.025 g, 0.225 mmol) in THF (20 ml) was refluxed for 1 hour changing colour from clear to yellow. On cooling the mixture was evaporated to dryness and dichloromethane added. The mixture was then filtered and the filtrate evaporated to dryness, giving a yellow oil. Microanalysis calculated for $C_{32}H_{72}N_2P_4S_4Pt$: C 41.2; H 7.8; N 3.0 %. Observed : C 46.0; H 8.5; N 2.4 %. ^{31}P - $\{^1H\}$ NMR ($CDCl_3$): 47.1 ppm, $^2J(^{31}P-^{195}Pt)$ 92.4 Hz. FTIR (KBr disc): ν (PNP) 1226; ν (PS) 529 cm^{-1} . FAB +ve MS: m/z 931 corresponds to $\{Pt[N(^nBu_2PS)_2]_2\}^+$.

$^iBu_2P(S)NHP(S)^iBu_2$ **11**. **11** was prepared with the same procedure as **10** giving a clear oily residue. This was then dissolved in the minimum of dichloromethane and cooled overnight in a freezer yielding colourless crystals (2.35 g, 6.37 mmol, 41 % yield, mp 66-68 °C). Microanalysis calculated for $C_{16}H_{37}NP_2S_2$: C 52.0; H 10.1; N 3.8 %. Observed : C 52.0; H 10.3 ; N 3.2 %. ^{31}P - $\{^1H\}$ NMR ($CDCl_3$): 68.3 ppm; 1H NMR ($CDCl_3$) 3.12 ppm NH proton. FTIR (dichloromethane solution, CsI cell at 100 microns): ν (N-H) 3323 cm^{-1} ; (KBr disc): ν (N-H) 3180; δ (N-H) 2720, 1367; ν (PNP) 916, 782 cm^{-1} .

$Zn[N(^iBu_2PS)_2]_2$ **17**. A solution of **11** (0.075 g, 0.203 mmol), $ZnCl_2$ (0.014 g, 0.103 mmol) and KO^tBu (0.023 g, 0.205 mmol) in THF (20 ml) was refluxed for 1 hour. On cooling the mixture was evaporated to dryness and dichloromethane added. The mixture was then filtered and the filtrate evaporated to dryness, giving a colourless oil. Microanalysis calculated for $C_{32}H_{72}N_2P_4S_4Zn$: C 47.9; H 9.0; N 3.5 %. Observed : C 51.5; H 9.5; N 3.0 %. ^{31}P - $\{^1H\}$ NMR ($CDCl_3$): 49.1 ppm. FTIR (KBr disc): ν (PNP) 1251, 1163, 782; ν (PS) 558, 538; ν (NPS) 398 cm^{-1} . FAB +ve MS: m/z 801 corresponds to $\{Zn[N(^iBu_2PS)_2]_2\}^+$.

$\text{Pd}[\text{N}(\text{}^i\text{Bu}_2\text{PS})_2]_2$ **23**. A solution of **11** (0.050 g, 0.136 mmol), PdCl_2COD (0.019 g, 0.067 mmol) and KO^iBu (0.015 g, 0.134 mmol) in THF (20 ml) was refluxed for 1 hour changing colour from yellow to red/orange. On cooling the mixture was evaporated to dryness and dichloromethane added. The mixture was then filtered and the filtrate evaporated to dryness, giving a dark red oil. Microanalysis calculated for $\text{C}_{32}\text{H}_{72}\text{N}_2\text{P}_4\text{S}_4\text{Pd}$: C 45.6; H 8.6; N 3.3 %. Observed : C 47.8; H 8.9; N 2.7 %. ^{31}P - $\{^1\text{H}\}$ NMR (CDCl_3): 49.7 ppm. FTIR (KBr disc): ν (PNP) 1258, 1165; ν (PS) 544; ν (NPS) 401 cm^{-1} . FAB +ve MS: m/z 843 corresponds to $\{\text{Pd}[\text{N}(\text{}^i\text{Bu}_2\text{PS})_2]_2\}^+$.

$\text{Pt}[\text{N}(\text{}^i\text{Bu}_2\text{PS})_2]_2$ **29**. A solution of **11** (0.050 g, 0.136 mmol), PtCl_2COD (0.025 g, 0.068 mmol) and KO^iBu (0.015 g, 0.134 mmol) in THF (20 ml) was refluxed for 1 hour changing colour from clear to yellow. On cooling the mixture was evaporated to dryness and dichloromethane added. The mixture was then filtered and the filtrate evaporated to dryness, giving a yellow oil. Microanalysis calculated for $\text{C}_{32}\text{H}_{72}\text{N}_2\text{P}_4\text{S}_4\text{Pt}$: C 41.2; H 7.8; N 3.0 %. Observed : C 45.9; H 8.1; N 2.5 %. ^{31}P - $\{^1\text{H}\}$ NMR (CDCl_3): 43.8 ppm, $^2J(^{31}\text{P}$ - $^{195}\text{Pt})$ 88.0 Hz. FTIR (KBr disc): ν (PNP) 1246, 1159; ν (PS) 557, 541; ν (NPS) 400 cm^{-1} . FAB +ve MS: m/z 931 corresponds to $\{\text{Pt}[\text{N}(\text{}^i\text{Bu}_2\text{PS})_2]_2\}^+$.

${}^s\text{Bu}_2\text{P}(\text{S})\text{NHP}(\text{S}){}^s\text{Bu}_2$ **12**. **12** was prepared with the same procedure as **10** giving a clear oily residue. This was then dissolved in the minimum of dichloromethane and cooled overnight in a freezer yielding colourless crystals (1.99 g, 5.39 mmol, 52 % yield, mp 93-95 $^\circ\text{C}$). Microanalysis calculated for $\text{C}_{16}\text{H}_{37}\text{NP}_2\text{S}_2$: C 52.0; H 10.1; N 3.8 %. Observed : C 52.4; H 9.9 ; N 3.7 %. ^{31}P - $\{^1\text{H}\}$ NMR (CDCl_3): 87.2 ppm; ^1H NMR (CDCl_3) 2.80 ppm NH proton. FTIR (dichloromethane solution, CsI cell at 100 microns): ν (N-H) 3323 cm^{-1} ; (KBr disc): ν (N-H) 3180; δ (N-H) 2720, 1367; ν (PNP) 916, 782 cm^{-1} . FAB +ve MS: m/z 370 corresponds to $\{\text{HN}(\text{}^s\text{Bu}_2\text{PS})_2\}^+$.

$\text{Zn}[\text{N}(\text{}^s\text{Bu}_2\text{PS})_2]_2$ **18**. A solution of **12** (0.108 g, 0.292 mmol), ZnCl_2 (0.020 g, 0.147 mmol) and KO^iBu (0.033 g, 0.294 mmol) in THF (20 ml) was refluxed for 1 hour. On cooling the mixture was evaporated to dryness and dichloromethane added. The mixture was then filtered and the filtrate evaporated to dryness, giving a colourless oil.

Microanalysis calculated for $C_{32}H_{72}N_2P_4S_4Zn$: C 47.9; H 9.0; N 3.5 %. Observed : C 48.7; H 9.0; N 2.9 %. ^{31}P - $\{^1H\}$ NMR ($CDCl_3$): 62.8 ppm. FTIR (KBr disc): ν (PNP) 1211, 773; ν (PS) 587, 537 cm^{-1} . FAB +ve MS: m/z 801 corresponds to $\{Zn[N(^tBu_2PS)_2]_2\}^+$.

$Pd[N(^tBu_2PS)_2]_2$ **24**. A solution of **12** (0.130 g, 0.352 mmol), $PdCl_2COD$ (0.050 g, 0.175 mmol) and KO^tBu (0.040 g, 0.357 mmol) in THF (20 ml) was refluxed for 1 hour changing colour from yellow to red/orange. On cooling the mixture was evaporated to dryness and dichloromethane added. The mixture was then filtered and the filtrate evaporated to dryness, giving a dark red oil. Microanalysis calculated for $C_{32}H_{72}N_2P_4S_4Pd$: C 45.6; H 8.6; N 3.3 %. Observed : C 49.5; H 9.0; N 2.6 %. ^{31}P - $\{^1H\}$ NMR ($CDCl_3$): 62.2 ppm. FTIR (KBr disc): ν (PNP) 1241, 1206; ν (PS) 575, 537 cm^{-1} . FAB +ve MS: m/z 843 corresponds to $\{Pd[N(^tBu_2PS)_2]_2\}^+$.

$Pt[N(^tBu_2PS)_2]_2$ **30**. A solution of **12** (0.050 g, 0.136 mmol), $PtCl_2COD$ (0.025 g, 0.068 mmol) and KO^tBu (0.015 g, 0.134 mmol) in THF (20 ml) was refluxed for 1 hour changing colour from clear to yellow. On cooling the mixture was evaporated to dryness and dichloromethane added. The mixture was then filtered and the filtrate evaporated to dryness, giving a yellow oil. Microanalysis calculated for $C_{32}H_{72}N_2P_4S_4Pt$: C 41.2; H 7.8; N 3.0 %. Observed : C 40.7; H 7.4; N 2.5 %. ^{31}P - $\{^1H\}$ NMR ($CDCl_3$): 58.1 ppm, $^2J(^{31}P-^{195}Pt)$ 88.0 Hz. FTIR (KBr disc): ν (PNP) 1261, 1208; ν (PS) 578, 533; ν (NPS) 437 cm^{-1} . FAB +ve MS: m/z 931 corresponds to $\{Pt[N(^tBu_2PS)_2]_2\}^+$.

$^nBu_2P(S)NHP(S)^iBu_2$ **13**. **13** was prepared with the same procedure as **10** giving a clear oily residue which was cooled in a freezer and over two months crystallised into a very low temperature melting solid. Microanalysis calculated for $C_{16}H_{37}NP_2S_2$: C 52.0; H 10.1; N 3.8 %. Observed : C 54.5; H 10.3; N 3.1 %. ^{31}P - $\{^1H\}$ NMR ($CDCl_3$): $\delta(P_A)$ 72.3(d), $\delta(P_X)$ 70.4(d) ppm. $^2J(^{31}P_A-^{31}P_X)$ 26.4 Hz. FTIR (KBr disc): δ (N-H) 1340; ν (PNP) 909, 745 cm^{-1} . FAB +ve MS: m/z 370 corresponds to $\{^nBu_2P(S)NHP(S)^iBu_2\}^+$.

Zn[ⁿBu₂P(S)NP(S)ⁱBu₂]₂ **19**. A solution of **13** (0.050 g, 0.136 mmol), ZnCl₂ (0.010 g, 0.073 mmol) and KO^tBu (0.015 g, 0.134 mmol) in THF (20 ml) was refluxed for 1 hour. On cooling the mixture was evaporated to dryness and dichloromethane added. The mixture was then filtered and the filtrate evaporated to dryness, giving a colourless oil. Microanalysis calculated for C₃₂H₇₂N₂P₄S₄Zn: C 47.9; H 9.0; N 3.5 %. Observed: C 51.9; H 9.7; N 3.0 %. ³¹P-¹H NMR (CDCl₃): δ(P_A) 51.5(d), δ(P_X) 49.6 ppm. ²J(³¹P_A-³¹P_X) 19.8 Hz. FTIR (KBr disc): ν (PNP) 1248, 1225, 807; ν (PS) 588, 552; ν (NPS) 421, 401 cm⁻¹. FAB +ve MS: m/z 801 corresponds to {Zn[ⁿBu₂P(S)NP(S)ⁱBu₂]₂}⁺.

Pd[ⁿBu₂P(S)NP(S)ⁱBu₂]₂ **25**. A solution of **13** (0.130 g, 0.352 mmol), PdCl₂COD (0.050 g, 0.175 mmol) and KO^tBu (0.040 g, 0.357 mmol) in THF (20 ml) was refluxed for 1 hour changing colour from yellow to red/orange. On cooling the mixture was evaporated to dryness and dichloromethane added. The mixture was then filtered and the filtrate evaporated to dryness, giving a dark red oil. Microanalysis calculated for C₃₂H₇₂N₂P₄S₄Pd: C 45.6; H 8.6; N 3.3 %. Observed : C 53.0; H 9.3; N 2.5 %. ³¹P-¹H NMR (CDCl₃): δ(P_A) 52.0(d), δ(P_X) 50.2(d) ppm. ²J(³¹P_A-³¹P_X) 16.8 Hz. FTIR (KBr disc): ν (PNP) 1220, 1164; ν (PS) 542 cm⁻¹. FAB +ve MS: m/z 843 corresponds to {Pd[ⁿBu₂P(S)NP(S)ⁱBu₂]₂}⁺.

ⁿBu₂P(S)NHP(S)^sBu₂ **14**. **14** was prepared with the same procedure as **10** giving a clear oily residue which was cooled in a freezer and over a period of two months crystallised into a very low temperature melting solid. Microanalysis calculated for C₁₆H₃₇NP₂S₂ : C 52.0; H 10.1; N 3.8 %. Observed : C 52.0; H 9.9; N 2.6 %. ³¹P-¹H NMR (CDCl₃): δ(P_A) 79.0(d), δ(P_X) 84.7(d) ppm. ²J(³¹P_A-³¹P_X) 30.8 Hz. FTIR (KBr disc): δ (N-H) 1347; ν (PNP) 913, 744 cm⁻¹. FAB +ve MS: m/z 370 corresponds to {ⁿBu₂P(S)NHP(S)^sBu₂}⁺.

Zn[ⁿBu₂P(S)NP(S)^sBu₂]₂ **20**. A solution of **14** (0.050 g, 0.136 mmol), ZnCl₂ (0.010 g, 0.073 mmol) and KO^tBu (0.015 g, 0.134 mmol) in THF (20 ml) was refluxed for 1 hour. On cooling the mixture was evaporated to dryness and dichloromethane added.

The mixture was then filtered and the filtrate evaporated to dryness, giving a colourless oil. $^{31}\text{P}\{-^1\text{H}\}$ NMR (CDCl_3): $\delta(\text{P}_\text{A})$ 50.4(d), $\delta(\text{P}_\text{X})$ 64.0(d) ppm. $^2\text{J}(^{31}\text{P}_\text{A}\text{-}^{31}\text{P}_\text{X})$ 26.4 Hz. FTIR (KBr disc): ν (PNP) 1259, 1204, 780; ν (PS) 579, 550; ν (NPS) 401 cm^{-1} . FAB +ve MS: m/z 801 corresponds to $\{\text{Zn}[\text{}^n\text{Bu}_2\text{P(S)NP(S)}^s\text{Bu}_2]_2\}^+$.

$\text{Pd}[\text{}^n\text{Bu}_2\text{P(S)NP(S)}^s\text{Bu}_2]_2$ **26**. A solution of **14** (0.050 g, 0.136 mmol), PdCl_2COD (0.019 g, 0.067 mmol) and KO^tBu (0.015 g, 0.134 mmol) in THF (20 ml) was refluxed for 1 hour changing colour from yellow to red/orange. On cooling the mixture was evaporated to dryness and dichloromethane added. The mixture was then filtered and the filtrate evaporated to dryness, giving a dark red oil. Microanalysis calculated for $\text{C}_{32}\text{H}_{72}\text{N}_2\text{P}_4\text{S}_4\text{Pd}$: C 45.6; H 8.6; N 3.3 %. Observed : C 47.1; H 9.3; N 2.1 %. $^{31}\text{P}\{-^1\text{H}\}$ NMR (CDCl_3): $\delta(\text{P}_\text{A})$ 50.8(d), $\delta(\text{P}_\text{X})$ 64.9(d) ppm. $^2\text{J}(^{31}\text{P}_\text{A}\text{-}^{31}\text{P}_\text{X})$ 19.3 Hz. FTIR (KBr disc): ν (PNP) 1260; ν (PS) 532; ν (NPS) 401 cm^{-1} . FAB +ve MS: m/z 843 corresponds to $\{\text{Pd}[\text{}^n\text{Bu}_2\text{P(S)NP(S)}^s\text{Bu}_2]_2\}^+$.

$^s\text{Bu}_2\text{P(S)NHP(S)}^i\text{Bu}_2$ **15**. **15** was prepared with the same procedure as **10** giving a clear oily residue which was cooled overnight in a freezer yielding colourless crystals (0.213 g, 0.577 mmol, 5.6 % yield, mp 20-30 $^\circ\text{C}$). Microanalysis calculated for $\text{C}_{16}\text{H}_{37}\text{NP}_2\text{S}_2$: C 52.0; H 10.1; N 3.8 %. Observed : C 51.5; H 10.1 ; N 3.7 %. $^{31}\text{P}\{-^1\text{H}\}$ NMR (CDCl_3): $\delta(\text{P}_\text{A})$ 76.0(d), $\delta(\text{P}_\text{X})$ 82.7(d) ppm. $^2\text{J}(^{31}\text{P}_\text{A}\text{-}^{31}\text{P}_\text{X})$ 30.8 Hz. FTIR (KBr disc): δ (N-H) 1337; ν (PNP) 918, 772 cm^{-1} . FAB +ve MS: m/z 370 corresponds to $\{\text{}^s\text{Bu}_2\text{P(S)NHP(S)}^i\text{Bu}_2\}^+$.

$\text{Zn}[\text{}^s\text{Bu}_2\text{P(S)NP(S)}^i\text{Bu}_2]_2$ **21**. A solution of **15** (0.050 g, 0.136 mmol), ZnCl_2 (0.010 g, 0.073 mmol) and KO^tBu (0.015 g, 0.134 mmol) in THF (20 ml) was refluxed for 1 hour. On cooling the mixture was evaporated to dryness and dichloromethane added. The mixture was then filtered and the filtrate evaporated to dryness, giving a colourless oil. Microanalysis calculated for $\text{C}_{32}\text{H}_{72}\text{N}_2\text{P}_4\text{S}_4\text{Zn}$: C 47.9; H 9.0; N 3.5 %. Observed : C 50.0; H 9.3; N 3.5 %. $^{31}\text{P}\{-^1\text{H}\}$ NMR (CDCl_3): $\delta(\text{P}_\text{A})$ 48.7(d), $\delta(\text{P}_\text{X})$ 63.4(d) ppm. $^2\text{J}(^{31}\text{P}_\text{A}\text{-}^{31}\text{P}_\text{X})$ 26.4 Hz. FTIR (KBr disc): ν (PNP) 1259, 1207, 780; ν (PS) 525; ν (NPS) 438 cm^{-1} . FAB +ve MS: m/z 801 corresponds to $\{\text{Zn}[\text{}^s\text{Bu}_2\text{P(S)NP(S)}^i\text{Bu}_2]_2\}^+$.

$\text{Pd}[\text{}^s\text{Bu}_2\text{P}(\text{S})\text{NP}(\text{S})\text{}^i\text{Bu}_2]_2$ **27**. A solution of **15** (0.050 g, 0.136 mmol), PdCl_2COD (0.019 g, 0.067 mmol) and KO^tBu (0.015 g, 0.134 mmol) in THF (20 ml) was refluxed for 1 hour changing colour from yellow to red/orange. On cooling the mixture was evaporated to dryness and dichloromethane added. The mixture was then filtered and the filtrate evaporated to dryness, giving a dark red oil. Microanalysis calculated for $\text{C}_{32}\text{H}_{72}\text{N}_2\text{P}_4\text{S}_4\text{Pd}$: C 45.6; H 8.6; N 3.3 %. Observed : C 44.5; H 8.5; N 3.1 %. ^{31}P - $\{^1\text{H}\}$ NMR (CDCl_3): $\delta(\text{P}_A)$ 49.1(d), $\delta(\text{P}_X)$ 64.3(d) ppm. $^2\text{J}(^{31}\text{P}_A-^{31}\text{P}_X)$ 18.2 Hz. FTIR (KBr disc): ν (PNP) 1248, 1164; ν (PS) 531 cm^{-1} . FAB +ve MS: m/z 843 corresponds to $\{\text{Pd}[\text{}^s\text{Bu}_2\text{P}(\text{S})\text{NP}(\text{S})\text{}^i\text{Bu}_2]_2\}^+$.

CHAPTER 4:
DIETHOXY-DIPHENYL-DITHIOIMIDODIPHOSPHINATE,
ITS MIXED SULFUR / OXYGEN ANALOGUES AND THEIR
COORDINATION CHEMISTRY

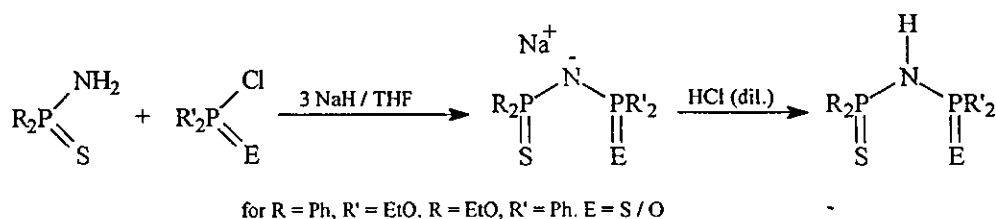
4.1. Introduction.

Further to our work on alkyl substituted dithioimidodiphosphinates with varying steric effects, we have also studied imidodiphosphinates with varying electronic effects, namely substituent groups of differing electronic character (ethoxy and phenyl), and differing donor atoms on each phosphorus. The three compounds $(\text{EtO})_2\text{P}(\text{S})\text{NHP}(\text{S})\text{Ph}_2$ (**31**), $(\text{EtO})_2\text{P}(\text{S})\text{NHP}(\text{O})\text{Ph}_2$ (**32**) and $(\text{EtO})_2\text{P}(\text{O})\text{NHP}(\text{S})\text{Ph}_2$ (**33**) were synthesised and coordinated to platinum, palladium and zinc.

RESULTS AND DISCUSSION

4.2. Ligand Syntheses.

The syntheses of **31**, **32** and **33** were based upon a literature preparation for preparing compounds with mixed substituent groups²¹ (Equation 4.1). The amine and halide are “clipped” together with sodium hydride in THF. It should be noted the mixed S / O compounds are unstable to heat. The salts were then protonated with dilute hydrochloric acid giving the neutral ligands as oils which were recrystallised from the minimum of dichloromethane and petroleum ether giving colourless crystals (70 - 80 % yields) pure by elemental analyses. Characteristic bands were observed



Eqn 4.1.

in the FTIR, ν (NH) 3060, δ (NH) 1344 - 1315, ν (PO) 1196 - 1186, ν (PNP) 976 - 936, 787 - 754 and ν (PS) 646 - 630 cm^{-1} . ν (NH) could not be confidently assigned for **31**.

The ^{31}P NMR spectra (CDCl_3 , Table 4.1) are of the AX type. For **31** the phosphorus centre with ethoxy substituents appears around 64 ppm as opposed to 53 ppm for the phenyl substituted phosphorus with ^2J phosphorus coupling of 22.0 Hz in reasonable agreement for disulfur compounds of this type. However it is interesting to note the decrease in frequency for the phosphorus centres when the sulfur is replaced by an oxygen. In **32** the phenyl substituted phosphorus centre is reduced by 33 ppm

Table 4.1. Chemical shifts and [P-P] coupling constants in ^{31}P NMR (CDCl_3) for $(\text{EtO})_2\text{P}(\text{E})\text{NHP}(\text{S})\text{Ph}_2$ (E = S/O) and $(\text{EtO})_2\text{P}(\text{S})\text{NHP}(\text{O})\text{Ph}_2$.

	δ / ppm		$^2\text{J} (^{31}\text{P}-^{31}\text{P}) / \text{Hz}$
	P_1	P_2	
$(\text{EtO})_2\text{P}(\text{S})\text{NHP}(\text{S})\text{Ph}_2$ 31	63.6	53.3	22.0
$(\text{EtO})_2\text{P}(\text{S})\text{NHP}(\text{O})\text{Ph}_2$ 32	64.1	19.7	17.6
$(\text{EtO})_2\text{P}(\text{O})\text{NHP}(\text{S})\text{Ph}_2$ 33	0.1	53.3	13.2

P_1 denotes the ethoxy substituted phosphorus atoms.

P_2 denotes the phenyl substituted phosphorus atoms.

and the ^2J [P-P] coupling is reduced by around 4 Hz in contrast to the ethoxy substituted phosphorus in **33** where the decrease is 64 ppm and the ^2J phosphorus coupling is reduced by 9 Hz. Evidently the larger differences seen in the case of **33** are due to a greater electron withdrawing effect. Furthermore solid state ^{31}P NMR was studied for **31** giving a doublet as expected (63.5, 52.6 ppm, $^2\text{J} \{^{31}\text{P}-^{31}\text{P}\} = 1324.5$ Hz) for the two inequivalent phosphorus environments.

All three compounds were studied by X-ray single crystal analysis. **31** was observed to be a unique *cisoid* dimer (Figure 4.1), the phosphorus with the phenyl substituents being pendant thus reducing any steric crowding. The SP...PS torsion angle is 87.0° which is comparable to the *cisoid* **1** (79°). The P(1)-S(1) bond at 1.937(1) Å is considerably longer than the pendant P(2)-S(2) bond length of 1.920(2)

Å as expected. Indeed the S \cdots H hydrogen bond is relatively strong at 2.452(3) Å while the N(1)-H(1n) bond length is 1.063(2) Å in good agreement with the alkyl substituted dimers from Chapter 3. The P-N bonds are 1.67 - 1.68 Å and the P-N-P bond angle is 129.9(2) °.

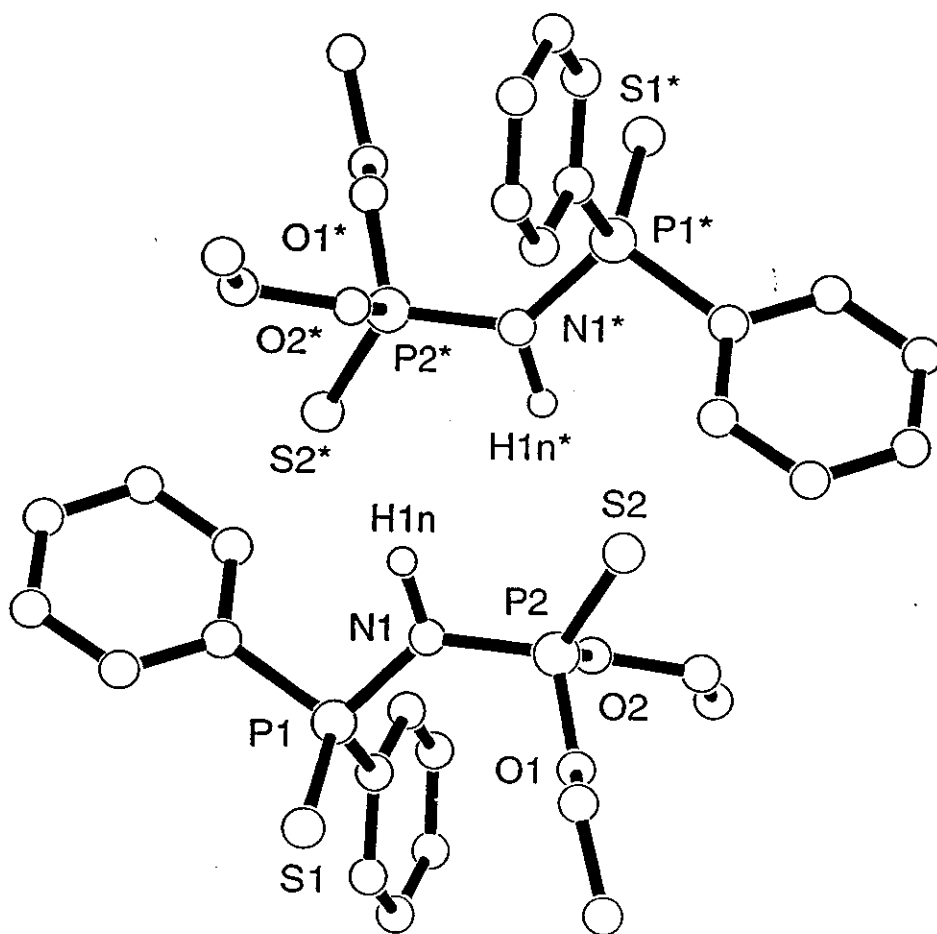


Figure 4.1. Crystal structure of (EtO) $_2$ P(S)NHP(S)Ph $_2$ dimer.

33 was found to be a typical *trans* dimer (Figure 4.2) with a SP...PO torsion angle of 172.3 °, much closer to the planar SPNPS backbone as has been observed previously. As expected the hydrogen bonding contact to form the dimer is through the oxygen, again with the phenyls substituted on the pendant phosphorus. The P(1)-

S(1) bond length is 1.931(1) Å and the P(2)-O(1) bond length is 1.457(2) Å. The P(2)-N(1) bond length of 1.632(3) Å is short compared to the P(1)-N(1) length of 1.679(3) Å. The N(1)-H(1n) bond length is 0.925(2) Å, the O⁻H hydrogen bond is 1.876(4) Å and the P-N-P bond angle is 130.5(1)°.

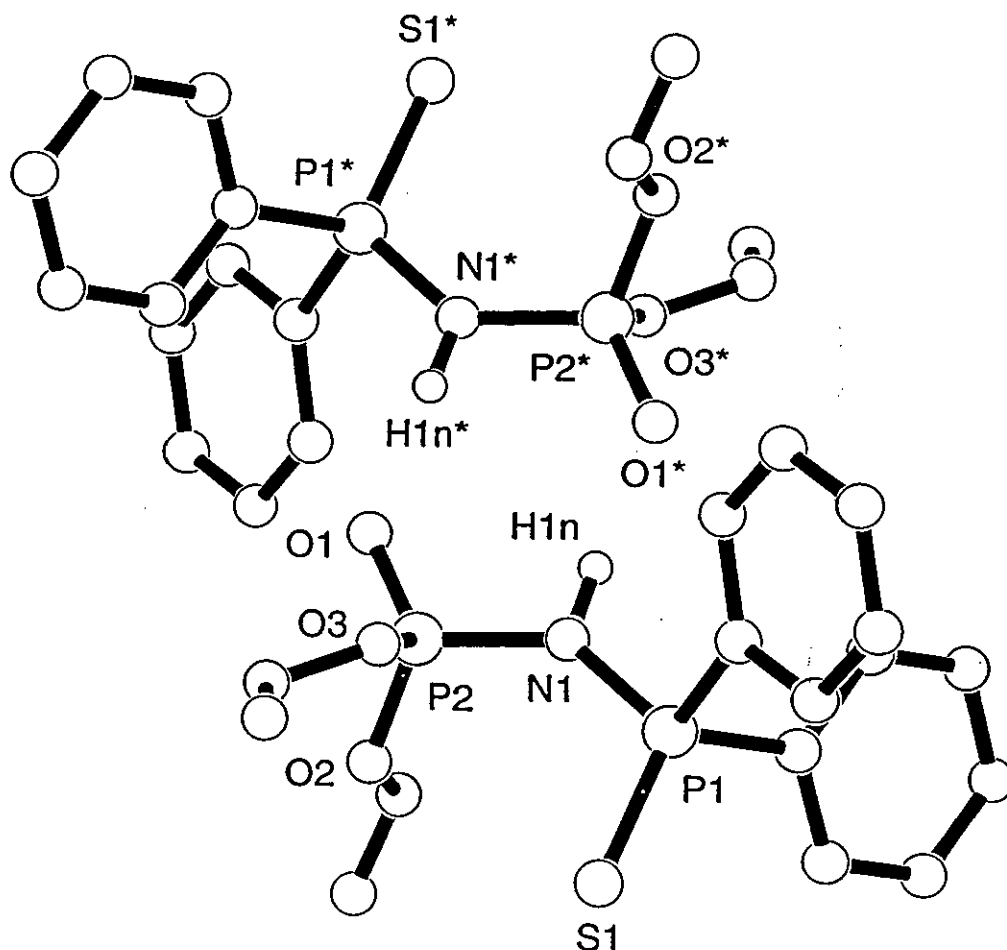


Figure 4.2. Crystal structure of (EtO)₂P(O)NHP(S)Ph₂ dimer.

In contrast to the *trans* dimers, **32** is a *cisoid* structure (Figure 4.3) with a SP...PO torsion angle of 79.5° and exists as an hydrogen bonded chain similar to **1**. Whilst the hydrogen bonding is through the oxygen, there is far too much steric hindrance from the phenyl substituents on the phosphorus to allow the formation of a dimer. The P(2)-S(1) bond length at 1.895(3) Å is slightly shorter than previously observed P-S bonds and the P(2)-N(1) bond length of 1.662(4) Å is not significantly

different to the P(1)-N(1) bond at 1.673(4) Å. The P(1)-O(1) bond is 1.476(3) Å, the N(1)-H(1n) bond is 1.064(3) Å and the P-N-P angle is 122.6(2) °, the smallest angle P-N-P observed in this work.

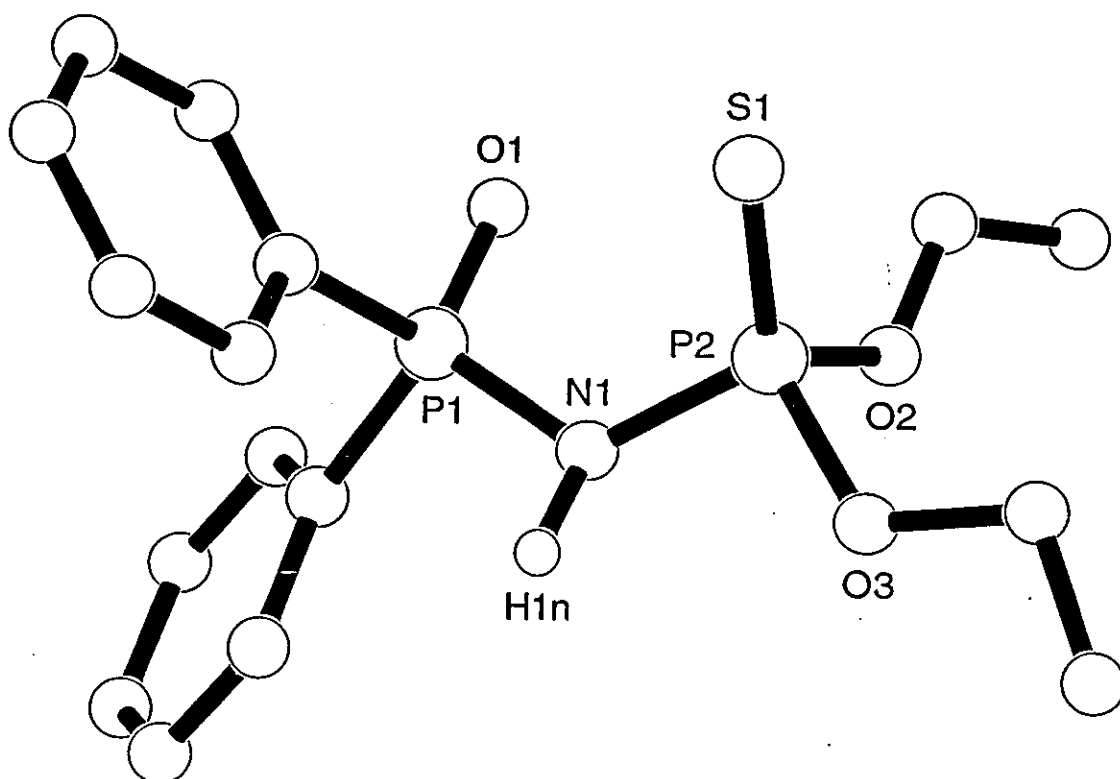


Figure 4.3. Crystal structure of $(\text{EtO})_2\text{P}(\text{S})\text{NHP}(\text{O})\text{Ph}_2$.

It is interesting to note (Table 4.2) how short the P-S bond length is for **32** (1.90 Å) in comparison to those for the other compounds (1.92 - 1.94 Å). Similarly the P-O distance for **33** is 0.02 Å shorter than that for **32** and the P-N bond lengths vary greatly in **33**, from 1.63 Å to 1.68 Å. All these observations can be explained by the electron withdrawing effect of the ethoxy groups. The short P-S bond length in **32** is due to two factors; the pendant sulfur and the electron withdrawing effect of the

Table 4.2. Selected bond lengths (Å) and angles (°) for (EtO)₂P(E)NHP(S)Ph₂ (E = S / O) and (EtO)₂P(S)NHP(O)Ph₂.

	31 (EtO) ₂ P(S)NHP(S)Ph ₂	33 (EtO) ₂ P(O)NHP(S)Ph ₂	32 (EtO) ₂ P(S)NHP(O)Ph ₂
S(1)-P(1)	1.937(1)	1.931(1)	-
S(2)-P(2)	1.920(2)	-	1.895(3)
O(1)-P(1)	-	-	1.476(3)
O(1)-P(2)	-	1.457(2)	-
P(1)-N(1)	1.681(3)	1.679(3)	1.673(4)
P(2)-N(1)	1.667(3)	1.632(3)	1.662(4)
P(1)-N(1)-P(2)	129.9(2)	130.5(1)	122.6(2)
S-P...P-E	87.0	172.3	79.5
N(1)-H(1n)	1.063(2)	0.925(2)	1.064(3)

ethoxy groups. Similarly the shortest P-O and P-N bonds are observed in **33** due to the combined electron withdrawing effects of the ethoxy substituents and the oxygen on the phosphorus involved. There is no obvious reason to explain the shortness of the N-H bond for **33**, the small P-N-P bond angle of 122.6(2) ° observed for **32**, or the varying S-P...P-E torsion angles. It is unlikely to be due to steric effects, both **31** and **33** contain a bulky phenyl substituted phosphorus with a sulfur donor atom, yet their torsion angles are 87.0 and 172.3 ° in contrast to the angle of 79.5° for **32** where the phenyl substituted phosphorus is attached to the much smaller oxygen donor atom.

4.3.1 Zinc Complexes of **31**, **33** and **32**.

One mole of zinc chloride and two moles of KO^tBu were refluxed with two moles of **31** or stirred at room temperature with two moles of **33** and **32** in THF. The solvent was then evaporated off, dichloromethane added and the mixture was filtered. The filtrate was evaporated to dryness yielding in each case an opaque white oil. For Zn[(EtO)₂P(O)NP(S)Ph₂]₂ (**36**) the oil yielded a small amount of crystals from the minimum of dichloromethane at - 10 °C which were subsequently studied by single crystal analysis. All complexes gave reasonable elemental analyses and the FAB +ve mass spectra revealed the expected parent ions of Zn[(EtO)₂P(S)NP(S)Ph₂]₂ (**34**) as well as (**36**) and Zn[(EtO)₂P(S)NP(O)Ph₂]₂ (**35**). Characteristic bands were observed

in the FTIR (Table 4.3). Again the characteristic shifts in the ν (PNP) vibration from around 950 to 1239 - 1262 cm^{-1} , the ν (PO) band from around 1190 to 1050 cm^{-1}

Table 4.3. FTIR assignments for $\text{Zn}[(\text{EtO})_2\text{P}(\text{E})\text{NHP}(\text{S})\text{Ph}_2]_2$ (E = S/O) and $\text{Zn}[(\text{EtO})_2\text{P}(\text{S})\text{NHP}(\text{O})\text{Ph}_2]_2$ (cm^{-1}).

	ν (PNP)	ν (PO)	ν (PS)	ν (NPS)
34	1239, 764	-	552	416
36	1255, 747	1057	583	421
35	1262, 747	1049	562	402

and the ν (PS) vibration from 640 to 552 - 583 cm^{-1} all signify the change in bond order within the ligand due to the delocalisation of the negative charge.

Signals observed in the ^{31}P NMR in CDCl_3 (Table 4.4) were two doublets of the AX type spectrum. The shift has decreased by 17 - 20 ppm for both phosphorus centres in the disulfur ligand, however somewhat surprisingly the ^2J phosphorus coupling has increased slightly. The shift of the ethoxy substituted phosphorus of 36 (with the oxygen donor atom) increased by 5 ppm upon coordination / deprotonation whilst the phenyl substituted phosphorus is in good agreement with 34. Furthermore the ^2J phosphorus coupling has increased by 9 Hz from 33. In contrast the shift of the phenyl substituted phosphorus of 35 (with the oxygen donor atom) has increased by only 1 ppm and the ^2J phosphorus coupling has increased by 6.5 Hz.

Table 4.4. Chemical shifts and [P-P] coupling constants in ^{31}P NMR (CDCl_3) for $\text{Zn}[(\text{EtO})_2\text{P}(\text{E})\text{NHP}(\text{S})\text{Ph}_2]_2$ (E = S/O) and $\text{Zn}[(\text{EtO})_2\text{P}(\text{S})\text{NHP}(\text{O})\text{Ph}_2]_2$.

	δ / ppm		^2J (^{31}P - ^{31}P) / Hz
	P_1	P_2	
$\text{Zn}[(\text{EtO})_2\text{P}(\text{S})\text{NP}(\text{S})\text{Ph}_2]_2$ 34	46.9	36.3	26.4
$\text{Zn}[(\text{EtO})_2\text{P}(\text{O})\text{NP}(\text{S})\text{Ph}_2]_2$ 36	5.4	35.6	22.0
$\text{Zn}[(\text{EtO})_2\text{P}(\text{S})\text{NP}(\text{O})\text{Ph}_2]_2$ 35	43.4	21.6	24.2

P_1 denotes the ethoxy and P_2 denotes the phenyl substituted phosphorus atoms.

The P-S and P-O bonds in the crystal structure of **36** (Figure 4.4) lengthen and the P-N bonds shorten upon deprotonation / coordination as indicated by the increase of the ν (PNP) vibration in the FTIR. The Zn-S bond is 0.025 Å shorter for **36** than for **2** and the S-P-N angles compare well. The S-P-N and O-P-N angles for **36** are equal and the P-N-P angle increased by 4 ° upon coordination.

Table 4.5. Selected bond lengths (Å) and angles (°) for (EtO)₂P(O)NHP(S)Ph₂, Zn[(EtO)₂P(O)NHP(S)Ph₂]₂ and Zn[ⁱPr₂P(S)NP(S)ⁱPr₂]₂.

	33 (EtO) ₂ P(O)NHP(S)Ph ₂	36 Zn[(EtO) ₂ P(O)NP(S)Ph ₂] ₂	2 Zn[ⁱ Pr ₂ P(S)NP(S) ⁱ Pr ₂] ₂
P(1)-S(1)	1.931(1)	2.013(2)	2.032(1)
P(2)-O(1)	1.457(2)	1.479(3)	-
P(1)-N(1)	1.679(3)	1.579(3)	1.581(2)
P(2)-N(1)	1.632(3)	1.551(3)	-
Zn-S(1)	-	2.318(1)	2.345(1)
Zn-O(1)	-	1.946(3)	-
S(1)-P(1)-N(1)	114.24(10)	118.4(1)	118.5(1)
O(1)-P(2)-N(1)	111.0(1)	118.5(2)	-
P(1)-N(1)-P(2)	130.5(1)	134.1(2)	140.5(3)
Zn-S(1)-P(1)	-	97.98(5)	107.1(1)
Zn-O(1)-P(2)	-	129.0(2)	-

The Zn-S-P angle is 97.98(5) °, unexpectedly low for a tetrahedral complex, 9 ° less than **2**. Such a small angle has only previously been observed for square planar complexes with an MS₂P₂N ring in the “chair” conformation. In contrast the very large Zn-O-P angle at 129.0(2) ° is the main reason for the Zn-O-P-N-P atoms to be in plane, indeed the ME₂P₂N ring (E = S / O) is only prevented from being planar by the sulfur atom.

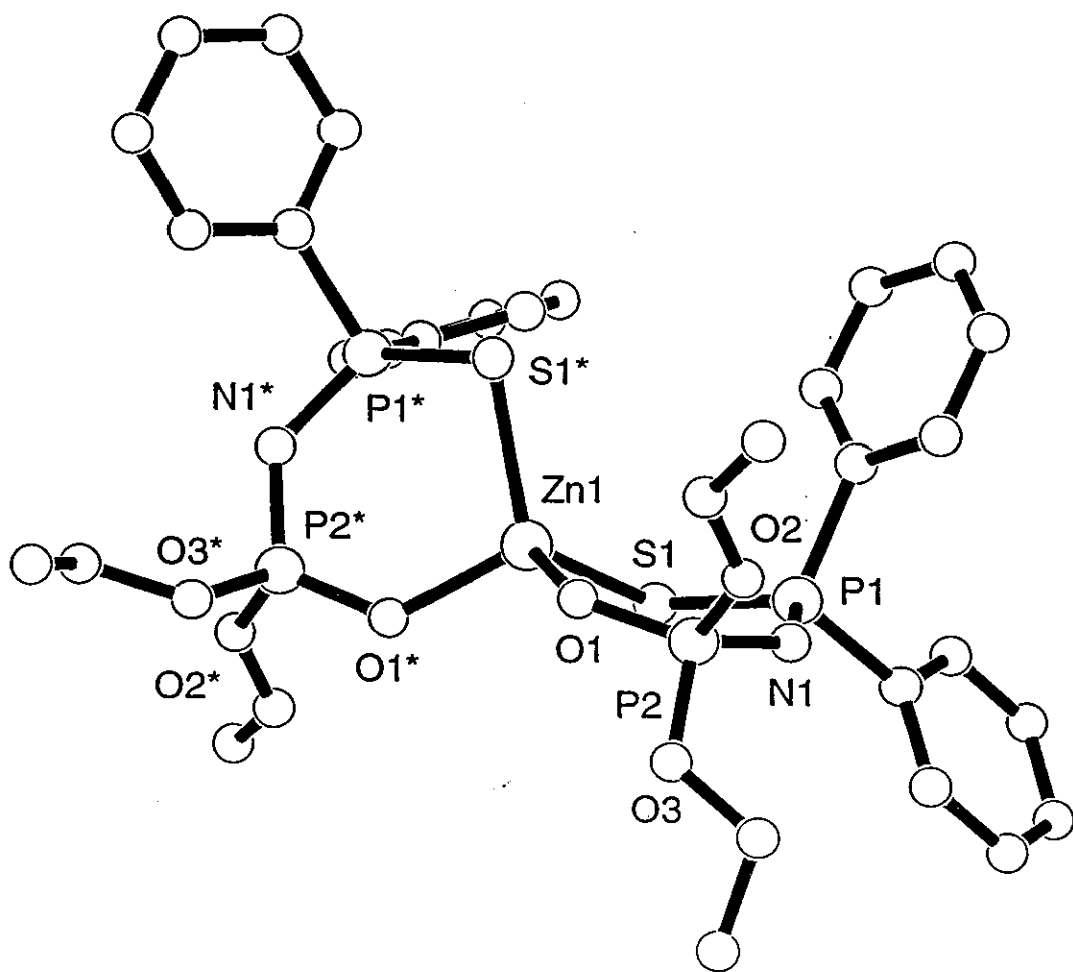


Figure 4.4. Crystal structure of $\text{Zn}[(\text{EtO})_2\text{P}(\text{O})\text{NP}(\text{S})\text{Ph}_2]_2$.

4.3.2 Square Planar Complexes of 31, 33 and 32.

One mole of MCl_2COD ($M = Pd, Pt$) and two moles of KO^tBu were refluxed with two moles of **31** or stirred at room temperature with two moles of **33** and **32** in THF. The solvent was then evaporated off and after the addition of dichloromethane the mixture was filtered. The filtrate was evaporated to dryness yielding deep red oils for the palladium complexes and yellow oils for the platinum complexes with the exception of $Pd[(EtO)_2P(S)NP(S)Ph_2]_2$ (**37**) and $Pt[(EtO)_2P(S)NP(S)Ph_2]_2$ (**38**) which yielded red and yellow solids. All were dissolved in the minimum of dichloromethane and hexane was added, though only **37** and **38** crystallised (95 % yield). In addition one mole of **31**, KO^tBu and $NaBPh_4$ were refluxed with one mole of $PtCl_2(PMe_3)_2$ in THF producing $Pt(PMe_3)_2[(EtO)_2P(S)NP(S)Ph_2]^+ BPh_4^-$ (**43**) which was isolated by evaporating to dryness, washing with methanol then recrystallising from acetone (76 % yield). Satisfactory elemental analyses were observed for all complexes and expected parent ions in the FAB +ve mass spectra were observed for the palladium complexes $Pd[(EtO)_2P(S)NP(O)Ph_2]_2$ (**39**) and $Pd[(EtO)_2P(O)NP(S)Ph_2]_2$ (**41**) at 843 m/z , and the platinum complexes $Pt[(EtO)_2P(S)NP(O)Ph_2]_2$ (**40**) and $Pt[(EtO)_2P(O)NP(S)Ph_2]_2$ (**42**) at 932 m/z . Bands observed in the FTIR for ν (PNP) were 1206 - 1259 cm^{-1} , ν (PS) were 539 - 570 cm^{-1} and ν NPS vibrations at 420 - 426 cm^{-1} were only observed for **37** and **38**. Surprisingly no bands were observed that could be confidently assigned as ν (PO). Furthermore **37**, **38** and **43** were studied by single crystal analysis.

37 was observed to be a typical square planar complex with the MS_2P_2N ring adopting the distorted boat formation (Figure 4.5). Interestingly the Pd-S(1) bond at 2.325(1) Å is shorter than the Pd-S(2) bond, whereas the S(1)-P(1) bond at 2.207(1) Å is longer than the S(2)-P(2) bond, and the P(1)-N(1) bond is approximately 0.028 Å longer than the P(2)-N(1) bond of 1.566(3) Å. The electron withdrawing effect of the ethoxy substituents causes the S(2)-P(2) and P(2)-N(1) bonds to be slightly shorter. Pd-S-P bond angles are 101.09(5) and 110.08(5)°, the S-P-N angles are 116.7(1) and 117.4(1)° and the P-N-P angle is 125.1(2)° as expected for a square planar distorted boat type structure.

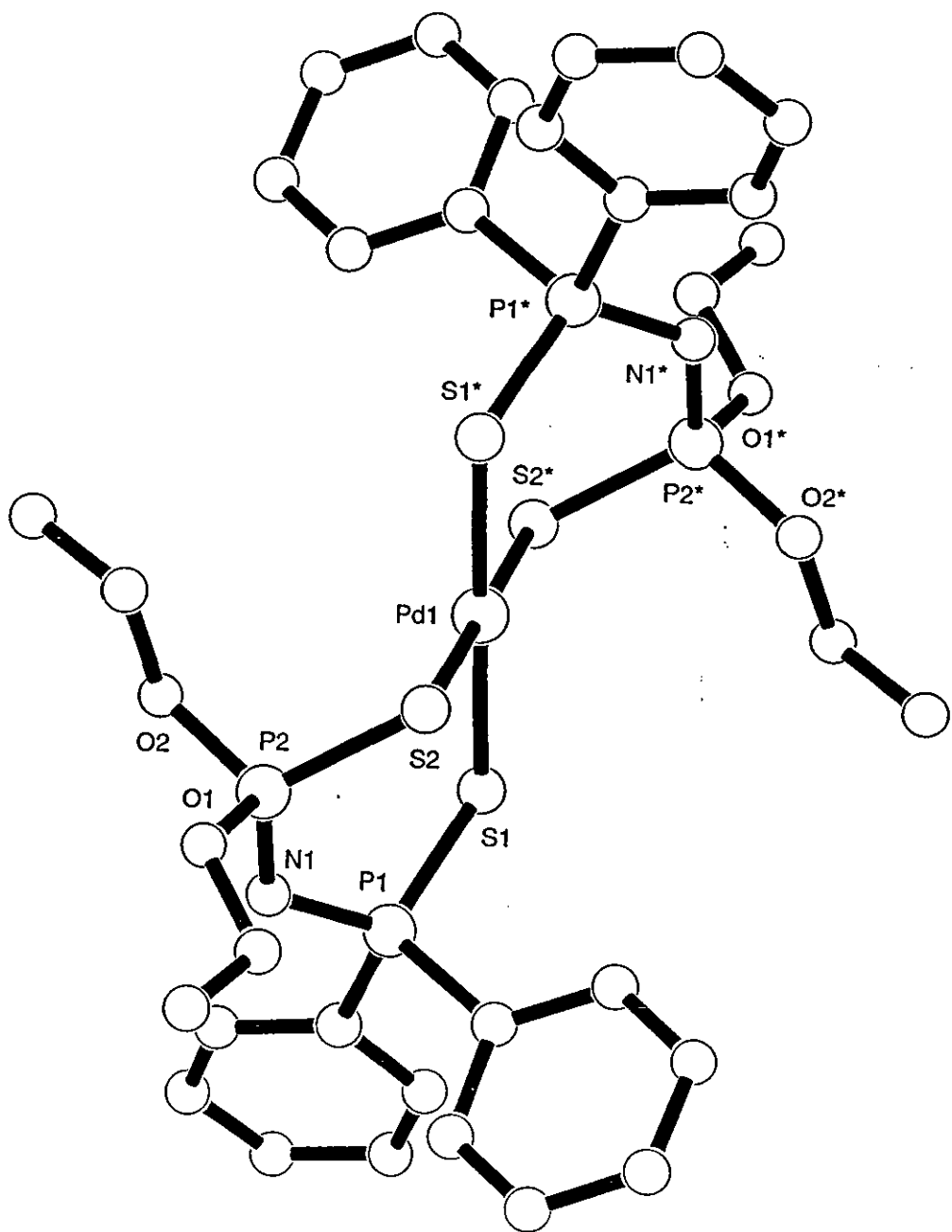


Figure 4.5. Crystal structure of $\text{Pd}[(\text{EtO})_2\text{P}(\text{S})\text{NP}(\text{S})\text{Ph}_2]_2$.

In contrast **38** showed a completely novel structure (Figure 4.6), one MS_2P_2N ring adopting the distorted boat formation and the other MS_2P_2N ring adopting the chair formation, so both known conformations of the MS_2P_2N ring for square planar complexes are observed in the same compound. Comparing values for the boat and chair conformations in the molecule (Table 4.6), the only significant bond length difference is between the P-N bonds where the P(2)-N(1) length is 0.1 Å less than P(1)-N(1) whereas the P-N bonds are very nearly equal for the chair part of the molecule. The more characteristic differences between the two conformations are in the bond angles. The M-S-P angles for the boat conformation are 105 - 112 ° as opposed to 100 - 102 ° for the chair conformation. The S-P-N angles are all very similar at 116 - 120 ° in contrast to the S-M-S angles which differ quite greatly by 8 ° implying the square planar geometry at the metal centre is somewhat distorted for the boat conformation. The boat P-N-P angle is 2.5 ° greater at 127.8 °.

Table 4.6. Selected bond lengths (Å) and angles (°) for $M[(EtO)_2P(S)NHP(S)Ph_2]_2$ (M = Pd, Pt).

	37		38	
	“Boat”	“Boat”	“Boat”	“Chair”
M-S(1)	2.3250(9)	2.338(4)	M-S(3)	2.330(4)
M-S(2)	2.345(1)	2.330(4)	M-S(4)	2.339(4)
S(1)-P(1)	2.027(1)	2.028(6)	S(3)-P(3)	2.027(5)
S(2)-P(2)	2.011(1)	2.008(6)	S(4)-P(4)	2.008(6)
P(1)-N(1)	1.594(3)	1.60(1)	P(3)-N(2)	1.60(1)
P(2)-N(1)	1.566(3)	1.49(2)	P(4)-N(2)	1.57(1)
S(1)-M-S(2)	81.66(3)	100.4(1)	S(3)-M-S(4)	92.8(1)
M-S(1)-P(1)	110.08(5)	105.2(2)	M-S(3)-P(3)	101.8(2)
M-S(2)-P(2)	101.09(5)	111.9(2)	M-S(4)-P(4)	99.5(2)
S(1)-P(1)-N(1)	116.7(1)	116.1(6)	S(3)-P(3)-N(2)	116.4(5)
S(2)-P(2)-N(1)	117.4(1)	118.1(6)	S(4)-P(4)-N(2)	119.9(5)
P(1)-N(1)-P(2)	125.1(2)	127.8(9)	P(3)-N(2)-P(4)	125.1(7)

Bond lengths for the two MS_2P_2N rings of the boat conformation are comparable with the exception of the P(1)-N(1) and P(2)-N(1) bonds which for **37** are 1.57 - 1.59 Å compared to 1.49(2) Å {P(2)-N(1)} and 1.60(1) Å {P(1)-N(1)} for **38**.

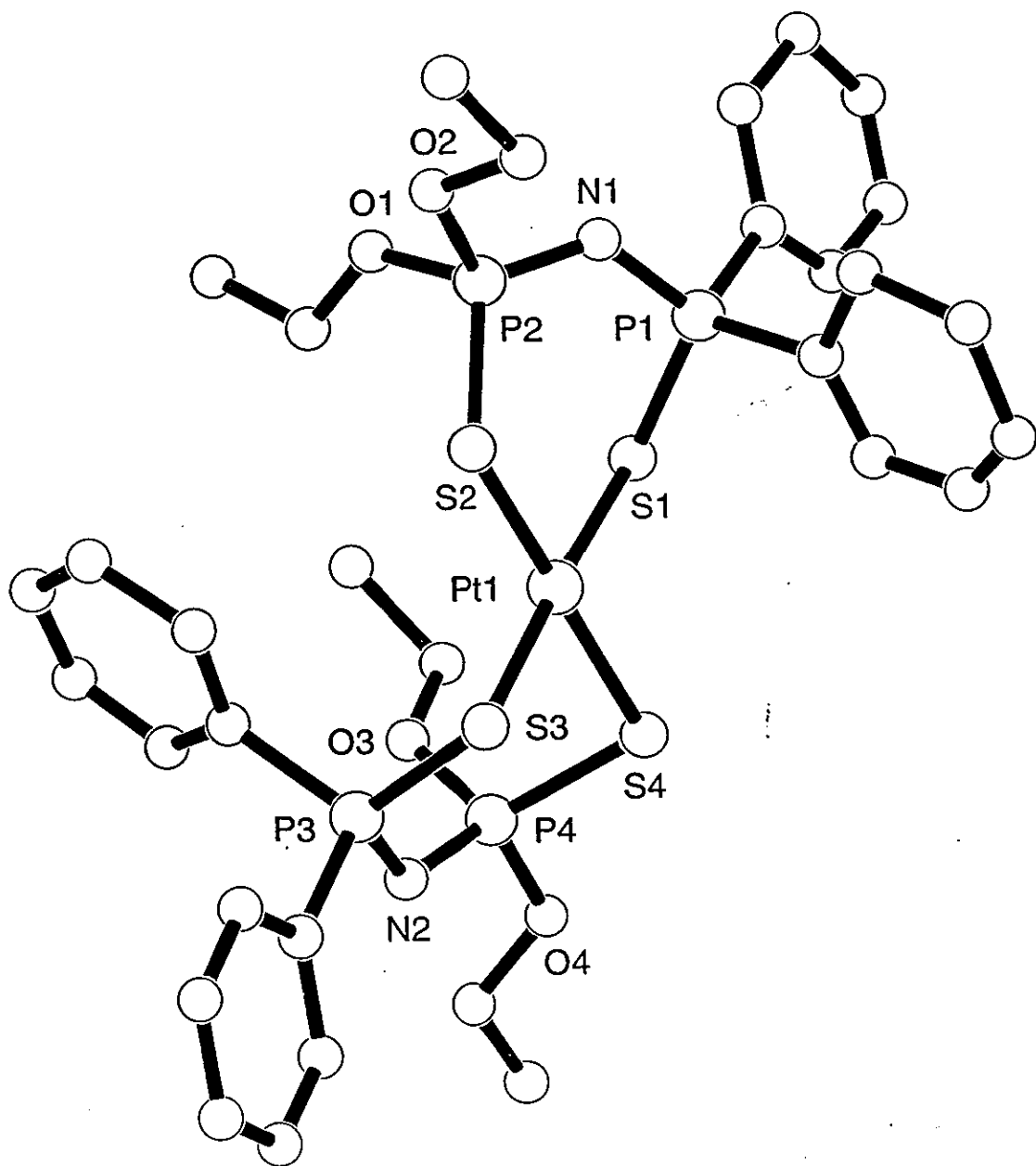


Figure 4.6. Crystal structure of $\text{Pt}[(\text{EtO})_2\text{P}(\text{S})\text{NP}(\text{S})\text{Ph}_2]_2$.

Furthermore the bond angles are quite different, the S-M-S angle for **37** is 18 ° less than for **38**. The M-S-P angles are slightly smaller for **37** at 101 - 110 ° compared to 105 - 112 ° for **38**. The S-P-N angles are comparable at 116 - 118 ° and the P-N-P angle for **38** at 127.8 ° is 3 ° greater than **37**.

In contrast the structure of the square planar bis(trimethylphosphine)platinum complex (Figure 4.7, Table 4.7) shows attributes that have been observed in square planar “chair”, “boat” and tetrahedral complexes. The Pt-S bond lengths differ by 0.02 Å and are 0.03 - 0.05 Å longer than those observed for **38**. In comparison the S(2)-P(2) bond length is 0.04 Å shorter than S(1)-P(1) and the P(2)-N(1) bond is 0.08 Å shorter than the P(1)-N(1) bond. These differences may best be explained by the electron withdrawing effect of the ethoxy substituents on the P(2) phosphorus, which

Table 4.7. Selected bond lengths (Å) and angles (°) for $\{\text{Pt}(\text{PMe}_3)_2[(\text{EtO})_2\text{P}(\text{S})\text{NP}(\text{S})\text{Ph}_2]\}^+$.

Bond lengths		Bond angles	
Pt-S(1)	2.371(3)	S(1)-Pt-S(2)	88.7(1)
Pt-S(2)	2.395(3)	Pt-S(1)-P(1)	97.3(1)
S(1)-P(1)	2.026(4)	Pt-S(2)-P(2)	108.1(2)
S(2)-P(2)	1.987(5)	S(1)-P(1)-N(1)	116.4(4)
P(1)-N(1)	1.608(9)	S(2)-P(2)-N(1)	120.1(4)
P(2)-N(1)	1.522(10)	P(1)-N(1)-P(2)	132.0(6)

as a result produce a slightly longer Pt-S(2) bond. The difference in Pt-S-P angles is significant, Pt-S(1)-P(1) at 97.3(1) ° is consistent with a “chair” type conformation for the PtS₂P₂N ring whereas the Pt-S(2)-P(2) angle of 108.1(2) ° implies a “boat” type conformation. Furthermore the large angles of S(2)-P(2)-N(1) at 120.1(4) ° and P(1)-N(1)-P(2) at 132.0(6) ° are more consistent with a tetrahedral “boat” type MS₂P₂N ring conformation rather than any sort of square planar complex. In this case the PtS₂P₂N ring can only be described as puckered.

Signals observed in the ³¹P NMR revealed an ABCD type spectrum (Figure 4.8, Table 4.8, Figure 4.9) with much ³J (³¹P-³¹P) coupling which was not observed for $\{\text{Pt}(\text{PMe}_3)_2[\text{N}(\text{Pr}_2\text{PS})_2]\}^+$.

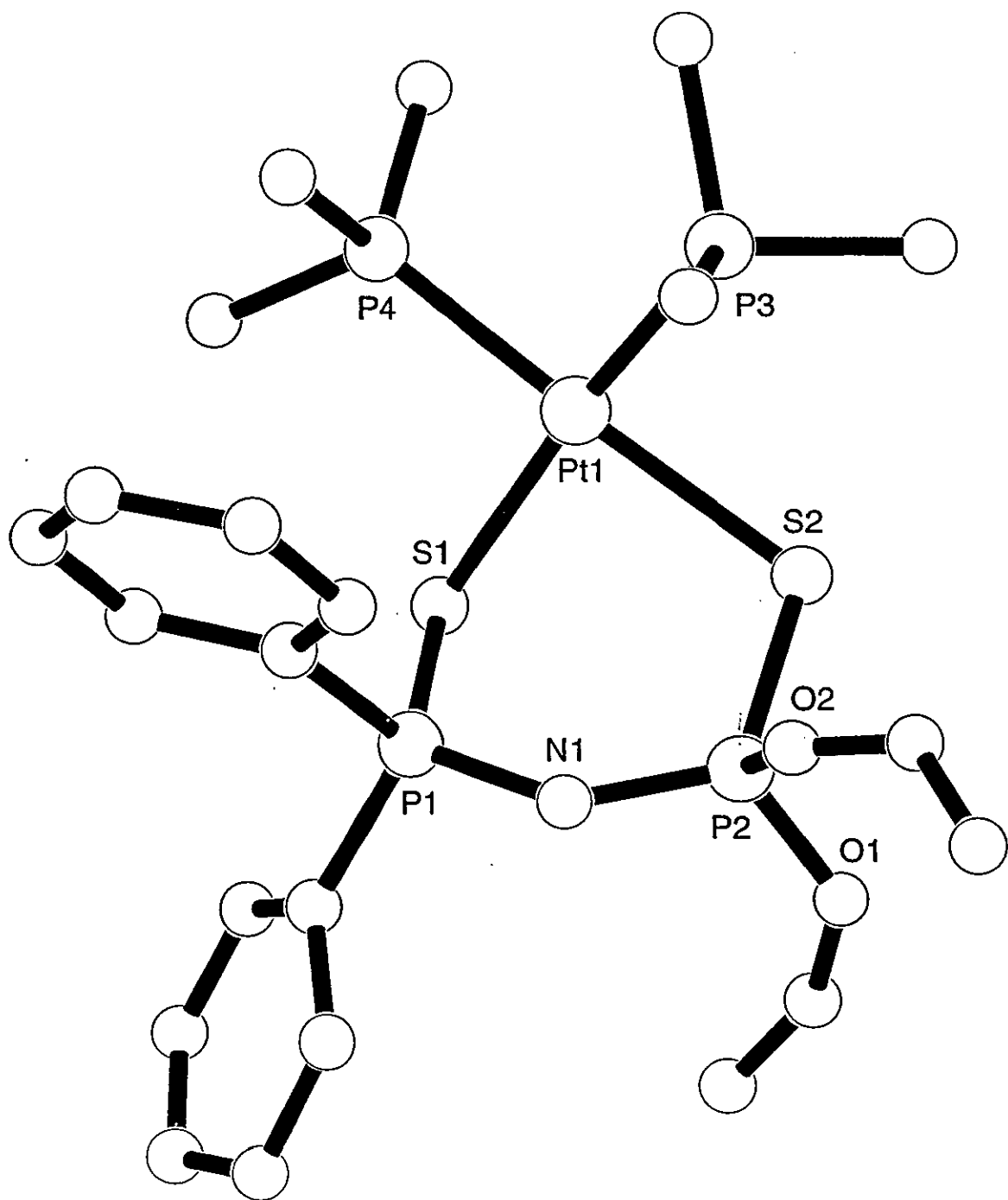


Figure 4.7. Crystal structure of $\{Pt(PMe_3)_2[(EtO)_2P(S)NP(S)Ph_2]\}^+$.

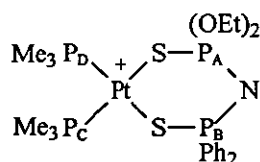


Figure 4.8. Phosphorus atoms labelled for $\{\text{Pt}(\text{PMe}_3)_2[(\text{EtO})_2\text{P}(\text{S})\text{NP}(\text{S})\text{Ph}_2]\}^+$.

P_A , P_B and P_C all give well resolved doublets of triplets, the platinum satellites were partially obscured for P_A and P_B . *Cis* ^3J [P-P] coupling was found to be of equal magnitude to *trans* ^3J [P-P] coupling for P_A and P_B . Despite the partial overlap of the triplets in the P_D signal seven peaks were observed as the difference between the $^3\text{J}[\text{P}_D-\text{P}_B]$ *trans* and the $^3\text{J}[\text{P}_D-\text{P}_A]$ *cis* coupling constants was resolved as 2.0 Hz. It is

Table 4.8. ^{31}P NMR parameters for $\{\text{Pt}(\text{PMe}_3)_2[(\text{EtO})_2\text{P}(\text{S})\text{NP}(\text{S})\text{Ph}_2]\}^+\text{BPh}_4^-$.

	δ/ppm	$[\text{J}(\text{P-P})]/\text{Hz}$				$[\text{J}(\text{P-Pt})]/\text{Hz}$ Pt
		P_A	P_B	P_C	P_D	
P_A	45.9	-				65.4
P_B	34.3	25.8	-			57.5
P_C	-19.8	7.9	9.9	-		3104.3
P_D	-18.0	7.9	9.9	21.8	-	3062.7

interesting to note the difference of 8 Hz between the $^2\text{J}(^{31}\text{P}_A-^{195}\text{Pt})$ and $^2\text{J}(^{31}\text{P}_B-^{195}\text{Pt})$ coupling constants. Despite the different electronic effects of the substituent groups on P_A and P_B , it could further be explained by the Pt-S-P bond angles (Pt-S- P_A 108.1°, Pt-S- P_B 97.3°). Given that a larger angle may imply a greater proportion of *s* character in the hybridised sulfur, this greater proportion of *s* character is likely to increase the magnitude of the platinum-phosphorus coupling⁵⁹. This assumption is supported by the crystal structure data.

Two sets of two doublets (AX type spectra) were observed for **37**, **38** and **41**, in each case the chemical shifts were very similar as was the coupling (Table 4.9). For **37** and **38** this is most likely due to the presence of the $\text{MS}_2\text{P}_2\text{N}$ ring “chair” and

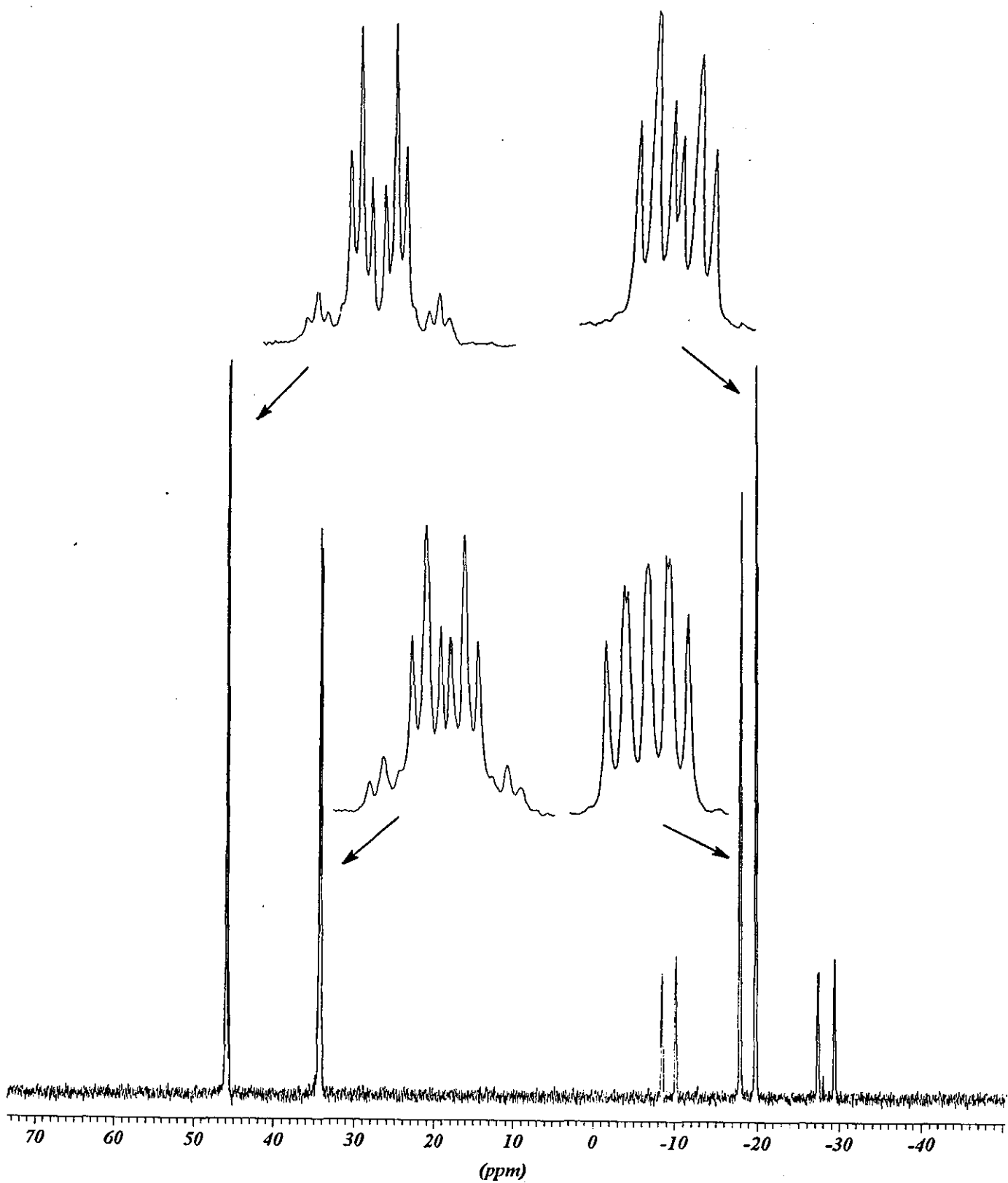


Figure 4.9. $^{31}\text{P}\{-^1\text{H}\}$ NMR spectrum of $\text{Pt}(\text{PMe}_3)_2[(\text{EtO})_2\text{P}(\text{S})\text{NP}(\text{S})\text{Ph}_2]^+ \text{BPh}_4^-$.

“boat” conformations (Figure 4.10). The crystal structure of **38** indicates there is very little energy difference between the two conformers in the solid state. Indeed considering the intensity of the two sets of doublets is approximately equal the two

Table 4.9. Chemical shifts and [P-P] coupling constants in ^{31}P NMR (CDCl_3) for $\text{M}[(\text{EtO})_2\text{P}(\text{E})\text{NHP}(\text{S})\text{Ph}_2]_2$ ($\text{M} = \text{Pd}, \text{Pt}; \text{E} = \text{S/O}$) and $\text{M}[(\text{EtO})_2\text{P}(\text{S})\text{NHP}(\text{O})\text{Ph}_2]_2$ ($\text{M} = \text{Pd}, \text{Pt}$).

	δ / ppm				$^2\text{J}(^{31}\text{P}-^{31}\text{P}) / \text{Hz}$	
	P_A	P_X	P_A'	P_X'	$[\text{P}_\text{A}-\text{P}_\text{X}]$	$[\text{P}_\text{A}'-\text{P}_\text{X}']$
$\text{Pd}[(\text{EtO})_2\text{P}(\text{S})\text{NP}(\text{S})\text{Ph}_2]_2$	50.5	40.5	50.4	40.9	27.5	26.7
$\text{Pt}[(\text{EtO})_2\text{P}(\text{S})\text{NP}(\text{S})\text{Ph}_2]_2$	44.2	37.8	44.1	38.3	25.6	25.3
$\text{Pd}[(\text{EtO})_2\text{P}(\text{O})\text{NP}(\text{S})\text{Ph}_2]_2$	3.9	3.6	28.4	27.4	24.5	29.7
$\text{Pt}[(\text{EtO})_2\text{P}(\text{O})\text{NP}(\text{S})\text{Ph}_2]_2$	0.4	24.9	-	-	23.4	-
$\text{Pd}[(\text{EtO})_2\text{P}(\text{S})\text{NP}(\text{O})\text{Ph}_2]_2$	58.6	21.8	-	-	13.4	-
$\text{Pt}[(\text{EtO})_2\text{P}(\text{S})\text{NP}(\text{O})\text{Ph}_2]_2$	65.4	19.7	-	-	18.7	-

$\text{P}_\text{A}/\text{A}'$ denotes the ethoxy and $\text{P}_\text{X}/\text{X}'$ denotes the phenyl substituted phosphorus atoms.

conformers may well be in equilibrium. Unfortunately no platinum satellites could be confidently resolved or assigned for any of the spectra, however **37** was studied by variable temperature ^{31}P NMR (d^6 -DMSO) increasing the sample temperature to 85 °C (Table 4.10). The two AX type spectra observed for **37** were not clearly resolved in d^6 -DMSO at 298 K, it is possible the stronger polarity of the solvent affects the “boat” versus “chair” conformational equilibrium of the $\text{MS}_2\text{P}_2\text{N}$ ring. At 318 K the doublets observed as signals representing the A and A' phosphorus atoms had merged into a single doublet whilst the signals representing the X and X' phosphorus atoms remained as two doublets. At 338 K the two remaining doublets had coalesced. We propose that at this temperature one $\text{MS}_2\text{P}_2\text{N}$ ring conformation predominates.

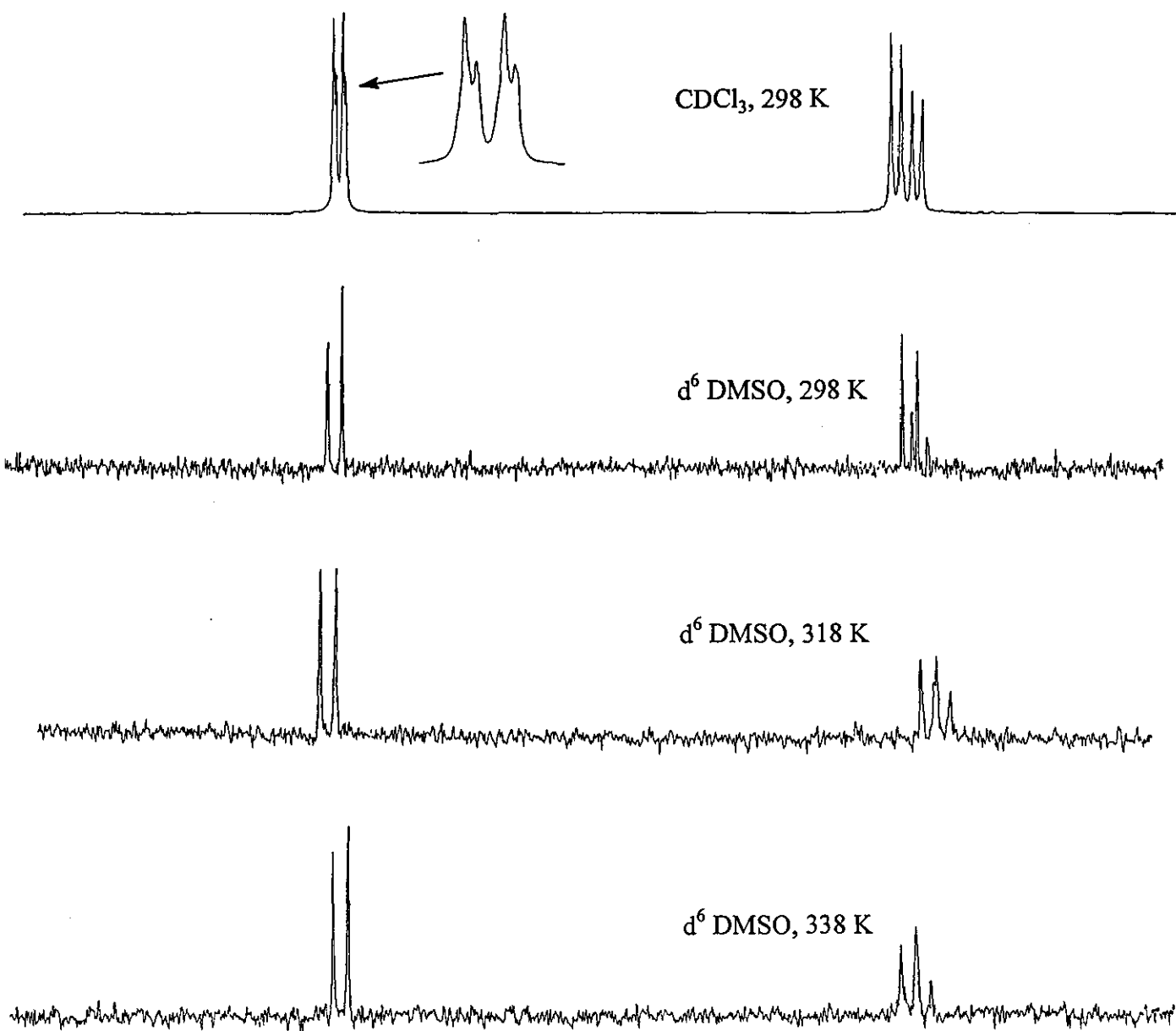


Figure 4.10. $^{31}\text{P}\{-^1\text{H}\}$ VT NMR spectra of $\text{Pd}[(\text{EtO})_2\text{P}(\text{S})\text{NP}(\text{S})\text{Ph}_2]_2$.

Table 4.10. Chemical shifts and phosphorus-phosphorus coupling constants in ^{31}P VT NMR of $\text{Pd}[(\text{EtO})_2\text{P}(\text{S})\text{NP}(\text{S})\text{Ph}_2]_2$.

$\text{Pd}[(\text{EtO})_2\text{P}(\text{S})\text{NP}(\text{S})\text{Ph}_2]_2$	δ / ppm				$J[\text{P}-\text{P}]$ / Hz	
	P_A	P_X	$\text{P}_{A'}$	$\text{P}_{X'}$	$[\text{P}_A-\text{P}_X]$	$[\text{P}_{A'}-\text{P}_{X'}]$
298 K (CDCl_3)	50.5	40.5	50.4	40.9	27.5	26.7
298 K (d^6 -DMSO)	54.1	44.3	-	44.1	26.9	25.1
318 K (d^6 -DMSO)	54.2	44.4	-	44.2	26.9	25.1
338 K (d^6 -DMSO)	54.3	44.5	-	-	26.0	-

$\text{P}_{A/A'}$ denotes the ethoxy and $\text{P}_{X/X'}$ denotes the phenyl substituted phosphorus atoms.

In regard to **41** there are many possible explanations for its two sets of doublets. It may simply be *cis* and *trans* isomers of the square planar complex or the “chair” and “boat” equilibrium. The most plausible explanation is probably differing donor atoms. The oxygen donor atom bound to the phosphorus with ethoxy substituents is quite “hard” so it may be pendant while coordination occurs through the sulfur and nitrogen atoms (Figure 4.11), similar to the reported palladium complex $^{53}\text{Pd}[(\text{PhO})_2\text{P}(\text{S})\text{NP}(\text{O})(\text{OPh})_2]_2$. Stronger 2J [P-P] coupling might be expected as the ethoxy substituted phosphorus is pendant and the phenyl substituted phosphorus is directly involved in the coordination which would explain the strongest 2J coupling observed in all the square planar complexes of 29.7 Hz for this compound. However

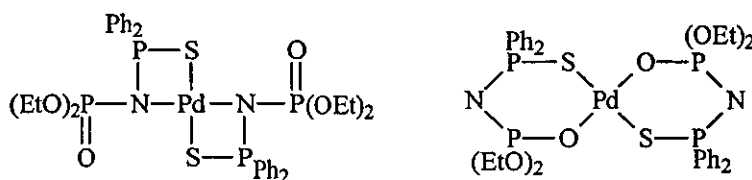


Figure 4.11. Proposed structures of $\text{Pd}[(\text{EtO})_2\text{P}(\text{O})\text{NP}(\text{S})\text{Ph}_2]_2$.

the shifts for the ethoxy substituted phosphorus atoms differ by only 0.3 ppm where a larger difference might be expected. The second compound present with 2J coupling of 24.5 Hz is most likely the expected complex (Figure 4.11) with sulfur and oxygen acting as the donor atoms.

The corresponding platinum complex has the lowest shift for the ethoxy substituted phosphorus (0.4 ppm) and similarly the lowest shift for the phenyl substituted phosphorus with sulfur donor atom (24.9 ppm), a decrease of 13 ppm from **38**. This contrasts with the marked increase in the shift of the ethoxy substituted phosphorus for **40** to 65.4 ppm, 15 ppm greater than for **38**. By the same token the phenyl substituted phosphorus does not decrease as greatly when attached to the oxygen donor atom. These differences may be due to the different electronic character of the substituents, most noticeably the electron withdrawing affect of the ethoxy groups.

4.4 Experimental

$\text{Ph}_2\text{P}(\text{S})\text{Cl}$ was formed by anaerobically refluxing diphenylchlorophosphine (12.30 g, 10.0 ml, 0.053 mol) with sulfur (1.70 g, 0.053 mol) overnight in toluene (30 ml). The solvent was evaporated off and the residual clear oil (13.31 g; $^{31}\text{P}\{-^1\text{H}\}$ NMR (CDCl_3): δ 79.4 ppm).

$\text{Ph}_2\text{P}(\text{S})\text{NH}_2$ was formed by bubbling ammonia gas through a solution of $\text{Ph}_2\text{P}(\text{S})\text{Cl}$ (4.00 g, 15.84 mmol) in ether (100 ml) for 20 minutes. After filtering the reaction mixture through celite, the filtrate was evaporated to dryness giving a white solid (3.62 g; $^{31}\text{P}\{-^1\text{H}\}$ NMR (CDCl_3): δ 59.7 ppm).

$(\text{EtO})_2\text{P}(\text{S})\text{NH}_2$ was formed by bubbling ammonia gas through a solution of diethylchlorothiophosphate (24.00 g, 20.0 ml, 0.127 mol) in ether (100 ml) for 20 minutes. After filtering the reaction mixture through celite, the filtrate was evaporated to dryness giving a residual oil (21.36 g; $^{31}\text{P}\{-^1\text{H}\}$ NMR (CDCl_3): δ 74.2 ppm).

$(\text{EtO})_2\text{P}(\text{S})\text{NHP}(\text{S})\text{Ph}_2$ **31**. Under anhydrous conditions, sodium hydride (60% dispersion in paraffin oil 1.69 g, 0.042 mol) was added to a solution of $(\text{EtO})_2\text{P}(\text{S})\text{NH}_2$ (2.38 g, 0.014 mol) in THF (30 ml) at 0 °C. The mixture was allowed to warm to room temperature and stirred for 30 minutes, then $\text{Ph}_2\text{P}(\text{S})\text{Cl}$ (3.53 g, 0.014 mol) was added dropwise at 0 °C. After addition was complete the mixture was warmed to room temperature and then refluxed overnight. Upon cooling methanol (5 ml) was added dropwise to destroy any excess sodium hydride. The volume of the THF was then reduced by half under vacuum and 2M aqueous HCl (50 ml) was added, producing a cloudy white mixture which was washed with dichloromethane (3 x 20 ml). The dichloromethane was dried over MgSO_4 then evaporated to dryness to give a white solid **31** which was recrystallised from dichloromethane and hexane (4.22 g, 0.011 mol, 78.3 % yield, mp 62 °C). Microanalysis calculated for $\text{C}_{16}\text{H}_{21}\text{NO}_2\text{P}_2\text{S}_2$: C 49.9; H 5.5; N 3.6 %. Observed: C 49.8; H 5.4; N 3.6 %. $^{31}\text{P}\{-^1\text{H}\}$ NMR (CDCl_3): $\delta(\text{P}_A)$ 63.6(d), $\delta(\text{P}_X)$ 53.3(d) ppm. $^2\text{J} (^{31}\text{P}_A\text{-}^{31}\text{P}_X)$ 22.0 Hz. FTIR (dichloromethane solution, CsI plates at 100 microns): ν (N-H) 3331 cm^{-1} ; (KBr disc): ν (N-H) 3200, δ (N-H) 1298; ν (PNP) 976, 768; ν (PS) 646, 634 cm^{-1} .

Zn[(EtO)₂P(S)NP(S)Ph₂]₂ **34**. A solution of **31** (0.100 g, 0.260 mmol), KO^tBu (0.029 g, 0.260 mmol) and ZnCl₂ (0.018 g, 0.132 mmol) in THF (20 ml) was refluxed for 1 hour. On cooling the mixture was evaporated to dryness and dichloromethane added. The mixture was then filtered and the filtrate evaporated to dryness yielding a colourless oil. Microanalysis calculated for C₃₂H₄₀N₂O₄P₄S₄Zn : C 46.1; H 4.8; N 3.4 %. Observed : C 49.3; H 6.1; N 3.1 %. ³¹P-{¹H} NMR (CDCl₃): δ(P_A) 46.9(d), δ(P_X) 36.3 ppm. ²J(³¹P_A-³¹P_X) 26.4 Hz. FTIR (KBr disc): ν (PNP) 1239, 764; ν (PS) 552; δ (NPS) 416 cm⁻¹. FAB +ve MS: m/z 833 corresponds to {Zn[(EtO)₂P(S)NP(S)Ph₂]₂}⁺.

Pd[(EtO)₂P(S)NP(S)Ph₂]₂ **37**. PdCODCl₂ (0.050 g, 0.175 mmol) was added to a solution of **31** (0.135 g, 0.351 mmol) and KO^tBu (0.039 g, 0.348 mmol) in THF (20 ml) and refluxed for 1 hour. The reaction changed colour from yellow to red/orange. On cooling the mixture was evaporated to dryness and dichloromethane added. The mixture was filtered and the filtrate evaporated to dryness. Crystals of **37** were grown from dichloromethane and hexane (0.145 g, 0.166 mmol, 94.7 % yield). Microanalysis calculated for C₃₂H₄₀N₂O₄P₄S₄Pd : C 43.9; H 4.6; N 3.2 %. Observed : C 43.6; H 4.6; N 2.8 %. ³¹P-{¹H} NMR (CDCl₃): δ(P_A) 50.5(d), δ(P_X) 40.5(d) ppm. ²J (³¹P_A-³¹P_X) 27.5 Hz. δ(P_{A'}) 50.4(d), δ(P_{X'}) 40.9(d) ppm. ²J (³¹P_{A'}-³¹P_{X'}) 26.7 Hz. FTIR (KBr disc): ν (PNP) 1206, 773; ν (PS) 563, 555; ν (NPS) 420 cm⁻¹.

Pt[(EtO)₂P(S)NP(S)Ph₂]₂ **38**. PtCODCl₂ (0.050 g, 0.134 mmol) was added to a solution of **31** (0.103 g, 0.267 mmol) and KO^tBu (0.030 g, 0.267 mmol) in THF (20 ml) and refluxed for 1 hour. The reaction changed colour from clear to yellow. On cooling the mixture was evaporated to dryness and dichloromethane added. The mixture was then filtered and the filtrate evaporated to dryness. Crystals of **38** were grown from dichloromethane and hexane (0.118 g, 0.123 mmol, 94.4 % yield). Microanalysis calculated for C₃₂H₄₀N₂O₄P₄S₄Pt : C 39.9; H 4.2; N 2.9 %. Observed : C 41.2; H 3.9; N 3.0 %. ³¹P-{¹H} NMR (CDCl₃): δ(P_A) 44.2(d), δ(P_X) 37.8(d) ppm. ²J (³¹P_A-³¹P_X) 25.6 Hz. δ(P_{A'}) 44.1(d), δ(P_{X'}) 38.3(d) ppm. ²J (³¹P_{A'}-³¹P_{X'}) 25.3 Hz. No

$^2J(^{195}\text{Pt}-^{31}\text{P})$ coupling was observed that could be confidently assigned. FTIR (KBr disc): ν (PNP) 1255, 1203; ν (PS) 576, 552, 542; ν (NPS) 426 cm^{-1} .

$[\text{Pt}(\text{PMe}_3)_2\{(\text{EtO})_2\text{P}(\text{S})\text{NP}(\text{S})\text{Ph}_2\}]^+ \text{BPh}_4^-$ **43**. $\text{Pt}(\text{PMe}_3)_2\text{Cl}_2$ (0.060 g, 0.144 mmol) and NaBPh_4 (0.049 g, 0.143 mmol) were added to a solution of **31** (0.055 g, 0.143 mmol) and KO^tBu (0.016 g, 0.143 mmol) in THF (30 ml) and refluxed for 1 hour. On cooling the mixture was evaporated to dryness and washed with methanol (2 x 5 ml). A white solid was filtered off and crystallised from acetone (0.114 g, 0.109 mmol, 75.6 % yield). Microanalysis calculated for $\text{C}_{46}\text{H}_{58}\text{P}_4\text{O}_2\text{S}_2\text{BNPt}$: C 52.6; H 5.6; N 1.3 %. Observed: C 52.2; H 5.6; N 1.1 %. $^{31}\text{P}-\{^1\text{H}\}$ NMR (CDCl_3): $\delta(\text{P}_A)$ 45.9(dt), $\delta(\text{P}_B)$ 34.3(dt), $\delta(\text{P}_C)$ -19.8(dt), $\delta(\text{P}_D)$ -18.0(m) ppm. $^2J(^{31}\text{P}_A-^{31}\text{P}_B)$ 25.8, $^2J(^{31}\text{P}_C-^{31}\text{P}_D)$ 21.8, $^3J(^{31}\text{P}_A-^{31}\text{P}_C)$ 7.9, $^3J(^{31}\text{P}_A-^{31}\text{P}_D)$ 7.9, $^3J(^{31}\text{P}_B-^{31}\text{P}_D)$ 9.9 Hz, $^3J(^{31}\text{P}_B-^{31}\text{P}_C)$ 9.9 Hz; $^2J(^{31}\text{P}_A-^{195}\text{Pt})$ 65.4, $^2J(^{31}\text{P}_B-^{195}\text{Pt})$ 57.5, $^1J(^{31}\text{P}_C-^{195}\text{Pt})$ 3104.3, $^1J(^{31}\text{P}_D-^{195}\text{Pt})$ 3062.7 Hz. FTIR (KBr disc): ν (PNP) 1267, 1206, 784; ν (PS) 570, 539 cm^{-1} .

$(\text{EtO})_2\text{P}(\text{S})\text{NHP}(\text{O})\text{Ph}_2$ **32**. A further amount of the amine made in the synthesis for **31**, $(\text{EtO})_2\text{P}(\text{S})\text{NH}_2$ (1.80 g, 10.6 mmol) was dissolved in THF (50 ml) and 3 molar equivalents of NaH (60% dispersion in paraffin oil 1.26 g, 31.2 mmol) was added dropwise at 0 °C. The mixture was allowed to warm to room temperature and stirred for 30 minutes, then $\text{Ph}_2\text{P}(\text{O})\text{Cl}$ (2.50 g, 10.6 mmol) was added dropwise at 0 °C. When the mixture was again at room temperature, it was stirred overnight. Methanol (5 ml) was then added dropwise to destroy any excess sodium hydride. The mixture was reduced by half under vacuum before 2M aqueous HCl (50 ml) was added, producing a white precipitate which was extracted with dichloromethane (3 x 20 ml). The dichloromethane was dried over MgSO_4 then evaporated to dryness to give a yellow oil which was recrystallised from the minimum of dichloromethane and petroleum ether (40-60) yielding colourless crystals upon cooling (2.87 g, 7.77 mmol, 73.1 % yield, mp 84 °C). Microanalysis calculated for $\text{C}_{16}\text{H}_{21}\text{NO}_3\text{P}_2\text{S}$: C 52.0; H 5.7; N 3.8 %. Observed: C 52.5; H 5.7; N 3.6 %. $^{31}\text{P}-\{^1\text{H}\}$ NMR (CDCl_3): $\delta(\text{P}_A)$ 64.1(d), $\delta(\text{P}_X)$ 19.7 ppm. $^2J(^{31}\text{P}_A-^{31}\text{P}_X)$ 17.6 Hz. FTIR (dichloromethane solution, CsI plates at

100 microns): ν (N-H) 3342 cm^{-1} ; (KBr disc): ν (N-H) not observed, δ (N-H) 1344; ν (PNP) 936, 913, 787; ν (PO) 1196, 1128; (PS) 607 cm^{-1} .

$\text{Zn}[(\text{EtO})_2\text{P}(\text{S})\text{NP}(\text{O})\text{Ph}_2]_2$ **35**. A solution of **32** (0.050 g, 0.135 mmol), KO^tBu (0.015 g, 0.134 mmol) and ZnCl_2 (0.010 g, 0.073 mmol) in THF (20 ml) was stirred for 1 hour. The mixture was then evaporated to dryness and dichloromethane added which was filtered and the filtrate evaporated to dryness yielding a colourless oil.

Microanalysis calculated for $\text{C}_{32}\text{H}_{40}\text{N}_2\text{O}_6\text{P}_4\text{S}_2\text{Zn}$: C 47.9; H 5.0; N 3.5 %. Observed : C 45.9; H 4.9; N 3.3 %. $^{31}\text{P}\{-^1\text{H}\}$ NMR (CDCl_3): $\delta(\text{P}_A)$ 43.4(d), $\delta(\text{P}_X)$ 21.6(d) ppm.

$^2\text{J}(^{31}\text{P}_A\text{-}^{31}\text{P}_X)$ 24.2 Hz. FTIR (KBr disc): ν (PNP) 1262, 1182, 747; ν (PO) 1161, 1127; ν (PS) 562; δ (NPS) 402 cm^{-1} . FAB +ve MS: m/z 801 corresponds to $\{\text{Zn}[(\text{EtO})_2\text{P}(\text{S})\text{NP}(\text{O})\text{Ph}_2]_2\}^+$.

$\text{Pd}[(\text{EtO})_2\text{P}(\text{S})\text{NP}(\text{O})\text{Ph}_2]_2$ **39**. PdCODCl_2 (0.019 g, 0.067 mmol) was added to a solution of **32** (0.050 g, 0.136 mmol) and KO^tBu (0.015 g, 0.134 mmol) in THF (20 ml) and stirred for 1 hour, changing colour from yellow to red/orange. The mixture was then evaporated to dryness and dichloromethane added which was filtered and the filtrate evaporated to dryness giving a dark red oil. Microanalysis calculated for $\text{C}_{32}\text{H}_{40}\text{N}_2\text{O}_6\text{P}_4\text{S}_2\text{Pd}$: C 45.6; H 4.8; N 3.3 %. Observed : C 45.4; H 5.0; N 3.1 %. $^{31}\text{P}\{-^1\text{H}\}$ NMR (CDCl_3): $\delta(\text{P}_A)$ 58.6(d), $\delta(\text{P}_X)$ 21.8(d) ppm. $^2\text{J}(^{31}\text{P}_A\text{-}^{31}\text{P}_X)$ 13.4 Hz. FTIR (KBr disc): ν (PNP) 1240; ν (PO) 1126; ν (PS) 625, 547 cm^{-1} . FAB +ve MS: m/z 843 corresponds to $\{\text{Pd}[(\text{EtO})_2\text{P}(\text{S})\text{NP}(\text{O})\text{Ph}_2]_2\}^+$.

$\text{Pt}[(\text{EtO})_2\text{P}(\text{S})\text{NP}(\text{O})\text{Ph}_2]_2$ **40**. PtCODCl_2 (0.020 g, 0.053 mmol) was added to a solution of **32** (0.039 g, 0.106 mmol) and KO^tBu (0.012 g, 0.107 mmol) in THF (20 ml) and stirred for 1 hour, changing colour from colourless to a yellow solution. The mixture was then evaporated to dryness and dichloromethane added which was filtered and the filtrate evaporated to dryness giving a yellow oil. Microanalysis calculated for $\text{C}_{32}\text{H}_{40}\text{N}_2\text{O}_6\text{P}_4\text{S}_2\text{Pt}$: C 41.3; H 4.3; N 3.0 %. Observed : C 39.2; H 4.3; N 2.4 %. $^{31}\text{P}\{-^1\text{H}\}$ NMR (CDCl_3): $\delta(\text{P}_A)$ 65.3(d), $\delta(\text{P}_X)$ 19.7(d) ppm. $^2\text{J}(^{31}\text{P}_A\text{-}^{31}\text{P}_X)$ 18.7 Hz. No $^2\text{J}(^{31}\text{P}\text{-}^{195}\text{Pt})$ coupling was observed that could confidently be assigned or calculated.

FTIR (KBr disc): ν (PNP) 1259, 1161; ν (PO) 1125; ν (PS) 548 cm^{-1} . FAB +ve MS: m/z 932 corresponds to $\{\text{Pt}[(\text{EtO})_2\text{P}(\text{S})\text{NP}(\text{O})\text{Ph}_2]_2\}^+$.

$(\text{EtO})_2\text{P}(\text{O})\text{NHP}(\text{S})\text{Ph}_2$ **33**. $\text{Ph}_2\text{P}(\text{S})\text{NH}_2$ (3.62 g, 15.54 mmol) was dissolved in THF (50 ml) and 3 mole equivalents of NaH (60% dispersion in paraffin oil, 1.86 g, 46.61 mmol) was added dropwise at 0 °C. The mixture was allowed to warm to room temperature and stirred for 30 minutes, then $(\text{EtO})_2\text{P}(\text{O})\text{Cl}$ (2.68 g, 2.25 ml, 15.54 mmol) was added dropwise at 0 °C. When the mixture was again at room temperature, it was stirred overnight. Methanol (5 ml) was then added dropwise to destroy any excess sodium hydride. The mixture was reduced by half under vacuum before 2M aqueous HCl (50 ml) was added, producing a white precipitate which was extracted with dichloromethane (3 x 20 ml). The dichloromethane was dried over MgSO_4 then evaporated to dryness to give another yellow oil which was recrystallised from the minimum of dichloromethane yielding colourless crystals upon cooling (4.62 g, 12.52 mmol, 80.6 % yield, mp 174 °C). Microanalysis calculated for $\text{C}_{16}\text{H}_{21}\text{NO}_3\text{P}_2\text{S}$: C 52.0; H 5.7; N 3.8 %. Observed: C 51.1; H 5.5; N 3.6 %. ^{31}P - $\{^1\text{H}\}$ NMR (CDCl_3): $\delta(\text{P}_A)$ 0.1(d), $\delta(\text{P}_X)$ 53.3(d) ppm. $^2\text{J} (^{31}\text{P}_A-^{31}\text{P}_X)$ 13.2 Hz. FTIR (dichloromethane solution, CsI plates at 100 microns): ν (N-H) 3334 cm^{-1} ; (KBr disc): δ (N-H) 1315; ν (PNP) 754; ν (PO) 1186; ν (PS) 630 cm^{-1} . FT Raman (capillary sample): ν (PO) 1159; ν (PS) 616 cm^{-1} .

$\text{Zn}[(\text{EtO})_2\text{P}(\text{O})\text{NP}(\text{S})\text{Ph}_2]_2$ **36**. A solution of **33** (0.050 g, 0.135 mmol), KO^tBu (0.015 g, 0.134 mmol) and ZnCl_2 (0.010 g, 0.073 mmol) in THF (20 ml) was stirred for 1 hour. The mixture was then evaporated to dryness and dichloromethane added which was filtered and the filtrate evaporated to dryness yielding a colourless oil. Microanalysis calculated for $\text{C}_{32}\text{H}_{40}\text{N}_2\text{O}_6\text{P}_4\text{S}_2\text{Zn}$: C 47.9; H 5.0; N 3.5 %. Observed: C 47.0; H 4.8; N 3.5 %. ^{31}P - $\{^1\text{H}\}$ NMR (CDCl_3): $\delta(\text{P}_A)$ 5.4(d), $\delta(\text{P}_X)$ 35.6(d) ppm. $^2\text{J} (^{31}\text{P}_A-^{31}\text{P}_X)$ 22.0 Hz. FTIR (KBr disc): ν (PNP) 1255, 1165, 747; ν (PO) 1112; ν (PS) 583; δ (NPS) 421 cm^{-1} . FAB +ve MS: m/z 801 corresponds to $\{\text{Zn}[(\text{EtO})_2\text{P}(\text{O})\text{NP}(\text{S})\text{Ph}_2]_2\}^+$.

$\text{Pd}[(\text{EtO})_2\text{P}(\text{O})\text{NP}(\text{S})\text{Ph}_2]_2$ **41**. PdCODCl_2 (0.019 g, 0.067 mmol) was added to a solution of **33** (0.050 g, 0.136 mmol) and KO^tBu (0.015 g, 0.134 mmol) in THF (20 ml) and stirred for 1 hour, changing colour from yellow to red/orange. The mixture was then evaporated to dryness and dichloromethane added which was filtered and the filtrate evaporated to dryness giving a dark red oil. Microanalysis calculated for $\text{C}_{32}\text{H}_{40}\text{N}_2\text{O}_6\text{P}_4\text{S}_2\text{Pd}$: C 45.6; H 4.8; N 3.3 %. Observed : C 44.4; H 4.9; N 3.1 %. ^{31}P - $\{^1\text{H}\}$ NMR (CDCl_3): $\delta(\text{P}_A)$ 3.9(d), $\delta(\text{P}_X)$ 28.4(d) ppm. ^2J ($^{31}\text{P}_A$ - $^{31}\text{P}_X$) 24.5 Hz. $\delta(\text{P}_A)$ 3.6(d), $\delta(\text{P}_X)$ 27.4(d) ppm. ^2J ($^{31}\text{P}_A$ - $^{31}\text{P}_X$) 29.7 Hz. FTIR (KBr disc): ν (PNP) 1231, 1165; ν (PO) 1112; ν (PS) 570, 513 cm^{-1} . FAB +ve MS: m/z 843 corresponds to $\{\text{Pd}[(\text{EtO})_2\text{P}(\text{O})\text{NP}(\text{S})\text{Ph}_2]_2\}^+$.

$\text{Pt}[(\text{EtO})_2\text{P}(\text{O})\text{NP}(\text{S})\text{Ph}_2]_2$ **42**. PtCODCl_2 (0.020 g, 0.053 mmol) was added to a solution of **33** (0.039 g, 0.106 mmol) and KO^tBu (0.012 g, 0.107 mmol) in THF (20 ml) and stirred for 1 hour, changing colour from colourless to a yellow solution. The mixture was then evaporated to dryness and dichloromethane added which was filtered and the filtrate evaporated to dryness giving a yellow oil. Microanalysis calculated for $\text{C}_{32}\text{H}_{40}\text{N}_2\text{O}_6\text{P}_4\text{S}_2\text{Pt}$: C 41.3; H 4.3; N 3.0 %. Observed : C 41.9; H 4.5; N 2.5 %. ^{31}P - $\{^1\text{H}\}$ NMR (CDCl_3): $\delta(\text{P}_A)$ 0.4(d), $\delta(\text{P}_X)$ 24.9(d) ppm. ^2J ($^{31}\text{P}_A$ - $^{31}\text{P}_X$) 23.4 Hz. No ^2J (^{31}P - ^{195}Pt) coupling was observed that could confidently be assigned or calculated. FTIR (KBr disc): ν (PNP) 1240, 1164; ν (PO) 1181; ν (PS) 618, 551 cm^{-1} . FAB +ve MS: m/z 932 corresponds to $\{\text{Pt}[(\text{EtO})_2\text{P}(\text{O})\text{NP}(\text{S})\text{Ph}_2]_2\}^+$.

CHAPTER 5:
**MOLECULAR MODELLING STUDIES AND A CRYOSCOPIC
INVESTIGATION INTO MOLECULAR WEIGHTS IN SOLUTION**

5.1 Introduction.

Molecular modelling has been closely involved with the metals extraction research effort at Zeneca and in recent years progress in the application of computer assisted modelling has allowed the rapid development of a great variety of molecular modelling techniques which have now become powerful tools. Therefore most crystal structures have been studied with the semi-empirical MOPAC 93 program⁶¹ using the MNDO⁶² method. The square planar complex, **6**, was studied with the *ab initio* ADF program⁶³ because there are no MNDO transition metal parameters with the exception of Zn, Cd and Hg. In order to compare the two methods **11** was also studied with ADF.

In addition one area of particular interest has been whether the compounds which exist as hydrogen bonded *trans* dimers in the solid state are dimers in solution, particularly in a non-polar solvent such as cyclohexane. Some studies were performed to calculate heats of formation in solution using the COSMO methodology. These were then used to evaluate the solution dimerisation energies. The five compounds **1**, **10**, **11**, **12** and **31** were studied cryoscopically and their molecular weights in solution determined. All calculations were carried out on a Silicon Graphics Indigo 2 at the Zeneca Specialties Research Molecular Modelling Section.

RESULTS AND DISCUSSION

5.21 MNDO Models of Neutral Ligands.

For the best comparison the neutral ligands have been split into different structural groups (Figure 5.1), the *cis* hydrogen bonded chain, the *trans* hydrogen bonded dimers and the *trans* hydrogen bonded chain. The starting point for all of the semi-empirical calculations was the crystal structure of each compound.

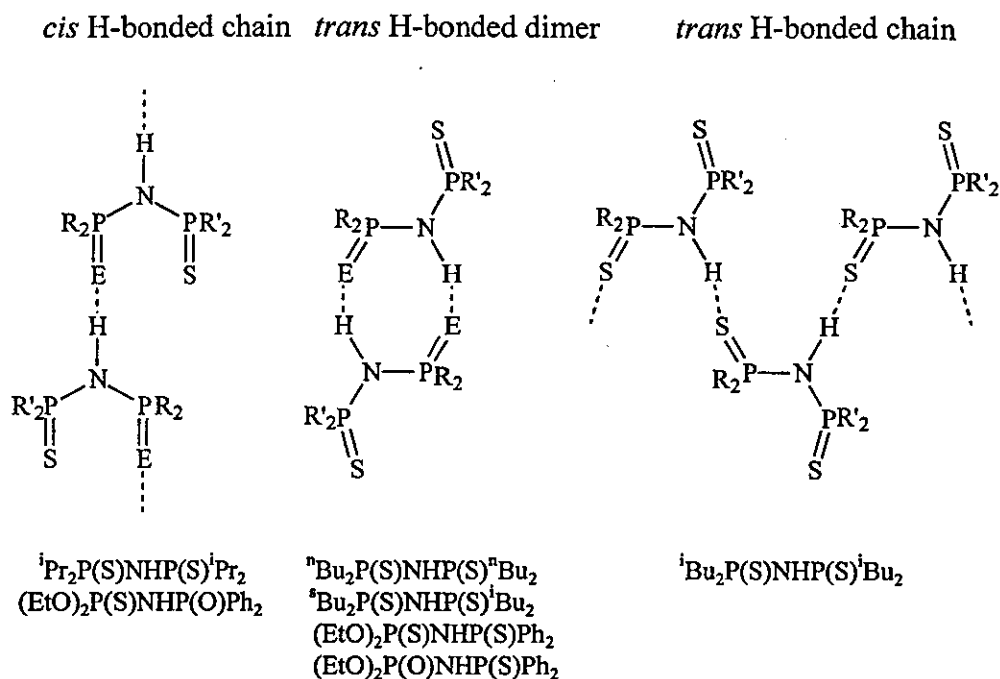


Figure 5.1. Differing types of structure in the solid state.

For the *cisoid* structures (Table 5.1) the agreement between calculated and observed P-S, P-O and P-N bond lengths is good, the greatest difference being 0.04 Å for the P-S bond in $(\text{EtO})_2\text{P}(\text{S})\text{NHP}(\text{O})\text{Ph}_2$. The P-N-P bond angles are also accurately predicted, differing by no more than 3°. However the calculated S-P...P-S torsion angle for ${}^i\text{Pr}_2\text{P}(\text{S})\text{NHP}(\text{S}){}^i\text{Pr}_2$ is out by 45° (Figure 5.2), closer to a *trans* geometry rather than *cis*, whereas the O-P...P-S torsion angle for $(\text{EtO})_2\text{P}(\text{S})\text{NHP}(\text{O})\text{Ph}_2$ agrees well.

Table 5.1. Comparison of bond lengths (Å) and angles (°) of the crystal structures and MNDO modelled structures of ${}^i\text{Pr}_2\text{P}(\text{S})\text{NHP}(\text{S}){}^i\text{Pr}_2$ and $(\text{EtO})_2\text{P}(\text{S})\text{NHP}(\text{O})\text{Ph}_2$.

Bond lengths/angles	${}^i\text{Pr}_2\text{P}(\text{S})\text{NHP}(\text{S}){}^i\text{Pr}_2$		$(\text{EtO})_2\text{P}(\text{S})\text{NHP}(\text{O})\text{Ph}_2$	
	Structure	MNDO Model	Structure	MNDO Model
E(1)-P(1)	1.94	1.92	1.48	1.51
S(2)-P(2) / S(1)-P(2)	1.95	1.92	1.90	1.94
P(1)-N(1)	1.68	1.68	1.67	1.69
P(2)-N(1)	1.68	1.70	1.66	1.66
P(1)-N(1)-P(2)	131.6	134.6	122.6	125.4
E(1)-P(1)...P(2)-S(2)	79.4	125.7	79.5	77.2

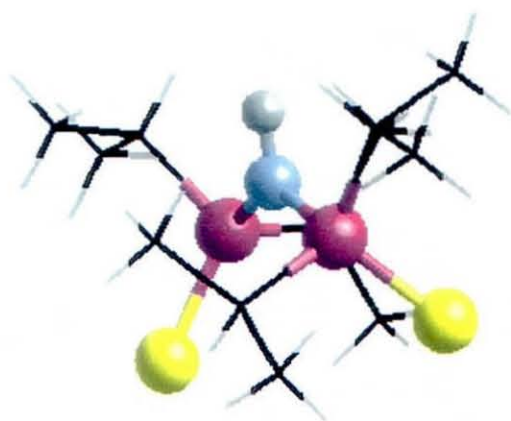
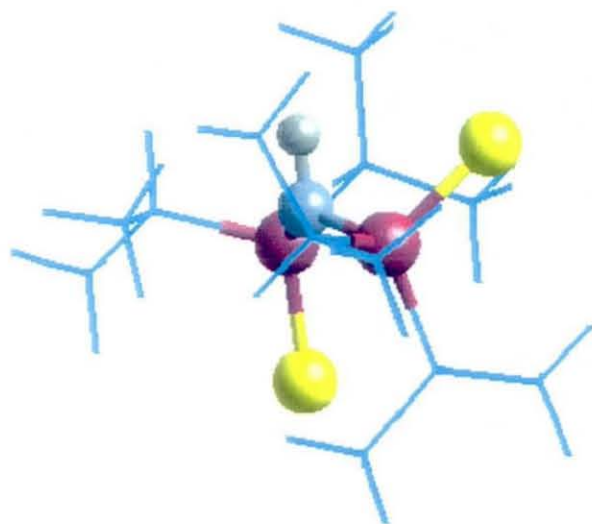


Figure 5.2. Comparison of the MNDO modelled structure (in blue) with the observed crystal structure of $i\text{-Pr}_2\text{P}(\text{S})\text{NHP}(\text{S})i\text{-Pr}_2$.

Heats of formation were calculated in two ways, one from the model of the crystal structure (ΔH_{F1}) and a further one from modelling the structure with the backbone of central atoms (S, P and N) constrained (ΔH_{F2}) so that the S-P...P-E (E = S / O) torsion angle observed in the crystal structure remained the same whilst the rest of the structure was allowed to “relax”, the purpose being to reduce any steric clash in the substituent groups present in the crystal structure.

The heat of formation (ΔH_{F2}) calculated for ${}^i\text{Pr}_2\text{P}(\text{S})\text{NHP}(\text{S}){}^i\text{Pr}_2$ with the S, P and N atoms constrained is $-71.06 \text{ kcalmol}^{-1}$, much lower than ΔH_{F1} value of $-4.35 \text{ kcalmol}^{-1}$. This large discrepancy indicates there is a great deal of steric clash in the iso-propyl substituents in ΔH_{F1} , however the ΔH_{F1} value may in part be due to the different torsion angle (125.7°). In contrast the ΔH_{F1} value for $(\text{EtO})_2\text{P}(\text{S})\text{NHP}(\text{O})\text{Ph}_2$ ($-71.06 \text{ kcalmol}^{-1}$) is 9 kcalmol^{-1} lower than the constrained ΔH_{F2} value of $-62.42 \text{ kcalmol}^{-1}$, possibly due to the changes in the P-N-P angle and E-P...P-S torsion angle in the unconstrained model.

For the butyl substituted *trans* dimer type compounds (Table 5.2), only the monomer was modelled. The agreement between calculated and observed P-S, P-O and P-N bond lengths is again very good. Moreover the P-N-P angle and S-P...P-S torsion angle are modelled better than for the *cis* type compounds, the largest difference being 1° . ΔH_{F1} values for ${}^n\text{Bu}_2\text{P}(\text{S})\text{NHP}(\text{S}){}^n\text{Bu}_2$ (Figure 5.3) and ${}^s\text{Bu}_2\text{P}(\text{S})\text{NHP}(\text{S}){}^i\text{Bu}_2$ are around 5 kcal mol^{-1} lower than their ΔH_{F2} values (Table 5.4), again this may be due to the changes in the P-N-P and the S-P...P-S torsion angles.

Table 5.2. Comparison of bond lengths (Å) and angles ($^\circ$) of the crystal structures and MNDO models of ${}^n\text{Bu}_2\text{P}(\text{S})\text{NHP}(\text{S}){}^n\text{Bu}_2$ and ${}^s\text{Bu}_2\text{P}(\text{S})\text{NHP}(\text{S}){}^i\text{Bu}_2$.

Bond lengths/angles	${}^n\text{Bu}_2\text{P}(\text{S})\text{NHP}(\text{S}){}^n\text{Bu}_2$		${}^s\text{Bu}_2\text{P}(\text{S})\text{NHP}(\text{S}){}^i\text{Bu}_2$	
	Structure	MNDO Model	Structure	MNDO Model
S(1)-P(1)	1.94	1.92	1.94	1.92
S(2)-P(2)	1.93	1.92	1.94	1.92
P(1)-N(1)	1.68	1.67	1.69	1.68
P(2)-N(1)	1.69	1.66	1.70	1.66
P(1)-N(1)-P(2)	132.1	133.2	133.1	134.2
S(1)-P(1)...P(2)-S(2)	179.0	179.8	179.4	179.2

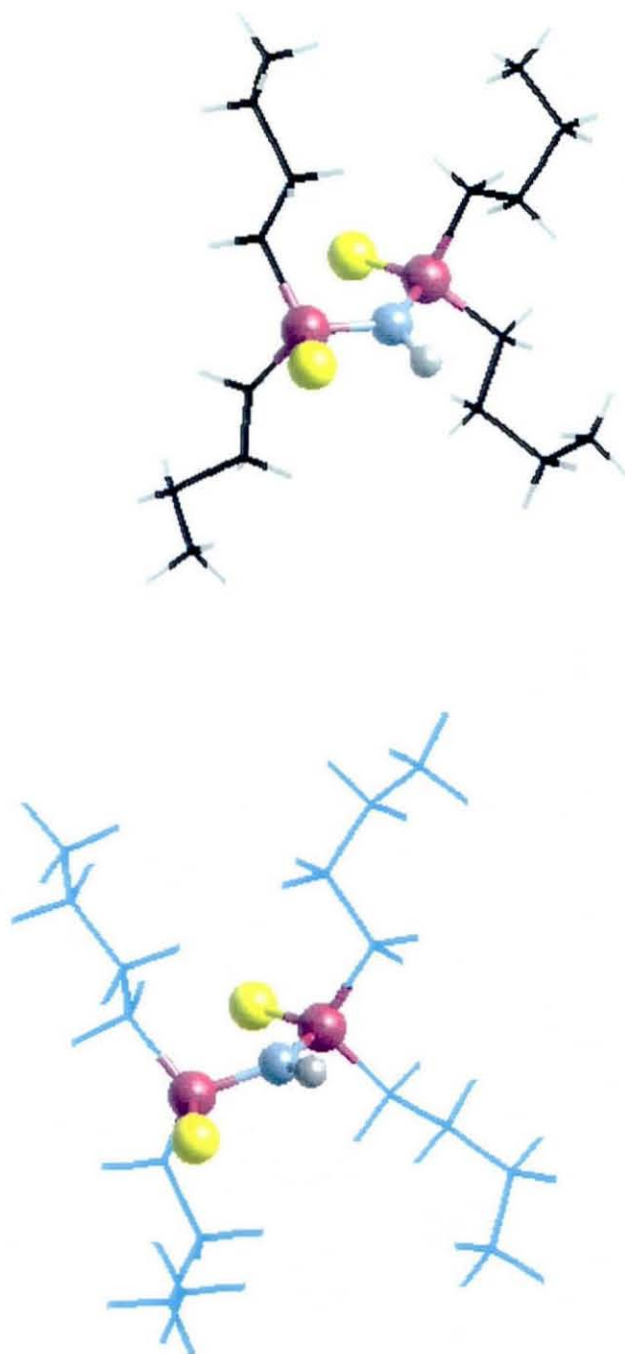


Figure 5.3. Comparison of the MNDO modelled structure (in blue) with the observed crystal structure of $n\text{Bu}_2\text{P}(\text{S})\text{NHP}(\text{S})n\text{Bu}_2$.

The modelled monomers of the *trans* dimer type compounds with ethoxy and phenyl group substituents (Table 5.3) also compare well with the observed structures with the exception of the S-P...P-S torsion angle for (EtO)₂P(S)NHP(S)Ph₂ which

Table 5.3. Comparison of bond lengths (Å) and angles (°) of the crystal structures and MNDO modelled structures of (EtO)₂P(S)NHP(S)Ph₂ and (EtO)₂P(O)NHP(S)Ph₂.

Bond lengths/angles	(EtO) ₂ P(S)NHP(S)Ph ₂		(EtO) ₂ P(O)NHP(S)Ph ₂	
	Structure	MNDO Model	Structure	MNDO Model
S(1)-P(1)	1.94	1.93	1.93	1.93
S(2)-P(2) / O(1)-P(2)	1.92	1.94	1.46	1.50
P(1)-N(1)	1.68	1.68	1.68	1.67
P(2)-N(1)	1.67	1.66	1.63	1.66
P(1)-N(1)-P(2)	129.9	134.0	130.5	131.9
E(1)-P(1)...P(2)-S(2)	87.0	75.2	172.3	175.3

differs by 12 ° from the model. It is somewhat surprising that this compound is a *trans* dimer at all with such a small torsion angle, however the ΔH_{F1} value (Table 5.4) of - 20.69 kcalmol⁻¹ is significantly lower than the constrained ΔH_{F2} value of - 14.90 kcalmol⁻¹ indicating the change in the torsion angle produces a calculated structure of lower heat of formation. Similarly ΔH_{F1} for (EtO)₂P(O)NHP(S)Ph₂ (- 75.05 kcalmol⁻¹) is lower than its constrained ΔH_{F2} value of - 68.81 kcalmol⁻¹.

Table 5.4. Heats of formation values for the modelled crystal (ΔH_{F1}) and constrained (ΔH_{F2}) structures of the *trans* dimer type compounds (kcalmol⁻¹).

	ⁿ Bu ₂ P(S)NHP(S) ⁿ Bu ₂	^s Bu ₂ P(S)NHP(S) ^s Bu ₂	(EtO) ₂ P(S)NHP(S)Ph ₂	(EtO) ₂ P(O)NHP(S)Ph ₂
ΔH_{F1}	- 45.238	- 22.998	- 20.690	- 75.049
ΔH_{F2}	- 39.881	- 17.705	- 14.903	- 68.814

The general trend for the *trans* dimer type compounds is that structures modelled with a constrained S, P and N backbone are less preferred than the conventionally modelled structures.

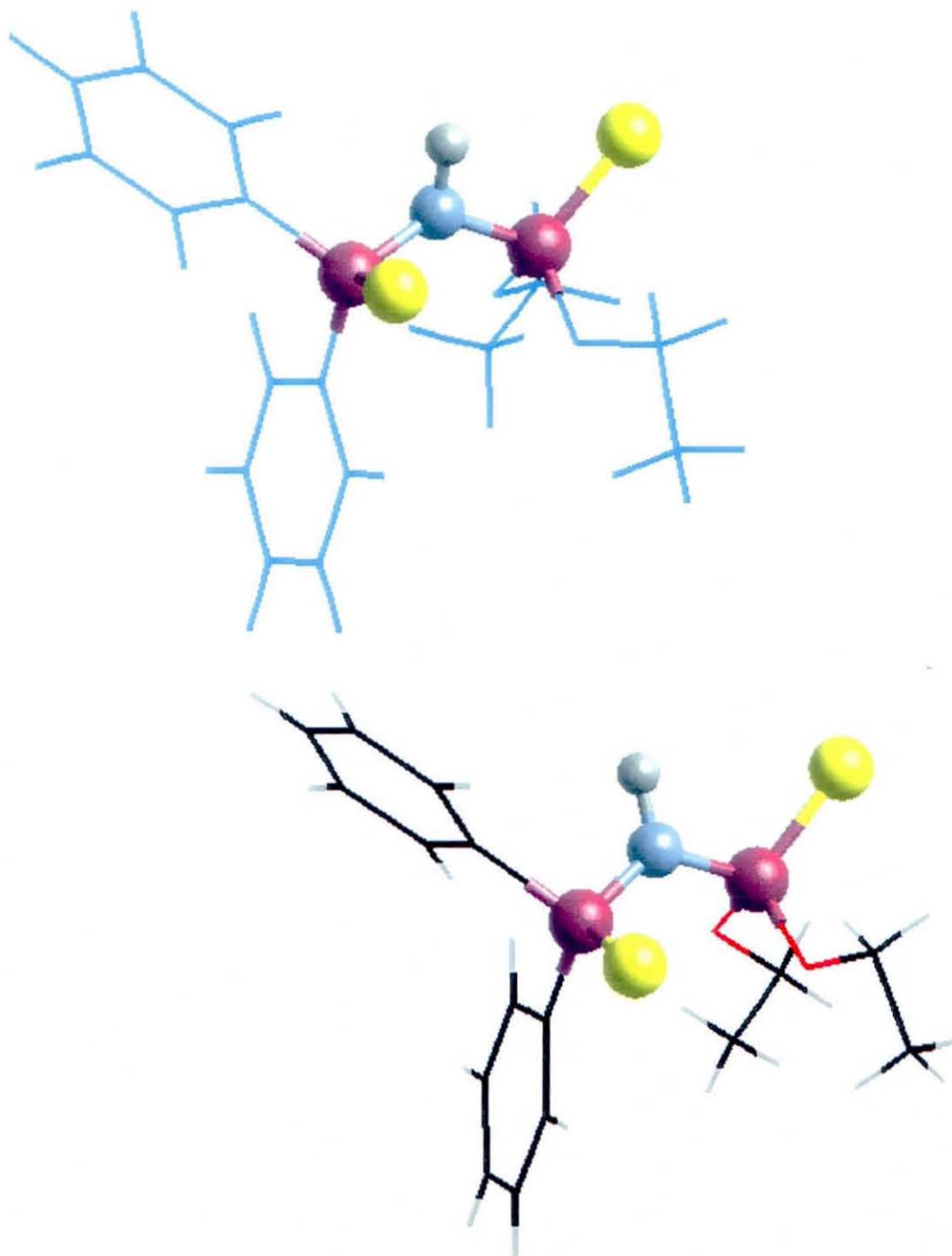


Figure 5.4. Comparison of the MNDO modelled structure (in blue) with the observed crystal structure of $(\text{EtO})_2\text{P}(\text{S})\text{NHP}(\text{S})\text{Ph}_2$.

The ${}^i\text{Bu}_2\text{P}(\text{S})\text{NHP}(\text{S}){}^i\text{Bu}_2$ compound was modelled both by MNDO and ADF in order to compare the two different methodologies (Table 5.5). Again the MNDO model (Figure 5.5) is in excellent agreement with the crystal structure with the exception of the S-P...P-S torsion angle which is 172° as opposed to the planar

Table 5.5. Comparison of bond lengths (Å) and angles ($^\circ$) of the crystal structure with the MNDO and the ADF modelled structures of ${}^i\text{Bu}_2\text{P}(\text{S})\text{NHP}(\text{S}){}^i\text{Bu}_2$.

Bond lengths/angles	${}^i\text{Bu}_2\text{P}(\text{S})\text{NHP}(\text{S}){}^i\text{Bu}_2$		
	Structure	MNDO Model	ADF Model
S(1)-P(1)	1.93	1.92	2.09
S(2)-P(2)	1.95	1.92	2.08
P(1)-N(1)	1.66	1.67	1.74
P(2)-N(1)	1.71	1.68	1.75
P(1)-N(1)-P(2)	133.0	132.4	129.6
S(1)-P(1)...P(2)-S(2)	179.8	172.2	171.6

torsion angle of 180° . However the ADF model is in poor agreement for bond lengths, the P-S bonds are 0.13 - 0.16 Å and the P-N bonds are 0.04 - 0.08 Å longer than observed in the crystal structure. The P-N-P angle and S-P...P-S torsion angle are both smaller than those observed but more comparable with the errors observed previously for MNDO. For a compound that is not a metal complex the ADF model is far less accurate than MNDO.

Further calculations have been made relating to the heats of formation of the dimers (ΔH_{FD}) compared to those of the monomers (ΔH_{FM}) (Table 5.6). All compounds of the *trans* geometry have been studied plus a MNDO model of ${}^s\text{Bu}_2\text{P}(\text{S})\text{NHP}(\text{S}){}^s\text{Bu}_2$. These compounds prefer the dimer state if $\Delta H_{\text{FD}}/2$ is more negative than the ΔH_{FM} value, ie. $(\Delta H_{\text{FD}}/2) - \Delta H_{\text{FM}} < 0$. From the calculations all the compounds appear to prefer the dimer state, though it is interesting to note the $\{(\Delta H_{\text{FD}}/2) - \Delta H_{\text{FM}}\}$ value for ${}^i\text{Bu}_2\text{P}(\text{S})\text{NHP}(\text{S}){}^i\text{Bu}_2$ is $-2.91 \text{ kcalmol}^{-1}$ despite the fact ${}^i\text{Bu}_2\text{P}(\text{S})\text{NHP}(\text{S}){}^i\text{Bu}_2$ is known not to be a dimer in the solid state. This figure is notably greater than those for the known *trans* dimers (-0.82 to $-1.91 \text{ kcalmol}^{-1}$). Furthermore the $\{(\Delta H_{\text{FD}}/2) - \Delta H_{\text{FM}}\}$ value for the *trans* dimer type model of ${}^s\text{Bu}_2\text{P}(\text{S})\text{NHP}(\text{S}){}^s\text{Bu}_2$ is even larger at $-3.51 \text{ kcalmol}^{-1}$.

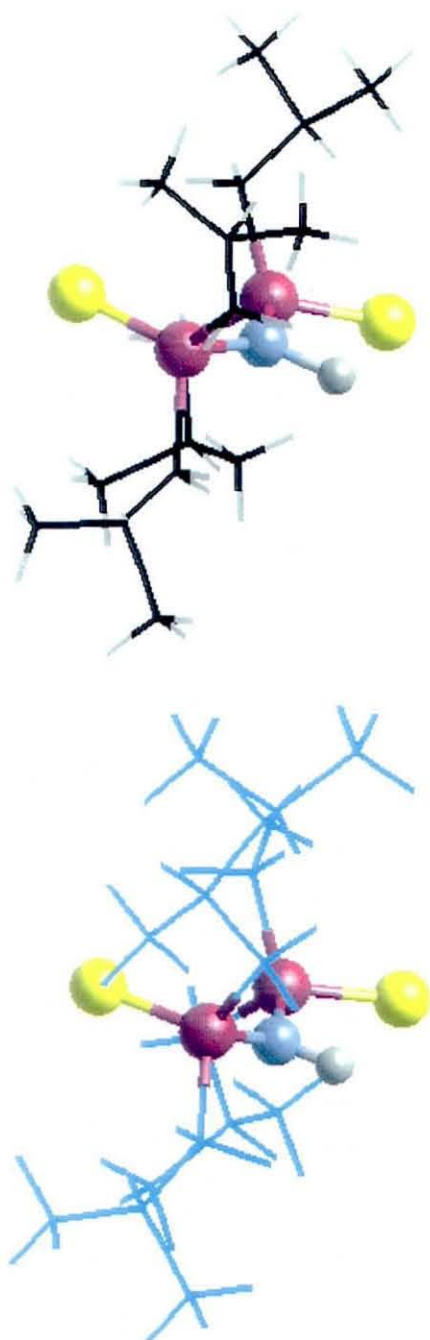


Figure 5.5. Comparison of the MNDO modelled structure (in blue) with the observed crystal structure of $i\text{Bu}_2\text{P}(\text{S})\text{NHP}(\text{S})i\text{Bu}_2$.

Calculated $(\Delta H_{FD}/2) - \Delta H_{FM}$ values relating to *trans* dimers observed in crystallography are no more negative than $-2.0 \text{ kcalmol}^{-1}$, implying the compound ${}^s\text{Bu}_2\text{P}(\text{S})\text{NHP}(\text{S}){}^s\text{Bu}_2$ is unlikely to exist as a *trans* dimer in the solid state.

Table 5.6. Monomer (ΔH_{FM}) and dimer (ΔH_{FD}) heats of formation for *transoid* compounds (kcalmol^{-1}). Calculations of unobserved structures in italics.

	ΔH_F Monomer	ΔH_F Dimer	$(\Delta H_{FD}/2) - \Delta H_{FM}$
${}^n\text{Bu}_2\text{P}(\text{S})\text{NHP}(\text{S}){}^n\text{Bu}_2$	-45.24	-94.29	-1.91
<i>${}^i\text{Bu}_2\text{P}(\text{S})\text{NHP}(\text{S}){}^i\text{Bu}_2$</i>	<i>-25.80</i>	<i>-57.41</i>	<i>-2.91</i>
<i>${}^s\text{Bu}_2\text{P}(\text{S})\text{NHP}(\text{S}){}^s\text{Bu}_2$</i>	<i>-10.81</i>	<i>-28.64</i>	<i>-3.51</i>
${}^s\text{Bu}_2\text{P}(\text{S})\text{NHP}(\text{S}){}^i\text{Bu}_2$	-23.00	-49.27	-1.64
$(\text{EtO})_2\text{P}(\text{S})\text{NHP}(\text{S})\text{Ph}_2$	-20.69	-43.02	-0.82
$(\text{EtO})_2\text{P}(\text{O})\text{NHP}(\text{S})\text{Ph}_2$	-75.05	-153.72	-1.81

Further heats of formation calculations were carried out using the COSMO method⁶⁴ for the monomers and dimers of ${}^n\text{Bu}_2\text{P}(\text{S})\text{NHP}(\text{S}){}^n\text{Bu}_2$, ${}^i\text{Bu}_2\text{P}(\text{S})\text{NHP}(\text{S}){}^i\text{Bu}_2$ and ${}^s\text{Bu}_2\text{P}(\text{S})\text{NHP}(\text{S}){}^s\text{Bu}_2$ in cyclohexane solution (Table 5.7) in an effort to predict whether these compounds might exist as dimers in solution. Again a large difference in the $(\Delta H_{FD}/2) - \Delta H_{FM}$ values is observed for **12** in comparison to **10** and **11**. Given that **10** and **11** adopt the *trans* geometry in the solid state, the results might tentatively suggest that **10** and **11** will be *trans* dimers in solution whilst **12**, with such a large $(\Delta H_{FD}/2) - \Delta H_{FM}$ value will be a monomer.

Table 5.7. Monomer (ΔH_{FM}) and dimer (ΔH_{FD}) heats of formation for *transoid* compounds in solution in C_6H_{12} (**10**, **11**, **12**) (kcalmol^{-1}).

	ΔH_F (solution)		$(\Delta H_{FD}/2) - \Delta H_{FM}$ (solution)
	Monomer	Dimer	
(10) ${}^n\text{Bu}_2\text{P}(\text{S})\text{NHP}(\text{S}){}^n\text{Bu}_2$ (C_6H_{12})	-53.70	-108.47	-0.54
(11) ${}^i\text{Bu}_2\text{P}(\text{S})\text{NHP}(\text{S}){}^i\text{Bu}_2$ (C_6H_{12})	-33.29	-68.17	-0.80
(12) ${}^s\text{Bu}_2\text{P}(\text{S})\text{NHP}(\text{S}){}^s\text{Bu}_2$ (C_6H_{12})	-17.99	-40.16	-2.09

5.22 MNDO Models of Tetrahedral Zinc Complexes.

The coordination complexes $\text{Zn}[\text{}^i\text{Pr}_2\text{P}(\text{S})\text{NP}(\text{S})\text{}^i\text{Pr}_2]_2$ (Figure 5.6) and $\text{Zn}[(\text{EtO})_2\text{P}(\text{O})\text{NP}(\text{S})\text{Ph}_2]_2$ (Figure 5.7) were also modelled with MNDO (Table 5.8). The bond lengths calculated for $\text{Zn}[\text{}^i\text{Pr}_2\text{P}(\text{S})\text{NP}(\text{S})\text{}^i\text{Pr}_2]_2$ all differ from those observed in the crystal structure by 0.05 - 0.06 Å, significantly less accurate than those calculated for the neutral ligands. For $\text{Zn}[(\text{EtO})_2\text{P}(\text{O})\text{NP}(\text{S})\text{Ph}_2]_2$ the P-S, P-O, Zn-S, and Zn-O bonds all differ by 0.02 - 0.05 Å, again in reasonable agreement. The exceptions are the P-N bonds which differ by 0.07 - 0.08 Å from the crystal structure.

Table 5.8. Comparison of bond lengths (Å) and angles ($^\circ$) of the crystal structures and MNDO models of $\text{Zn}[\text{}^i\text{Pr}_2\text{P}(\text{S})\text{NP}(\text{S})\text{}^i\text{Pr}_2]_2$ and $\text{Zn}[(\text{EtO})_2\text{P}(\text{O})\text{NP}(\text{S})\text{Ph}_2]_2$.

Bonds/angles	$\text{Zn}[\text{}^i\text{Pr}_2\text{P}(\text{S})\text{NP}(\text{S})\text{}^i\text{Pr}_2]_2$		$\text{Zn}[(\text{EtO})_2\text{P}(\text{O})\text{NP}(\text{S})\text{Ph}_2]_2$	
	Structure	MNDO model	Structure	MNDO model
S(1)-P(1)	2.03	1.97	2.01	1.98
O(1)-P(2)	-	-	1.48	1.53
P(1)-N(1)	1.58	1.64	1.58	1.65
P(2)-N(1)	-	-	1.55	1.63
Zn-S(1)	2.35	2.30	2.32	2.34
Zn-O(1)	-	-	1.95	1.92
S(1)-Zn-S(2)	112.4	98.2	-	-
S(1)-Zn-O(1)	-	-	109.5	97.1
Zn-S(1)-P(1)	107.1	116.0	98.0	113.3
Zn-O(1)-P(2)	-	-	129.0	137.8
S(1)-P(1)-N(1)	118.5	117.8	118.4	117.8
O(1)-P(2)-N(1)	-	-	118.5	119.6
P(1)-N(1)-P(2)	140.5	125.3	134.1	121.4

By comparison the bond angles show very poor agreement. Calculated S-Zn-E angles (E = S / O) are around 12 $^\circ$ smaller and P-N-P angles are approximately 14 $^\circ$ smaller than those observed in the crystal structures. In contrast the calculated Zn-E-P angles are 9 - 15 $^\circ$ greater than in the crystal structures. The only calculated angles that are at all accurate are the E-P-N angles which are all within 1 $^\circ$. These differences may be due to crystal packing effects as bond angles are believed to be easier to deform than lengths.

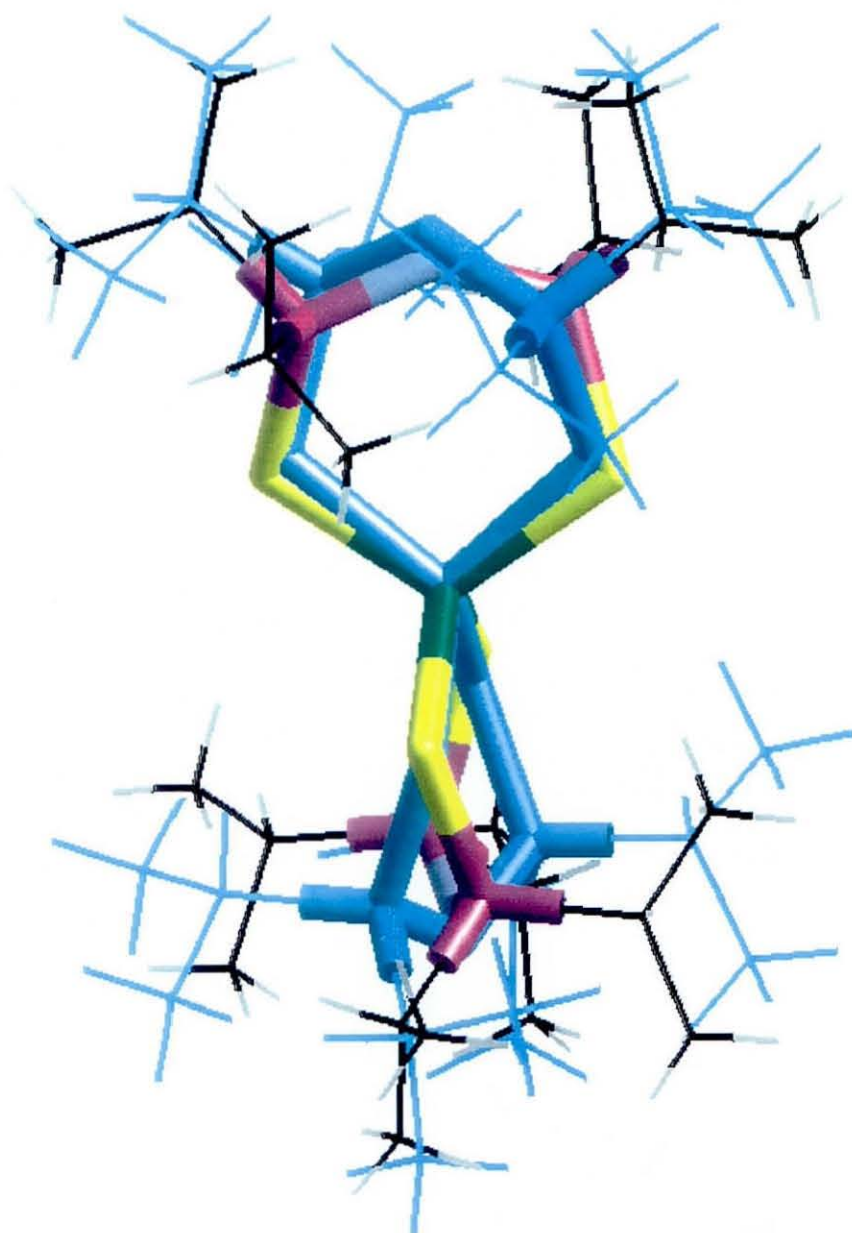


Figure 5.6. Comparison of the MNDO modelled structure (in blue) with the observed crystal structure of $\text{Zn}[\text{}^i\text{Pr}_2\text{P}(\text{S})\text{NP}(\text{S})\text{}^i\text{Pr}_2]_2$.

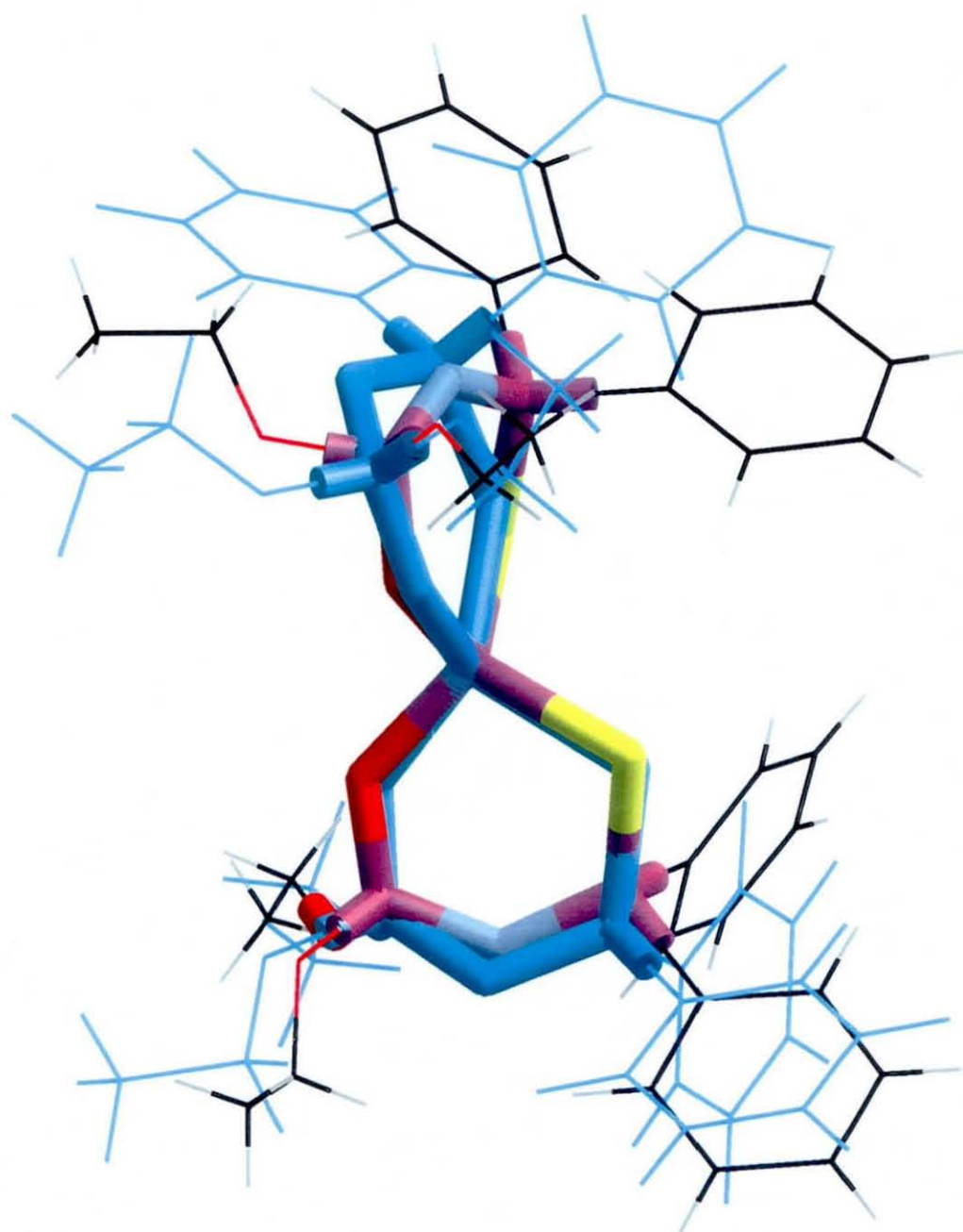


Figure 5.7. Comparison of the MNDO modelled structure (in blue) with the observed crystal structure of $\text{Zn}[(\text{EtO})_2\text{P}(\text{O})\text{NP}(\text{S})\text{Ph}_2]_2$.

5.23 ADF Model of a Square Planar Palladium Complex.

Calculated P-S bond lengths for the ADF model of $\text{Pd}[\text{}^i\text{Pr}_2\text{P}(\text{S})\text{NP}(\text{S})\text{}^i\text{Pr}_2]_2$ (Figure 5.8) differed by 0.15 Å from observed values (Table 5.9). The P-N and Pd-S calculated bond lengths were more accurate being 0.07 - 0.09 Å greater than observed lengths. In contrast the bond angles compared reasonably well, the S-Pd-S and S-P-N angles differ by only 2° from observed values and the P-N-P angle differs by 5°. These calculated angles are certainly more accurate than those found for the zinc complexes using MNDO. The exceptions are the Pd-S-P angles where the calculated angles were 6 - 12° smaller than those observed. Indeed the Pd-S(2)-P(2) angle at 96.4° might be expected in a “chair” type $\text{MS}_2\text{P}_2\text{N}$ ring conformation observed previously for platinum complexes. In many ways the calculated structure could be considered as a mixture of the “boat” and “chair” conformations producing an hybrid $\text{MS}_2\text{P}_2\text{N}$ ring conformation. The only possible example of such an hybrid previously observed in this work is the crystal structure of 43, where Pt-S-P bond angles were 97.3 and 108.1°, surprisingly similar to those calculated here. A tentative observation might then be made that the program implies the difference in energy between the “boat” and “chair” conformations of the $\text{MS}_2\text{P}_2\text{N}$ ring is extremely small.

Table 5.9. Comparison of bond lengths (Å) and angles (°) of the crystal structure and ADF modelled structure of $\text{Pd}[\text{}^i\text{Pr}_2\text{P}(\text{S})\text{NP}(\text{S})\text{}^i\text{Pr}_2]_2$.

Bond lengths/angles	$\text{Pd}[\text{}^i\text{Pr}_2\text{P}(\text{S})\text{NP}(\text{S})\text{}^i\text{Pr}_2]_2$	
	Structure	ADF model
S(1)-P(1)	2.03	2.19
S(2)-P(2)	2.02	2.17
P(1)-N(1)	1.60	1.68
P(2)-N(2)	1.59	1.68
Pd-S(1)	2.34	2.41
Pd-S(2)	2.35	2.41
S(1)-Pd-S(2)	100.7	102.6
Pd-S(1)-P(1)	114.0	108.4
Pd-S(2)-P(2)	108.6	96.4
S(1)-P(1)-N(1)	119.1	120.8
S(2)-P(2)-N(1)	117.1	117.4
P(1)-N(1)-P(2)	130.2	125.3

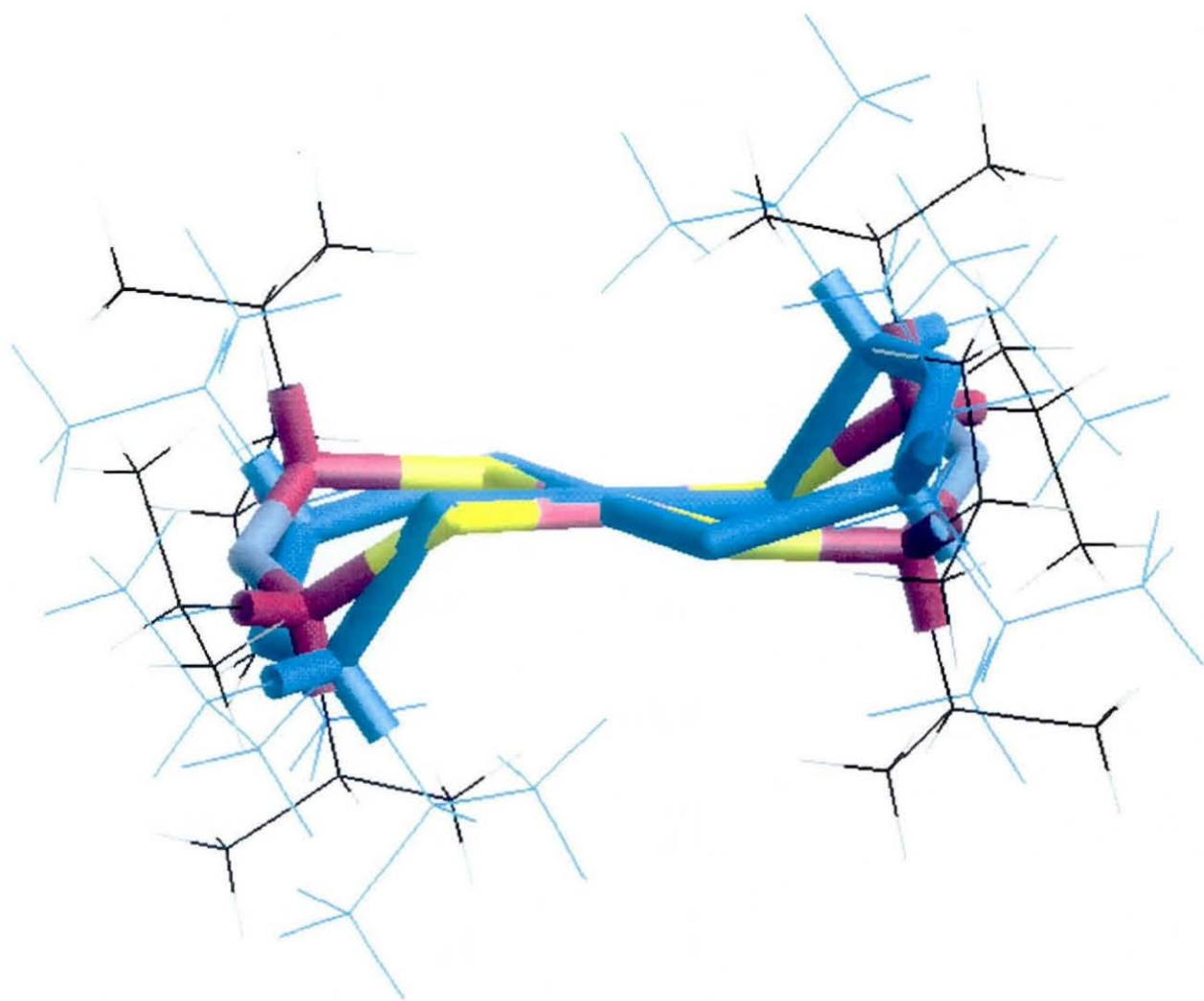


Figure 5.8. Comparison of the ADF modelled structure (in blue) with the observed crystal structure $\text{Pd}[\text{}^i\text{Pr}_2\text{P}(\text{S})\text{NP}(\text{S})\text{}^i\text{Pr}_2]_2$.

5.31 Studies on the Conformation of Neutral Ligands in Solution.

The compounds of particular interest were the symmetrical propyl and butyl substituted dithioimidodiphosphinates and $(\text{EtO})_2\text{P}(\text{S})\text{NHP}(\text{S})\text{Ph}_2$. It is interesting to note in the FAB +ve mass spectrum of ${}^i\text{Pr}_2\text{P}(\text{S})\text{NHP}(\text{S}){}^i\text{Pr}_2$ the parent ion peak was 627 m/z corresponding to a dimer $[\text{HN}({}^i\text{Pr}_2\text{PS})_2]_2$. This was somewhat surprising as in the solid state this compound is observed in the *cisoid* form in a hydrogen bonded chain. However it is possible that when the solution of ${}^i\text{Pr}_2\text{P}(\text{S})\text{NHP}(\text{S}){}^i\text{Pr}_2$ is ionised the dimer is formed.

In order to determine whether these compounds exist as monomers or dimers in solution, analytical techniques were used where spectra could be observed from the sample in both the solid state and solution (NMR, FTIR). Having observed the solid state ${}^{31}\text{P}$ NMR spectrum of the *trans* dimer type ${}^n\text{Bu}_2\text{P}(\text{S})\text{NHP}(\text{S}){}^n\text{Bu}_2$ compound where the two phosphorus atoms were observed to be inequivalent (77.8, 67.8 ppm) due to hydrogen bonding, a solution ${}^{31}\text{P}$ NMR spectrum of the same compound was run in a non-polar solvent (cyclohexane). A singlet was observed (71.0 ppm) indicating the phosphorus centres were equivalent and that no dimer was present. It is likely this is due to a rapid exchange between monomer and dimer in solution that is too fast to resolve.

Comparing the difference in values observed for the ν (NH) vibration in solution IR (DCM, CsI cell) and solid state IR spectra (KBr disc) with S...H hydrogen bond lengths of the compounds indicated a general trend (Table 5.10, Figure 5.9).

Table 5.10. Comparison of the shifts in ν (NH) vibrations from solution and solid state FTIR (cm^{-1}) with S...H hydrogen bond lengths in the crystal structures (\AA).

	ν (NH) solid	ν (NH) solution	$\nu_{\text{solution}} - \nu_{\text{solid}}$	S...H (\AA)
${}^i\text{Pr}_2\text{P}(\text{S})\text{NHP}(\text{S}){}^i\text{Pr}_2$	3243	3320	77	2.60
${}^s\text{Bu}_2\text{P}(\text{S})\text{NHP}(\text{S}){}^s\text{Bu}_2$	3225	3319	94	-
$(\text{EtO})_2\text{P}(\text{S})\text{NHP}(\text{S})\text{Ph}_2$	3200	3331	131	2.45
${}^i\text{Bu}_2\text{P}(\text{S})\text{NHP}(\text{S}){}^i\text{Bu}_2$	3180	3323	143	2.51
${}^n\text{Bu}_2\text{P}(\text{S})\text{NHP}(\text{S}){}^n\text{Bu}_2$	3172	3325	153	2.44
$(\text{EtO})_2\text{P}(\text{O})\text{NHP}(\text{S})\text{Ph}_2$	3059	3334	275	1.88
$(\text{EtO})_2\text{P}(\text{S})\text{NHP}(\text{O})\text{Ph}_2$	3057	3342	285	1.60

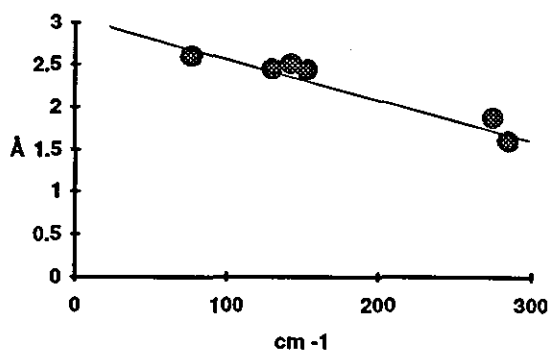


Figure 5.9. Plot of $\nu_{\text{solution}} - \nu_{\text{solid}}$ (x axis) versus $\text{S}\cdots\text{H}$ (y axis).

The greater the value of $\nu_{\text{solution}} - \nu_{\text{solid}}$ the shorter the hydrogen bond. Not surprisingly the compounds which hydrogen bond through oxygen donor atoms have far greater $\nu_{\text{solution}} - \nu_{\text{solid}}$ values as there is a significant reduction in the strength of the hydrogen bonding when the compounds are in dichloromethane solution, implying therefore that these compounds do not exist as dimers in dichloromethane.

Furthermore from a line of best fit we can estimate the $\text{S}\cdots\text{H}$ hydrogen bond for ${}^t\text{Bu}_2\text{P}(\text{S})\text{NHP}(\text{S}){}^t\text{Bu}_2$ will be between 2.60 and 2.70 Å.

However the results of the compounds modelled as *transoid* dimers in continuum with the same dielectric constant as cyclohexane (${}^n\text{Bu}_2\text{P}(\text{S})\text{NHP}(\text{S}){}^n\text{Bu}_2$, ${}^i\text{Bu}_2\text{P}(\text{S})\text{NHP}(\text{S}){}^i\text{Bu}_2$ and ${}^t\text{Bu}_2\text{P}(\text{S})\text{NHP}(\text{S}){}^t\text{Bu}_2$) to simulate a solution of the compounds in their respective solvents (Table 5.7) do imply the ${}^n\text{Bu}_2\text{P}(\text{S})\text{NHP}(\text{S}){}^n\text{Bu}_2$ and ${}^i\text{Bu}_2\text{P}(\text{S})\text{NHP}(\text{S}){}^i\text{Bu}_2$ compounds will probably be dimers in solution and the ${}^t\text{Bu}_2\text{P}(\text{S})\text{NHP}(\text{S}){}^t\text{Bu}_2$ compound will probably be a monomer in solution.

5.32 Introduction to Solution Molecular Mass Determinations on Tetrabutylthioimidodiphosphinates and Related Compounds.

The solution structures of the imidodiphosphinates (**1**, **10**, **11**, **12** and **31**) were investigated by cryoscopic (depression of freezing point of a solvent) determination of their relative molecular masses in order to ascertain whether the association found in their solid state structures (mediated by the N-H...S hydrogen bond) is maintained in solution. Selected compounds were examined at various concentrations in cyclohexane and benzene solution.

5.33 Experimental for Cryoscopy.

Cryoscopic molecular mass measurements provide an accurate means by which solution molecular mass (M_r) and thereby the degree of association (n) [where $n = M_r / M_r(\text{monomer})$] may be determined. Where non-integer values of n are found, variable-concentration cryoscopic measurements are able to identify equilibrium species present in solution. The apparatus used (Figure 5.10) consists of a flat-bottomed inner glass sample tube surrounded by an outer cooling jacket filled with circulating ethanol (whose temperature is maintained at around 3 °C by a cryostat). An air jacket separates the inner tube from the cooling jacket to prevent supercooling of the solution. Standard inert atmosphere techniques were used throughout, the side-arm of the apparatus allowing a dry, oxygen-free argon atmosphere to be maintained during measurements. The freezing point of each solution was recorded using a Beckmann thermometer (reading to ± 0.002 °C with the aid of an eyepiece). Benzene (specifically purified for cryoscopic measurements) and cyclohexane (spectrophotometric grade) were pre-dried over molecular sieve and purged with argon prior to use. Initially the freezing point of pure solvent was determined before a known mass of the compound was introduced into the apparatus under a stream of dry argon. The freezing point of the resulting solution was then determined and hence the freezing point depression (ΔT). From the cryoscopic equation⁶⁵ (Equation 5.1) M_r could then be calculated.

$$M_r = \frac{1000 \times K \times w_s}{\Delta T \times w_b}$$

(where K = cryoscopic constant specific to the solvent,
 w_s = mass of solute and w_b = mass of solvent)

Eqn 5.1.

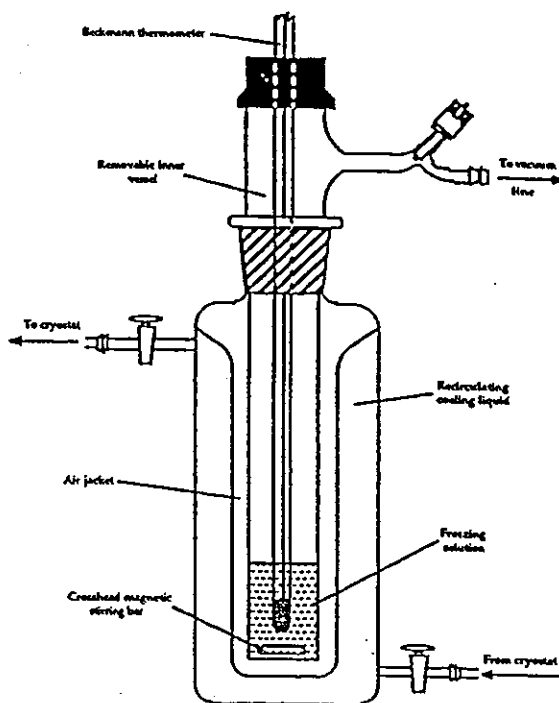


Figure 5.10. The cryoscopy apparatus.

5.34 Cryoscopic Results and Discussion.

For benzene K was determined by measuring ΔT for a known mass of $(C_6H_5)_2$, $M_r = 154.22$ g, ($K = 5.18$ gK). For cyclohexane time constraints dictated that the literature value ($K = 20.0$ gK) was used. For all cryoscopic experiments freezing points were determined at least three times until consecutive readings were consistent. The errors quoted are due to a precision of ± 0.004 °C in ΔT . All other errors (eg., in w_s , w_b , etc) were deemed relatively insignificant. For some of the measurements made in cyclohexane difficulty was experienced in achieving consistent temperature readings (probably due to unavailability of ultra-pure solvent). In these cases an average of up

to seven readings was taken and errors in ΔT were assumed to cover the range of these readings. This treatment results in the high errors reported in these cases.

In benzene solution (Table 5.11) all the compounds except ${}^n\text{Bu}_2\text{P}(\text{S})\text{NHP}(\text{S}){}^n\text{Bu}_2$ are, within error, monomeric, that is to say at the concentrations studied none of the intermolecular N-H...S hydrogen bonding found in the solid state is maintained in benzene solution). This lack of association in benzene is supported by the variable-concentration measurements of ${}^i\text{Bu}_2\text{P}(\text{S})\text{NHP}(\text{S}){}^i\text{Bu}_2$ and ${}^s\text{Bu}_2\text{P}(\text{S})\text{NHP}(\text{S}){}^s\text{Bu}_2$ which show no increase in n on increasing concentration. In comparison ${}^n\text{Bu}_2\text{P}(\text{S})\text{NHP}(\text{S}){}^n\text{Bu}_2$ exhibits a measurable degree of oligomerisation in

Table 5.11. Cryoscopic results in benzene.

Compound	w_s (g)	w_b (g)	conc. (M)	M_r (monomer)	M_r (expt.)	n^* (degree of association)
${}^{\text{Pr}}_2\text{P}(\text{S})\text{NHP}(\text{S}){}^{\text{Pr}}_2$	0.151	27.50	0.0153	313	332±15	1.06±0.05
${}^n\text{Bu}_2\text{P}(\text{S})\text{NHP}(\text{S}){}^n\text{Bu}_2$	0.159	24.47	0.0154	369	427±15	1.16±0.05
${}^i\text{Bu}_2\text{P}(\text{S})\text{NHP}(\text{S}){}^i\text{Bu}_2$	0.200	26.40	0.0179	369	386±14	1.05±0.04
${}^i\text{Bu}_2\text{P}(\text{S})\text{NHP}(\text{S}){}^n\text{Bu}_2$	0.286	26.40	0.0257	369	381±10	1.03±0.03
${}^s\text{Bu}_2\text{P}(\text{S})\text{NHP}(\text{S}){}^s\text{Bu}_2$	0.100	25.00	0.0095	369	371±24	1.01±0.06
${}^s\text{Bu}_2\text{P}(\text{S})\text{NHP}(\text{S}){}^n\text{Bu}_2$	0.203	25.00	0.0192	369	377±13	1.02±0.04
$(\text{EtO})_2\text{P}(\text{S})\text{NHP}(\text{S})\text{Ph}_2$	0.209	24.13	0.0197	385	385±13	1.00±0.03

Table 5.12. Cryoscopic results in cyclohexane.

Compound	w_s (g)	w_b (g)	conc. (M)	M_r (monomer)	M_r (expt.)	n^* (degree of association)
${}^n\text{Bu}_2\text{P}(\text{S})\text{NHP}(\text{S}){}^n\text{Bu}_2$	0.050	22.78	0.0046	369	610±32	1.65±0.08
${}^n\text{Bu}_2\text{P}(\text{S})\text{NHP}(\text{S}){}^i\text{Bu}_2$	0.106	22.78	0.0098	369	655±18	1.78±0.06
${}^i\text{Bu}_2\text{P}(\text{S})\text{NHP}(\text{S}){}^i\text{Bu}_2$	0.053	21.59	0.0052	369	446±47	1.21±0.13
${}^s\text{Bu}_2\text{P}(\text{S})\text{NHP}(\text{S}){}^s\text{Bu}_2$	0.096	22.79	0.0089	369	415±27	1.12±0.08

$$n^* = M_r(\text{monomer}) / M_r(\text{experimental}).$$

benzene solution. In view of its solid state structure it is reasonable to assume that such oligomerisation is mediated by the N-H...S hydrogen bonding.

The measurements made in cyclohexane solution suggest that all three butyl-substituted compounds oligomerise to some extent, that is to say in this less polar solvent a greater degree of hydrogen bonding is maintained on dissolution. The greatest degree of association is observed for ${}^n\text{Bu}_2\text{P}(\text{S})\text{NHP}(\text{S}){}^n\text{Bu}_2$ which is consistent with observations made of the benzene solutions. Furthermore an increase in concentration results in an increase in n . This is indicative of a monomer / dimer equilibrium operating in solution.

APPENDIX

Single Crystal X-Ray Crystallography.

Details of crystallographic parameters, data collections, reflections (measured reflections, independent reflections, observed reflections, reflection / parameter ratio) and refinements ($\langle F \{000}\rangle$, minimum / maximum transmission, final R and R' , maximum Δ / σ , largest difference peak / hole) for the crystal structures of **10**, **11**, **15**, **31**, **32**, **33**, **36**, **37**, **38** and **43** are summarised in Table I. Details of crystallographic parameters, data collections, reflections and refinements for the crystal structures of **1**, **2**, **3**, **4**, **6**, **7** and **8** have recently been published^{66,67}. Crystals were mounted on quartz fibres using araldite. Data were collected using Cu radiation and ω scans at room temperature with a Rigaku AFC7S diffractometer. Intensities were corrected for Lorentz-polarisation and for absorption (DIFABS)⁶⁸. The structures were solved by the heavy atom method^{69,70} or by direct methods⁷¹. In all cases except **32**, all of the non-hydrogen atoms were refined anisotropically. In **32**, the 30 % oxygen atom in the disordered region was refined isotropically. All other non-hydrogen atoms in **32** were refined anisotropically. The positions of the C-H hydrogen atoms were idealised whilst the N-H atoms were allowed to refine isotropically. Refinements were by full matrix least squares based on F using teXsan⁷².

Table I

	ⁿ Bu ₂ P(S)NHP(S) ⁿ Bu ₂ (10)	ⁱ Bu ₂ P(S)NHP(S) ⁱ Bu ₂ (11)	^s Bu ₂ P(S)NHP(S) ^s Bu ₂ (15)
Empirical formula	C ₁₆ H ₃₇ NP ₂ S ₂	C ₁₆ H ₃₇ NP ₂ S ₂	C ₁₆ H ₃₇ NP ₂ S ₂
<i>M</i>	369.54	369.54	369.54
Crystal colour, habit	clear, prism	clear, plate	clear, block
Crystal dimensions / mm	0.32 X 0.32 X 0.25	0.30 X 0.02 X 0.30	0.20 X 0.20 X 0.30
Space group	<i>P</i> -1 (#2)	<i>P</i> 2 ₁ / <i>n</i> (#14)	<i>P</i> -1 (#2)
<i>a</i> / Å	10.035(4)	12.339(4)	10.812(3)
<i>b</i> / Å	12.298(2)	9.033(6)	12.218(2)
<i>c</i> / Å	9.225(3)	21.681(3)	9.792(2)
α / °	93.13(2)	90.	112.48(1)
β / °	96.06(3)	106.28(2)	99.79(2)
γ / °	94.32(2)	90.	71.91(2)
<i>U</i> / Å ³	1126.7(5)	2319(1)	1134.2(5)
<i>D_c</i> / g cm ⁻³	1.089	1.058	1.082
μ / cm ⁻¹	34.33	33.35	34.1
2 θ max / °	120.2	120.1	120.1
<i>F</i> (000)	404.00	808.00	404.00
Measured reflections	3583	3903	3209
Independent reflections (<i>R</i> _{int})	3360 (0.064)	3712 (0.027)	3003 (0.049)
Observed reflections [<i>I</i> > 3.0 σ (<i>I</i>)]	2304	1335	2224
Reflection / parameter ratio	12.06	6.99	10.25
Minimum / maximum transmission	0.53 / 1.00	0.51 / 1.00	0.90 / 1.00
Final <i>R</i> , <i>R</i> '	0.075, 0.064	0.060, 0.050	0.055, 0.050
Maximum Δ / σ	3.78	0.34	7.12
Largest difference peak hole / eÅ ⁻³	0.32	0.18	0.40

	(EtO) ₂ P(S)NHP(S)Ph ₂ (31)	(EtO) ₂ P(S)NHP(O)Ph ₂ (32)	(EtO) ₂ P(O)NHP(S)Ph ₂ (33)
Empirical formula	C ₁₆ H ₂₁ NO ₂ P ₂ S ₂	C ₁₆ H ₂₁ NO ₃ P ₂ S	C ₁₆ H ₂₁ NO ₃ P ₂ S
<i>M</i>	385.41	369.35	369.35
Crystal colour, habit	clear, block	clear, block	clear, block
Crystal dimensions / mm	0.21 X 0.21 X 0.32	0.15 X 0.15 X 0.40	0.26 X 0.30 X 0.32
Space group	<i>P</i> ₂ /c (#14)	<i>P</i> -1 (#2)	<i>P</i> ₂ /n (#14)
<i>a</i> / Å	13.648(4)	10.196(4)	9.275(3)
<i>b</i> / Å	9.393(3)	19.301(2)	8.688(3)
<i>c</i> / Å	15.209(3)	10.080(1)	23.438(2)
α / °	90.	102.93(1)	90.
β / °	95.27(2)	98.40(2)	98.54(1)
γ / °	90.	83.25(2)	90.
<i>U</i> / Å ³	1941.3(9)	1905.4(8)	1867.8(8)
<i>D</i> _c / g cm ⁻³	1.319	1.287	1.313
μ / cm ⁻¹	41.03	32.08	32.72
2 θ max / °	120.3	110.2	120.1
<i>F</i> (000)	808.00	776.00	776.00
Measured reflections	3247	5168	3205
Independent reflections (<i>R</i> _{int})	3103 (0.060)	4800 (0.064)	2999 (0.093)
Observed reflections [<i>I</i> > 3.0 σ (<i>I</i>)]	2295	3717	2232
Reflection / parameter ratio	10.98	8.77	10.68
Minimum / maximum transmission	0.77 / 1.00	0.68 / 1.00	0.80 / 1.00
Final <i>R</i> , <i>R</i> '	0.041, 0.039	0.057, 0.050	0.043, 0.043
Maximum Δ / σ	0.20	0.58	0.06
Largest difference peak hole / eÅ ⁻³	0.28	0.30	0.35

	Zn[(EtO) ₂ P(O)NP(S)Ph ₂] ₂ (36)	Pd[(EtO) ₂ P(S)NP(S)Ph ₂] ₂ (37)	Pt[(EtO) ₂ P(S)NP(S)Ph ₂] ₂ (38)
Empirical formula	C ₃₂ H ₄₀ O ₆ P ₄ S ₂ N ₂ Zn	C ₃₂ H ₄₀ O ₄ P ₄ S ₄ N ₂ Pd	C ₃₂ H ₄₀ O ₄ P ₄ S ₄ N ₂ Pt
<i>M</i>	802.07	875.21	963.90
Crystal colour, habit	clear, block	yellow, needle	yellow, plate
Crystal dimensions / mm	0.10 X 0.10 X 0.33	0.12 X 0.17 X 0.33	0.20 X 0.20 X 0.10
Space group	<i>C</i> 2/ <i>c</i> (#15)	<i>P</i> -1 (#2)	<i>P</i> -1 (#2)
<i>a</i> / Å	19.614(4)	9.710(3)	11.342(6)
<i>b</i> / Å	10.468(1)	12.554(4)	20.813(5)
<i>c</i> / Å	19.780(2)	8.890(3)	8.630(6)
α / °	90.	98.95(3)	93.66(3)
β / °	108.32(1)	91.19(3)	105.44(6)
γ / °	90.	112.74(2)	89.51(3)
<i>U</i> / Å ³	3855.6(9)	983.3(5)	1959(1)
<i>D_c</i> / g cm ⁻³	1.382	1.478	1.633
μ / cm ⁻¹	38.41	76.30	102.84
2 θ max / °	120.1	120.2	120.1
<i>F</i> (000)	1664.00	448.00	960.00
Measured reflections	3161	3102	6160
Independent reflections (<i>R</i> _{int})	3058 (0.122)	2906 (0.074)	5818 (0.122)
Observed reflections [<i>I</i> > 3.0 σ (<i>I</i>)]	2322	2569	3467
Reflection / parameter ratio	10.85	11.95	8.16
Minimum / maximum transmission	0.67 / 1.00	0.77 / 1.00	0.64 / 1.00
Final <i>R</i> , <i>R</i> '	0.044, 0.039	0.030, 0.041	0.060, 0.059
Maximum Δ / σ	0.28	0.09	2.58
Largest difference peak hole / eÅ ⁻³	0.31	0.40	1.36

	Pt(PMe ₃) ₂ [(EtO) ₂ P(S)NP(S)Ph ₂] ⁺ BPh ₄ ⁻ (43)
Empirical formula	C ₄₆ H ₅₈ NBO ₂ P ₄ S ₂ Pt
<i>M</i>	1050.88
Crystal colour, habit	clear, plate
Crystal dimensions / mm	0.15 X 0.05 X 0.50
Space group	<i>P</i> -1 (#2)
<i>a</i> / Å	14.776(3)
<i>b</i> / Å	17.332(4)
<i>c</i> / Å	9.726(4)
α / °	102.63(3)
β / °	96.39(3)
γ / °	93.65(2)
<i>U</i> / Å ³	2405(1)
<i>D_c</i> / g cm ⁻³	1.451
μ / cm ⁻¹	78.69
2 θ max / °	119.8
\underline{E} (000)	1064.00
Measured reflections	7413
Independent reflections (<i>R</i> _{int})	7094 (0.135)
Observed reflections [<i>I</i> > 3.0 σ (<i>I</i>)]	5272
Reflection / parameter ratio	9.89
Minimum / maximum transmission	0.38 / 1.00
Final <i>R</i> , <i>R</i> '	0.060, 0.068
Maximum Δ / σ	0.08
Largest difference peak hole / eÅ ⁻³	1.55

REFERENCES

1. C. A. McAuliffe in *Comprehensive Coordination Chemistry*, eds. G. Wilkinson, R. D. Gillard and J. A. McCleverty, Pergamon Press, Oxford, 1987, Volume 2, p.989.
2. A. Pidcock in *Transition Metal Complexes of Phosphorus, Arsenic and Antimony Ligands*, ed. C. A. McAuliffe, Macmillan, London, 1973, p.3.
3. C. A. Tolman; *Chem. Rev.*, 1977, 77, 313.
4. C. A. McAuliffe and W. A. Levason, *Phosphine, Arsine and Stibine Complexes of the Transition Elements*, Elsevier, Amsterdam, 1979.
5. R. J. Puddephatt; *Chem. Soc. Rev.*, 1983, 99.
6. I. Haiduc; I. Silaghi-Dumitrescu; *Coord. Chem. Rev.*, 1986, 74, 127.
7. B. Chaudret; B. Delavaux; R. Poilblanc; *Coord. Chem. Rev.*, 1988, 86, 191.
8. B. Divisia; *Tetrahedron*, 1979, 35, 181.
9. S. O. Grim; E. D. Walton; *Inorg. Chem.*, 1980, 1982.
10. S. O. Grim; J. D. Mitchell; *Inorg. Chem.*, 1977, 1762.
11. S. O. Grim; L. C. Satek; J. D. Mitchell; *Inorg. Chem.*, 1980, 35B, 832.
12. J. D. Woollins; *J. Chem. Soc., Dalton Trans.*, 1996, 2893.
13. A. Schmidpeter; H. Groeger; *Z. Anorg. Allg. Chem.*, 1966, 345, 106.
14. A. Schmidpeter; J. Ebeling; *Chem. Ber.*, 1968, 101, 815.
15. R. A. Shaw; E. H. M. Ibrahim; *Angew. Chem. Int. Ed. Engl.*, 1967, 6(6), 556.
16. F. T. Wang; J. Najdzionek; K. L. Leneker; H. Wasserman; D. M. Braitsch; *Synth. React. Inorg. Met.-Org. Chem.*, 1978, 8(2), 119.
17. P. Bhattacharyya; A. M. Z. Slawin; M. B. Smith; J. D. Woollins; *Inorg. Chem.*, 1996, 35, 3675.
18. P. Bhattacharyya; J. Novosad; J. Phillips; A. M. Z. Slawin; D. J. Williams; J. D. Woollins; *J. Chem. Soc., Dalton Trans.*, 1995, 1607.
19. H. Steinberger; W. Kuchen; *Z. Naturforsch.*, 1974, 29b, 611.
20. N. G. Zabiroy; F. M. Shamsevaleev; R. A. Cherkasov; *Zh. Obshch. Khim.*, 1991, 61(6), 1474.
21. L. Meznik; A. Marecek; *Z. Chem.*, 1981, 8, 294.
22. H. Noth; *Z. Naturforsch.*, 1982, 37b, 1491.

- 23 S. Husebye; K. Maartmann-Moe; *Acta Chem. Scand.*, 1983, A37(5), 439.
- 24 P. B. Hitchcock; J. F. Nixon; I. Silaghi-Dumitrescu; I. Haiduc; *Inorg. Chim. Acta*, 1985, 96, 77.
- 25 S. Kulpe; I. Seidel; E. Herrmann; *Crystal Res. Technol.*, 1984, 19, 661.
- 26 M. Nouaman; Z. Zak; E. Herrmann; O. Navratil; *Z. Anorg. Allg. Chem.*, 1993, 619, 1147.
- 27 C. Silvestru; R. Rosler; I. Haiduc; R. Cea-Olivares; G. Espinosa-Perez; *Inorg. Chem.*, 1995, 34, 3352.
- 28 R. Cea-Olivares; H. Noth; *Z. Naturforsch.*, 1987, 42b, 1507.
- 29 A. M. Z. Slawin; J. Ward; D. J. Williams; J. D. Woollins; *J. Chem. Soc., Chem. Commun.*, 1994, 421.
- 30 I. Haiduc; R. Cea-Olivares; S. Hernandez-Ortega; C. Silvestru; *Polyhedron*, 1995, 14, 2041.
- 31 H. Bock; H. Schodel; Z. Havlas; E. Herrmann; *Angew. Chem. Int. Ed. Engl.*, 1995, 34, 1355.
- 32 G. P. McQuillan; I. A. Oxtan; *Inorg. Chim. Acta*, 1978, 29, 69.
- 33 O. Siiman; J. Vetuskey; *Inorg. Chem.*, 1980, 19, 1672.
- 34 R. Czernuszewicz; E. Maslowsky, Jr.; K. Nakamoto; *Inorg. Chim. Acta*, 1980, 40, 199.
- 35 O. Siiman; H. Gray; *Inorg. Chem.*, 1974, 13, 1185.
- 36 M. Churchill; J. Wormald; *Inorg. Chem.*, 1971, 10, 1778.
- 37 M. Churchill; J. Cooke; J. Fennessey; J. Wormald; *Inorg. Chem.*, 1971, 10, 1031.
- 38 S. Husebye; K. Maartmann-Moe; *Acta Chem. Scand.*, 1983, A37, 219.
- 39 S. Bjornevag; S. Husebye; K. Maartmann-Moe; *Acta Chem. Scand.*, 1982, A36, 195.
- 40 A. Laguna; M. Laguna; M. Nieves Fraile; E. Fernandez; P. G. Jones; *Inorg. Chim. Acta*, 1988, 150, 233.
- 41 J. R. Phillips; A. M. Z. Slawin; A. J. P. White; D. J. Williams; J. D. Woollins; *J. Chem. Soc., Dalton Trans.*, 1995, 2467.
- 42 D. J. Williams; C. O. Quicksall; K. M. Barkigia; *Inorg. Chem.*, 1982, 21, 2097.

- 43 I. Haiduc; C. Silvestru; H. W. Roesky; H-G. Schmidt; M. Noltemeyer; *Polyhedron*, 1993, 12, 69.
- 44 R. Rossi; A. Marchi; L. Magon; U. Casellato; S. Tamburini; R. Graziani; *J. Chem. Soc., Dalton Trans.*, 1991, 263.
- 45 N. Zuniga-Villareal; C. Silvestru; M. Reyes Lezama; S. Hernandez-Ortega; C. Alvarez Toledano; *J. Organomet. Chem.*, 1995, 496, 169.
- 46 C. P. Huber; M. L. Post; O. Siiman; *Acta Cryst.*, 1978, B34, 2629.
- 47 R. Rossi; A. Marchi; L. Marvelli; L. Magon; M. Peruzzini; U. Casellato; R. Graziani; *J. Chem. Soc., Dalton Trans.*, 1993, 723.
- 48 M. Rietzel; H. W. Roesky; K. V. Kalti; M. Noltemeyer; M. C. R. Symons; A. Abu-Raqabah; *J. Chem. Soc., Dalton Trans.*, 1991, 1285.
- 49 C. S. Browning; D. H. Farrar; D. C. Frankel; *Inorg. Chim. Acta.*, 1996, 241, 111.
- 50 R. O. Day; R. R. Holmes; A. Schmidpeter; K. Stoll; L. Howe; *Chem. Ber.*, 1991, 124, 2443.
- 51 C. Silvestru; I. Haiduc; R. Cea-Olivares; A. Zimbron; *Polyhedron*, 1994, 13, 3159.
- 52 R. Rosler; J. E. Drake; C. Silvestru; J. Yang; I. Haiduc; *J. Chem. Soc., Dalton Trans.*, 1996, 391.
- 53 O. Navratil; E. Herrmann; G. Grossmann; J. Teply; *Collect. Czech. Chem. Commun.*, 1990, 55, 364.
- 54 R. Cea-Olivares; J. Novosad; J. D. Woollins; A. M. Z. Slawin; V. Garcia-Montalvo; G. Espinosa-Perez; P. Garcia y Garcia; *J. Chem. Soc., Chem. Commun.*, 1996, 519.
- 55 M. Rietzel; H. W. Roesky; K. V. Kalti; H. G. Schmidt; R. Herbst-Irmer; M. Noltemeyer; G. M. Sheldrick; M. C. R. Symons; A. Abu-Raqabah; *J. Chem. Soc., Dalton Trans.*, 1990, 2387.
- 56 H. Ishikawa; T. Kido; T. Umeda; H. Ohyama; *Biosci. Biotech. Biochem.*, 1992, 56, 1882.
- 57 C. Alvarez; L. Barkaoui; N. Goasdoue; J. C. Daran; N. Platzer; H. Rudler; J. Vaissermann; *J. Chem. Soc., Chem. Commun.*, 1989, 1507.
- 58 O. Navratil; M. Fofana; J. Smola; *Z. Chem.*, 1984, 24, 30.

- 59 P. S. Pregosin; R. W. Kunz in *³¹P and ¹³C NMR of Transition Metal Phosphine Complexes*, eds. P. Diehl, E. Flucks and R. Kosfeld, Springer-Verlag, 1979, p.17.
- 60 K. Furusawa; M. Sekine; T. Hata; *J. Chem. Soc., Perkin I Trans.*, 1976, 1711.
- 61 MOPAC: A General Molecular Orbital Package, QCPE Program 455, Department of Chemistry, Indiana University, Bloomington, IN 47405, USA.
- 62 M. J. S. Dewar; W. J. Thiel; *J. Am. Chem. Soc.*, 1977, 99, 4899.
- 63 ADF 2.0 © Theoretical Chemistry, Vrije Universiteit De Buelelaan, 1083 1081 HV, Amsterdam, The Netherlands.
- 64 A. Klamt; G. Schuurmann; *J. Chem. Soc., Perkin Trans. 2*, 1993, 799.
- 65 M. G. Davidson; R. Snaith; D. Stalke; D. S. Wright; *J. Org. Chem.*, 1993, 58, 2810.
- 66 D. C. Cupertino; R. W. Keyte, A. M. Z. Slawin; D. J. Williams; J. D. Woollins; *Inorg. Chem.*, 1996, 35, 2695.
- 67 D. C. Cupertino; R. W. Keyte; A. M. Z. Slawin; D. J. Williams; J. D. Woollins; *Polyhedron*, in press.
- 68 DIFABS: N. Walker; D. Stuart; *Acta Cryst.*, 1983, A39, 158.
- 69 SAP191: Fan Hai-Fu (1991). Structure Analysis Programs with Intelligent Control, Rigaku Corporation, Tokyo, Japan.
- 70 PATTY: P. T. Beurskens; G. Admiraal; G. Beurskens; W. P. Bosman; S. Garcia-Granda; R. O. Gould; J. M. M. Smits; C. Smykalla. (1992). The DIRDIF program system, Technical Report of the Crystallography Laboratory, University of Nijmegen, The Netherlands.
- 71 SIR 92: A. Altomare; M. C. Burla; M. Camalli; M. Cascarano; C. Giacovazzo; A. Guagliardi; G. Polidori; *J. Appl. Cryst.*,
- 72 teXsan: Crystal Structure Analysis Package, Molecular Structure Corporation (1985 & 1992).

